UNIVERSITY OF CALIFORNIA SAN DIEGO

Using Light to Improve CAR T Cell Immunotherapy Development and Applications

A dissertation submitted in partial satisfaction of the requirements for the degree Doctor of Philosophy

in

Bioengineering

by

Molly Elizabeth Allen

Committee in charge:

Professor Yingxiao Wang, Chair
Professor John Chang
Professor Shu Chien
Professor Victor Nizet
Professor Geert Schmid-Schönbein
Professor Xiangdong Xu

2019

The Dissertation of Molly Elizabeth Allen is approved, and it is acceptable in quality and form for publication on microfilm and electronically:

_____

_____

_____

_____

_____

_____
Chair

University of California San Diego

2019

DEDICATION

This Dissertation is dedicated to my partner Ryan Abuan
whose love and support kept me sane long enough to complete it.

TABLE OF CONTENTS

LIST OF SYMBOLS AND ABBREVIATIONS

4-OHT: (Z)-4-hydroxytamoxifen

α-: anti-

A.U.: arbitrary units

aa: amino acid(s)

antigen^{-}: negative for antigen expression

antigen^{+}: positive for antigen expression

biLINuS: bipartite light-inducible nuclear localization signals

bp: base pairs

CaM: calmodulin

CAR(s): chimeric antigen receptor(s)

CDS(s): coding sequence(s)

CRISPR: clustered regularly interspaced short palindromic repeats

CTLA-4: cytotoxic T-lymphocyte-associated antigen 4

ECFP: enhanced cyan fluorescent protein

EGFP: enhanced green fluorescent protein

ERK: extracellular signal regulated kinase

ERT2: T2 mutant Estrogen Receptor ligand binding domain

Fc: crystallizable fragment

FRET: Fluorescence resonance energy transfer

IgG: immunoglobulin G

IL-2: Interleukin 2

ITAM(s): immunoreceptor tyrosine-based activation motif(s)

JNK: c-Jun N-terminal kinase

kb: kilobase pairs

LOV2: light-oxygen-voltage-sensing domain

mApple: a monomeric red fluorescent protein

mCherry: a monomeric red fluorescent protein

MHCII: major histocompatibility complex class II

mNG: monomeric NeonGreen fluorescent protein

mTurq: a monomeric cyan fluorescent protein

NFAT: nuclear factor of activated T cells

NF-κB: nuclear factor κ-light-chain-enhancer of activated B cells

NIR: near infrared

nMag: negative magnet of the light-inducible Magnet system

PA-Cre: photoactivatable Cre recombinase

PD-1: programmed cell death protein 1

PLL: poly-L-lysine

pMag: positive magnet of the light-inducible Magnet system

PTK(s): protein tyrosine kinase(s)

R-GECO: red fluorescent genetically-encoded calcium ion indicator for optical imaging

scFv: single chain variable fragment

Tam: tamoxifen

TamPA-Cre: tamoxifen and photoactivatable Cre recombinase

tBFP: truncated blue fluorescent protein

TF(s): transcription factor(s)

UCNP(s): up-conversion nanoparticle(s)

VPR: VP64-p65-Rta transcriptional activation domain

Ypet: a yellow fluorescent protein

Zap70: T cell receptor associated protein kinase 70

LIST OF FIGURES

LIST OF TABLES

LIST OF SUPPLEMENTARY FILES

Supplementary File 1: Excel spreadsheet of genetic constructs and oligonucleotides.

Supplementary File 2: Time-lapse fluorescence microscopy video of calcium biosensor R-GECO1.2^{+} Jurkat T cells stimulated with 1μM ionomycin (40x).

Supplementary File 3: Time-lapse fluorescence microscopy video of an α-CD19 CAR^{+} Jurkat T cell (green) actively binding to two CD19^{+} Target cells (red). (Merged bright field and pseudo-colored fluorescence images, 100x).

ACKNOWLEDGEMENTS

First and foremost, I would like to acknowledge Professor Yingxiao Wang for his generous support as my PI and doctoral committee Chair. With his bottomless wells of optimism and enthusiasm, he has taught me to embrace my creativity and to confidently apply novel synthetic biology approaches to overcome the many challenges in my field. Many thanks, Peter!

Having joined a lab specializing in FRET-based biosensor development, I am especially humbled by the opportunity to bring CAR T cell research and applications into this lab. I have Dr. Xiangdong Xu to thank for helping me bridge the gap between basic research and translational medicine.

I am also grateful for opportunity to work with and learn from so many highly-skilled, intelligent, and collaborative members of the Wang Lab, both past and present. A special thank you to my immunotherapy subgroup teammates for making invaluable contributions to my research endeavors and for allowing me to contribute to theirs!

Finally, I would like to thank my collaborator Phillip Kyriakakis for both his direct contributions to my research and his invaluable mentorship. Phil's passion and ingenuity inspired me push through many of the rough patches I encountered during my time as a grad student, he truly inspired me to become a better researcher.

Chapter 4, in part, is currently being prepared for submission for publication of the material as it may appear in ACS Synthetic Biology, 2019, Thangaraj, Jeyan; Kyriakakis, Phillip; Pan, Yijia; Limsakul, Praopim; Wu, Yiqian; Huang, Ziliang; Wang, Yingxiao; Molly Elizabeth Allen was the primary investigator and author of this material.

VITA

2007-2008	Research Assistant, Bay Area Regenerative Sciences Institute
2008-2009	Research Assistant, University of California, Berkeley
2009-2010	Research Assistant, CellASIC Corporation
2010	Bachelor of Science, University of California, Berkeley
2010-2012	Research Associate, CellASIC Corporation (acquired by EMD Millipore in 2012)
2012-2019	Research Assistant, University of California San Diego
2014	Master of Science, University of California San Diego
2019	Doctor of Philosophy, University of California San Diego

PUBLICATIONS

Pan, Yijia, Sangpil Yoon, Jie Sun, Ziliang Huang, Changyang Lee, **Molly Allen**, Yiqian Wu et al. "Mechanogenetics for the remote and noninvasive control of cancer immunotherapy." *Proceedings of the National Academy of Sciences* (2018): 201714900. Published January 17, 2018.

Limsakul, Praopim, Qin Peng, Yiqian Wu, **Molly E. Allen**, Jing Liang, Albert G. Remacle, Tyler Lopez et al. "Directed Evolution to Engineer Monobody for FRET Biosensor Assembly and Imaging at Live-Cell Surface." *Cell chemical biology* (2018). Published April 19, 2018.

Tang, Xia, Yanyan Liu, Qian Xiao, Qingping Yao, **Molly Allen**, Yingxiao Wang, Lizhi Gao, Yingxin Qi, and Ping Zhang. "Pathological cyclic strain promotes proliferation of vascular smooth muscle cells via the ACTH/ERK/STAT3 pathway." *Journal of Cellular Biochemistry* (2018). Published June 26, 2018.

Ouyang, Mingxing Qin Qin, Pengzhi Wang, Rongxue Wan, **Molly Allen**, Shannon Laub, Linhong Deng, Shaoying Lu, and Yingxiao Wang. "Sensitive FRET biosensor reveals Fyn kinase regulation by sub-membrane localization." *American Chemical Society Sensors* (2018). Published December 27, 2018.

Ziliang Huang, Yiqian Wu, Yijia Pan, **Molly Allen**, Ya-Ju Chang, Shu Chien, Yingxiao Wang. "A light inducible gene activation system toward controllable cell-based therapeutics." *Nature Communications*. Submitted: November 15, 2017. In revision.

ABSTRACT OF THE DISSERTATION

Using Light to Improve CAR T Cell Immunotherapy Development and Applications

by

Molly Elizabeth Allen

Doctor of Philosophy in Bioengineering

University of California San Diego, 2019

Professor Yingxiao Wang, Chair

Cancer is the second-leading cause of death worldwide. Over the past two decades, chimeric antigen receptor (CAR) T cell therapy has emerged as a promising alternative to traditional surgical, radiation and chemotherapy cancer treatments. Genetically engineered CAR T cells are designed to target and eradicate cancer cells *in vivo*. However, it remains difficult to identify a set of truly cancer-specific surface antigens to target—a critical requirement to prevent potentially fatal CAR T cell on-target off-tumor toxicity against other healthy tissues elsewhere in the body. I develop a variety of CARs and Receptors and assess their function using

genetically encoded fluorescent protein-based biosensors to rapidly detect the pre-transcriptional molecular events leading to CAR-mediated T cell activation. I next propose the novel concept of using light to spatially and temporally limit CAR expression in T cells localized to the tumor site in order to limit on-target off-tumor toxicity in distant healthy tissues. After creating and evaluating a variety of light-sensitive protein-based optogenetic systems to control CAR expression, I uncover three limitations. First, even when kept in the dark, some light-sensitive engineered T cells prematurely express CAR. Second, engineered T cells stimulated with light only weakly upregulate CAR expression. Third, the amount of blue light exposure necessary to induce CAR expression is phototoxic to the T cells. To overcome these limitations, I create the first light-inducible optogenetic system capable of driving robust CAR expression in T cells only following stimulation with minimal, non-toxic amounts of blue light. To do so, I create and optimize a novel genetic AND-gate by integrating components of tamoxifen-inducible Cre recombinase systems with a blue light-inducible split Cre system driven by heterodimerization between the highly sensitive Magnet system protein domains, nMag and pMag. To prevent premature CAR expression, the cytosol-localizing mutant T2 estrogen receptor ligand binding domain (ERT2) is fused to the N-terminal half of the CreN-nMag fusion protein, thus physically separating it from its nuclear-localized binding partner NLS-pMag-CreC. Without tamoxifen to drive ERT2-CreN-nMag protein translocation into the nucleus, the high levels of spontaneous, premature Cre-loxP recombination native to the original photoactivatable split Cre system is significantly suppressed. Upon stimulation with both tamoxifen and blue light, T cells engineered with this novel optogenetic system undergo efficient Cre-loxP recombination to express CAR, with high sensitivity to low-intensity, short-duration blue light exposure. I demonstrate that the new tamoxifen- and photo-activatable split-Cre recombinase system, called

TamPA-Cre, can be applied to strictly control localized CAR expression and subsequent T cell activation. The TamPA-Cre system has the potential to limit on-target off-tumor toxicity against distant healthy tissues in a way that was not previously possible.

CHAPTER 1:

Introduction

In 2018, an estimated 9.6 million people across the globe lost their lives to cancer. Second only to heart disease, cancer is the leading cause of death worldwide.[1] Over the past two decades, chimeric antigen receptor (CAR) T cell therapy has emerged from the field of immuno-oncology as a targeted approach for cancer treatment.[2] In CAR T cell therapy, a cancer patient's own T cells are genetically engineered *ex vivo* to express a chimeric antigen receptor. The CAR is designed to allow the engineered T cells to target a tumor associated antigen (TAA) expressed on the surface of cancer cells. Engineered CAR T cells are returned to the patient where, upon binding to TAA^+ cancer cells, they launch an immune effector response to kill the cancer cells.[3]

Current third generation CARs are transmembrane fusion proteins consisting of an extracellular antigen-recognition domain (typically an antibody-derived single chain variable fragment (scFv)), along with two or more intracellular costimulatory domains, and finally the T cell receptor (TCR) CD3-zeta activation domain. Whereas these intracellular domains are normally divided among different proteins within the T cell, CARs are designed to allow for T cell activation with a single trigger by combining all necessary components into one molecule.

CAR T cells that target the B cell-specific antigen CD19 have been successfully employed to treat several lymphomas and leukemias.[4-7] In fact, treatments have been so successful that, in 2017, the U.S. Food And Drug Administration (FDA) approved an anti(α)-CD19 CAR-T cell therapy known as Kymriah® (tisagenlecleucel) in 2017 to treat refractory acute lymphoblastic leukemia (ALL) in children and young adults (Novartis). However, because CD19 is present on all B cells, α-CD19 CAR T cells kill both malignant and heathy B cells indiscriminately. The process by which CAR T cells attack heathy tissues within the body along

with the targeted malignant cells is known as on-target off-tumor toxicity. Fortunately, in the case of CD19, CAR-mediated B-cell aplasia is uniquely survivable with life-long immunoglobulin-replacement therapy.

However, most on-target off-tumor toxicities pose serious risk to patient safety.[8-11] In early CAR T cell therapy clinical trials, α-HER2 CAR T cells targeting $HER2^+$ breast cancer cells proved fatal to the patient when healthy $HER2^+$ pulmonary tissues were also attacked by CAR T cells.[12] CAR T cells targeting Carbonic Anhydrase IX (CAIX)—a TAA overexpressed in renal cell carcinoma—also attacked healthy biliary epithelial cells found to express low levels of CAIX, ultimately resulting in liver toxicity.[13] Another clinical trial ended prematurely in 2017 when CAR T cells targeting carcinoembryonic antigen (CEACAM5), present on gastrointestinal malignancies, were found to also attack healthy $CEACAM5^+$ pulmonary and intestinal tissues.[14]

Furthermore, CAR T cells can launch too strong of a response, leading to dangerous side effects like cytokine storms and tumor lysis syndrome.[15] On the other hand, insufficient or non-sustained T cell activation is also an issue. While most CARs consist of the CD28 and/or the 4-1BB costimulatory domains along with the CD3-zeta activation domain, other potential costimulatory domains (e.g. ICOS, OX-40, DR3, CD27, CD30) and combinations thereof have yet to be widely exploited.[16-17] Such costimulatory signals are crucial in regulating activated T proliferation, cytokine production, differentiation, cytotoxic function, memory formation, and survival.[18] Coinhibitory receptors (e.g. cytotoxic T-lymphocyte-associated antigen 4 (CTLA-4) and programmed cell death protein 1 (PD-1)) can also be targeted for knockdown or inactivation to boost T cell activation signals.[18-19]

Current methods used to screen for optimal CAR designs as well as on-target off-tumor reactivity are labor intensive, often based on cell populations, and/or are low-throughput. Such

assays detect T cell activation by measuring post-translational outputs, such as changes in protein expression or cytokine production, that occur days after stimulation. However, T cell activation begins with a complex interplay of signaling pathways upstream of these transcriptionally-regulated changes. T cell activation requires two basic types of signals: activating and costimulatory.[20-23] The activating signal begins when the T cell antigen-specific receptor (TCR) binds an antigen on the major histocompatibility complex class II (MHCII) of antigen-presenting cells. Coreceptors also bind to MHCII and lead to activation of Src-family protein tyrosine kinases (PTKs) such as Lck and Fyn, and Syk-family PTKs such as the zeta chain of T cell receptor associated protein kinase 70 (Zap70). Tyrosine phosphorylation of several targets by PTKs trigger further activation of several molecules including mitogen-activated protein kinases like extracellular signal regulated kinase (ERK) and c-Jun N-terminal kinase (JNK), as well as the Ca^{2+}-driven nuclear factor of activated T cells (NFAT). Costimulatory signals are antigen-independent and are conducted through various costimulatory receptors, such as CD28 which is critical in the activation of the nuclear factor κ-light-chain-enhancer of activated B cells (NF-κB) pathway.[16] Together, NFAT, c-Jun, c-Fos, and NF-κB transcription factors drive the expression of cytokines like interleukin 2 (IL-2)[19] which in turn drives a multitude of downstream T cell activation responses.[24] T cells also employ antigen-independent coinhibitory receptors (e.g. CTLA-4, PD-1) which block such pathways to prevent downstream activation. The intricate balance of these signaling pathways govern antigen-mediated T cell cytoskeletal rearrangement, proliferation, differentiation, survival, and effector functions.[20-23]

In Chapter 2, I seek to expedite current CAR screening techniques by using protein-based genetically encoded biosensors to detect early pre-transcriptional signs of T cell activation in single cells that occur within seconds to minutes following stimulation. Such biosensors have

been critical in elucidating the spatiotemporal dynamics of important cellular pathways in living cells.[25-27] Biosensors can translate an intracellular biochemical process of interest into an altered protein configuration which can be read as a change in fluorescence.[28] Some biosensors are designed to conditionally alter proper fluorophore protein folding, which can change the intensity of the fluorescent signal. Other biosensors utilize fluorescence resonance energy transfer (FRET) to conditionally alter fluorescence. FRET is a phenomenon in which energy from an excited donor fluorophore is transferred in a non-radiative fashion to a nearby acceptor fluorophore. Donor-acceptor FRET pairs must have sufficient donor-emission and acceptor-excitation spectral overlap, and must be properly oriented and within close proximity (<10nm) in order for FRET to occur.[25, 28-29] Changes in fluorescence or FRET efficiency can be driven by promoting or disrupting their proper protein configuration. If a biological process of interest (e.g. an increase in intracellular calcium ions) can cause a conformational change in an engineered protein, this conditional change can be exploited to alter the fluorescent properties of an attached fluorophore or FRET pair reporter. For example, the FRET-based YC3.6 calcium biosensor reports calcium ion concentrations using FRET via Ca^{2+}-mediated binding of the calmodulin and M13 domains between the FRET fluorescent protein pair.[30-31] If such biosensors are proven to be effective reporters of T cell activation, their use has the potential to expedite CAR T cell research and development.

In addition to improving CAR screening techniques, I sought to prevent on-target off-tumor toxicity more directly using a synthetic biology approach. To circumvent the difficulty of identifying a tumor-specific antigen, several genetically-encoded Boolean logic gates have been created to allow CAR T cells to interpret a combination of multiple antigen inputs.[32] For example, healthy tissue known to also express the targeted antigen can be avoided using a NOT

logic gate, in which CAR T cells co-express an inhibitory[33] or cell death-inducing[34] receptor against another healthy tissue-specific antigen. To target tumor cells with a unique combination of antigens, AND logic gates have been generated in CAR T cells by splitting CAR costimulatory and activation domains between two unique antigen-specific receptors. In this approach, recognition of both antigens is required to drive full CAR-mediated T cell effector function.[15] Similarly, costimulatory and activation CAR domains can be reconstituted via small-molecule-driven dimerization, but failure to limit such diffusible small molecules to the tumor site *in vivo* leaves normal tissues susceptible to on-target off-tumor toxicity.[35] More recently, the mechanically-sensitive synNotch receptor has been used to automatically drive the transcription of CAR upon binding to the target cell.[36] Antigen recognition can also be altered at the protein level using tumor-targeting single-chain variable fragment adaptor molecules to tune and gate CAR activity.[37] However, in both systems, if the same pair of antigens happen to also be present on healthy cells, patients are at risk of on-target off-tumor toxicity.

Therefore, in Chapters 3 and 4, I explore whether an external stimulus could be used to spatially limit CAR-mediated T cell activation to the site of the tumor, thus avoiding on-target off-tumor toxicity in distant tissues. Light is an ideal external stimulus with high spatiotemporal resolution, readily available at low cost. Light can be applied non-invasively with precise control over the time, intensity, and location of the applied stimulus. Furthermore, unlike stimulation using drugs or small molecules, light can be instantly removed to halt CAR T cell activity as necessary.

In the field of optogenetics, genetically-encoded light-sensitive proteins have been developed to undergo functional changes upon light stimulation. A multitude of versatile optogenetic “light switches” have been developed to both study and actuate cellular functions.

Rhodopsin-type optogenetic proteins control ion channels and are widely used in the neuroscience field to induce cellular depolarization in neurons, yet rhodopsins have also been used to recruit T cells to tumor sites with some success.[38] Non-opsin-based optogenetic tools precisely control a greater variety of cellular functions by modulating gene expression, enzymatic function, protein translocation, and more.[39-40] Optogenetic protein systems like PhyB-PIF3 and BphP1-PpsR2 are sensitive to red, far-red, or near-infrared light (NIR). Although long wavelength red light advantageously penetrates deeper into tissues, it is also a highly diffuse stimulus. With the core need of limiting CAR T cell activity to the specific tumor site, shorter wavelength light provides higher spatial resolution. On the other hand, systems like UVB8 and Dronpa rely on intense violet or ultraviolet light which can directly damage DNA.[41-42]

Therefore, I considered optogenetic systems that respond to 400-500nm wavelength light. The limited tissue penetration (<1 mm) of such short wavelengths has been overcome with implantable micron-scale inorganic light emitting diodes controlled wirelessly with radio frequencies[43] or NIR light,[44] or by stimulating antigen-targeted, blue-light-emitting lanthanide-doped upconversion nanoparticles (UCNP) with NIR light.[45-46] These solutions take advantage of the tissue-penetrating nature of NIR light to stimulate highly localized blue light. As has been extensively reviewed,[39-40] several genetically encoded blue-light-sensitive proteins such as *As*Lov2, GIGANTEA-FKF1, VVD, Magnet, and Cry2-CIB1 have been used to transcriptionally regulate gene expression reversibly. While removing blue light from these systems advantageously turns off CAR expression, these transcriptional regulation systems often suffer from leaky inducible promoters and weak light-induced gene expression. My colleague, Ziliang Huang, developed a novel blue light-induced optogenetic system (LINTAD) designed to help prevent protein expression without light stimulation due to leaky inducible promoters. Using the

CAR constructs I developed, I explored the efficacy of this system in transcriptionally regulating CAR expression using light, as laid out in Chapter 3.

In order to combat the weak CAR expression driven by light-inducible transcriptional regulation systems, I switched my focus to blue light sensitive genome-editing systems to permanently switch on gene expression.[47-49] The enzyme Cre recombinase is widely used to delete or invert DNA coding sequences (CDSs) in the genome flanked by 34bp long loxP recognition sites. Cre recombination is commonly controlled by inducing nuclear localization using the drug tamoxifen. In these systems, the Cre protein is fused with the cytosol-localizing mutant T2 estrogen receptor ligand binding protein domain (ERT2).[50-52] Without tamoxifen, ERT2-Cre fusion proteins are sequestered outside of the nucleus, thus preventing Cre-loxP recombination in the genome. Administering the diffusible drug tamoxifen allows ERT2-Cre proteins to enter into the nucleus where Cre-loxP recombination can occur. However, Cre recombination can also be induced using light. In these systems, the Cre protein is split into two separate non-functional proteins, commonly referred to as CreN and CreC for the N-terminal and C-terminal protein halves, respectively. Cre recombinase function can be restored upon blue light stimulation by fusing CreN and CreC light-sensitive heterodimerizing protein domains, like Cry2 and CIB1 or nMag and pMag (negative and positive Magnet proteins). However, subject to the same undesirable non-light-induced premature heterodimerization seen in optogenetic transcription-based system, the light-sensitive split Cre systems likewise drove a degree of premature, permanent CAR expression without light stimulation. In Chapter 4, I create a novel tamoxifen- and light-inducible optogenetic system to prevent on-target off-tumor toxicity driven by premature CAR expression, yet sensitive to low intensity blue light stimulation following drug administration. To the best of this author's knowledge, this is the first example of a robust,

well-gated optogenetic system capable of inducing CAR expression in T cells with high spatiotemporal control.

CHAPTER 2:

Using Biosensors to Rapidly Detect CAR-Mediated T Cell Activation

2.1 Introduction

I decided to explore the potential use of these biosensors as tools to identify early signs of CAR-mediated T cell activation at the single cell level. Many genetically-encoded biosensors can be used to monitor components of the T cell activation pathway. For example, biosensors have been developed to detect changes in Lck,[53] Fyn,[54] Zap70,[55] ERK,[56-57] JNK,[58] protein kinase A and Ras,[27, 59] as well as for reporting intracellular calcium levels.[60-63] Biosensors can detect some of the first molecular signaling cascade events, and thus, provide a relatively immediate readout. An ideal candidate for such a biosensor would be sensitive enough to detect molecular events at physiologically-relevant levels with a robust readout (i.e. change in intensity or FRET). Biosensors must also be shown to accurately and reliably predict downstream T cell activation, as reported by currently accepted methods.

2.2 Results and Discussion

After evaluating the great variety of T cell-activation-related biosensors, I selected two for evaluation—one detecting an early molecular event (calcium ion mobilization), and one detecting a downstream event (ERK phosphorylation). Both molecular signaling pathway events occur upstream from the transcriptional and protein expression changes that are currently used to evaluate T cell activation, such as CD69 expression and IL-2 secretion.

Anti(α)-CD19 CAR is arguably the best studied and successful of the CARs, showing great success in clinical trials.[2-3, 15-16, 18, 64] Most B cells and their malignant forms express the CD19 antigen on their cell surface. Because B cell aplasia is treatable, α-CD19 CAR T cells have

the potential to wipe out many previously incurable B cell malignancies. Therefore, I opted to use a third generation α-CD19 CAR to study T cell activation and biosensor evaluation (see Supplementary File 1 for genetic construct details). The antigen CD38 has also been identified as a non-Hodgkin B cell lymphoma marker, against which an α-CD38 CAR was created to successfully target and eliminate such cells *in vitro* and in mouse models.[65] Therefore, I similarly designed and developed an α-CD38 CAR. A "headless" CAR lacking an antigen-specific scFv was also created to serve as a negative control for antigen-mediated T cell activation.

The leukemia-derived Jurkat (clone E6-1) T cell line has been used for decades to study T cell activation.[66] Simulation methods for both non-specific and TCR-specific activation are well established. Furthermore, numerous TCR signaling component knockdown and knockout mutants are also available for study. Though not a perfect model for primary T cell function, Jurkat T cells serve as a reasonable *in vitro* T cell model in which to evaluate both biosensor and CAR functionality.

2.2.1 Evaluation of candidate genetically-encoded biosensors

One of the earliest signs of T cell activation is a sudden increase in intracellular calcium ions.[61-63] Although a variety of non-genetically encoded calcium dyes are convenient and available,[67] such dyes do not exist for other signaling pathway events of interest. Genetically-encoded calcium biosensors serve as an important positive control to confirm model cell functionality as well as to establish appropriate methods of introducing, expressing, and evaluating other biosensors. I chose to test two of the many available genetically encoded calcium biosensors in Jurkat T cells: the intensity-based R-GECO1.2[60] and the FRET-based YC3.6[30-31] biosensors. R-GECO1.2 is a red-shifted GCaMP-type calcium biosensor that

increases in fluorescent intensity upon binding to calcium ions. The mApple red fluorescent protein is flanked by the calmodulin (CaM)-binding domain M13 and a CaM domain. Binding of calcium causes an interaction between M13 and CaM which reorganizes mApple causing an increase in fluorescence intensity. The FRET-based YC3.6 biosensor similarly utilizes the calcium-mediated interaction between M13 and CaM to bring a donor fluorophore into favorable proximity and orientation with an acceptor fluorophore causing an increase in FRET. I used a variant of this construct developed in-house in which the original ECFP/YFP FRET pair for the mTurquoise/Ypet FRET pair in YC3.6 because it exhibits a larger FRET change upon ionomycin stimulation than YC3.6 in Jurkat T cells while reflecting the same dynamics (data not shown). Both R-GECO1.2 and YC3.6 biosensors were investigated due to their spectral orthogonality and thus compatibility with other potential biosensors. While calcium influx alone is not sufficient to trigger full T cell activation, responses from these biosensors will serve as an important early indicator of T cell activation.

During T cell activation, the serine/threonine protein kinase ERK 1/2 dimer is activated through the mitogen-activated protein kinase (MAPK)-ERK pathway.[20-21] Activated ERK 1/2 phosphorylates cytosolic targets and nuclear transcription factors (TFs) responsible for up-regulating gene expression.[22-23] Importantly, ERK 1/2 activates c-Fos and NF-κB TFs which are necessary for driving expression of the IL-2 gene. IL-2 cytokine production is a key indicator of full T cell activation and many assays use IL-2 production as a quantitative readout.[24] Therefore, I utilized the FRET-based ERK biosensor EKAREV[29] (Extracellular signal-regulated Kinase Activity Reporter Enhanced Visualization) as the pre-IL-2 reporter for T cell activation. For creating the EKAREV biosensor stable Jurkat cell line, I replaced the original Ypet CDS for a codon-diversified dYpet CDS[54] to reduce sequence similarity with ECFP (Fig. 2.1), thus

preventing recombination introduced by lentiviral gene transfer.[68] Because ERK is activated in the cytosol, the biosensor includes a nuclear exclusion sequence (NES) to prevent it from translocating to the nucleus, ensuring that FRET changes in the ERK biosensor are not affected by translocation into the nucleus.

2.2.1.1 Non-specific stimulation of calcium biosensors

In order to confirm functionality of the calcium biosensors, ionomycin was used to increase intracellular calcium ion concentration. Ionomycin is an ionophore which effectively punches holes in the cell membrane allowing extracellular calcium ions (1 mM) to enter the cell (50-100 nM).[61] After allowing R-GECO1.2 and YC3.6 Jurkat T cells to attach to a poly-L-lysine (PLL)- or IgG-coated glass bottom dishes, cells were imaged on a fluorescence microscope under 40x magnification. Cells at multiple positions were imaged 10 minutes prior to stimulation to establish the mean baseline fluorescent intensities of each biosensor. Then, ionomycin (1μM) or vehicle control dissolved in prewarmed cell culture medium was added to the dish after which imaging was immediately resumed to track biosensor response for at least 15 minutes. Image analysis was conducted for each cell to evaluate fluorescence intensity changes (R-GECO1.2) or ratiometric FRET changes (YC3.6 FRET/mTurquoise).

In the absence of stimulation, calcium biosensors indicated that Jurkat T cells were already exhibiting short-lived, asynchronous "spikes" of high calcium ion concentrations of varying frequency and fold-change (Fig. 2.2A). Though these spontaneous spikes in intracellular calcium ion concentration have been previously reported,[61-63] I tested several experimental procedure parameters to ensure none had affected calcium ion dynamics in the Jurkat cell line stably expressing R-GECO1.2. First, I compared cells plated on PLL- and non-binding IgG-

coated glass bottom dishes (Fig. 2.2B-C). While R-GECO1.2^{+} Jurkat T cells only attached to PLL-coated surfaces, ultimately PLL and IgG groups did not exhibit significantly different calcium ion dynamics. Mimicking ionomycin stimulation by adding cell culture medium (with vehicle control) also did not affect calcium dynamics (Fig. 2.2D), nor did washing away unattached cells before imaging (Fig. 2.2E). Therefore, changes in intracellular calcium ion dynamics in Jurkat T cells were not influenced by these experimental parameters.

Extracellular calcium ion influx was triggered by ionomycin stimulation. Jurkat cell lines stably expressing the calcium biosensor R-GECO1.2 or YC3.6 were monitored before and after stimulation (Fig. 2.3A-B, S2.1A-D). After ionomycin stimulation, both biosensors reported a rapid increase in intracellular calcium ions (~2 min) followed by a short period of rapid decrease (1 min), then a gradual decrease until leveling off after 5-10 min above baseline measurements (Supplementary File 2). While both biosensors reported similar intracellular calcium ion dynamics, R-GECO1.2 exhibited a slightly larger dynamic range (~3.5-fold) than YC3.6 (~3-fold). Therefore, moving forward, I chose to use the intensity-based R-GECO1.2 calcium biosensor to monitor intracellular calcium ions.

2.2.1.2 T cell-specific stimulation of calcium and ERK biosensors

Next, Jurkat cell lines stably expressing R-GECO1.2 and EKAREV calcium biosensors were tested with a physiologically-relevant T cell-activating stimulus to ensure sufficient biosensor sensitivity. T cell receptor (TCR)- and costimulatory receptor-mediated T cell activation was triggered by stimulating Jurkat T cells with α-CD3/α-CD28 antibody clusters. Using similar experimental and image analysis procedures, I found that the baseline-normalized intracellular calcium ion concentration reported by R-GECO1.2 (Fig. 2.3C, S2.1E) also rapidly

increased (~1.5 min), then gradually decreased (~3 min) until leveling off at measurements 2.3-fold higher than baseline. Whereas non-specific stimulation of cells by ionomycin produced a relatively consistent calcium ion influx response in cells (Fig. S2.1D), T cell specific stimulation with CD3-CD28 antibody clusters elicited a wide range of responses (Fig. S2.1E). The non-specific mechanism of ionomycin indiscriminately exposes cells to high extracellular calcium ion concentrations (1mM). On the other hand, stimulation through TCR- and costimulatory-pathways first triggers cytoplasmic calcium ion influx from the endoplasmic reticulum, which then triggers cell membrane calcium release-activated calcium channels to allow for additional extracellular calcium ion influx.[21] Therefore, control of intracellular calcium ion concentration through this complex pathway will naturally vary between cells within a heterogenous population. Setting aside those cells that did not respond (< 1.6-fold change), T cell-specific stimulation induced a greater 2.6-fold increase in biosensor response on average than for ionomycin stimulation (1.9-fold increase).

Antibody clusters were also used to trigger T cell activation in Jurkat cell lines expressing the ERK biosensor EKAREV which reports increases in ERK phosphorylation with increases in FRET ratiometric measurements between the codon-diversified Ypet and ECFP pair. Five minutes after triggering Jurkat T cell activation using CD3/CD28 antibody clusters, average ERK phosphorylation rapidly increased, exhibiting a prolonged overall 1.17-fold increase in the FRET/ECFP ratio (Figure 2.3D, S2.1F). However, there was considerable heterogeneity between cell responses. Approximately 18.5% of cells did not respond (<1% change) and 25.9% of cells exhibited only a minor response (<10% change), while the rest of the cells responded with an average 1.31-fold increase in phosphorylation. Despite this response heterogeneity, this data

confirmed the EKAREV biosensor was indeed able to detect T cell activation-related ERK phosphorylation.

2.2.2 Development and Evaluation of Candidate Chimeric Antigen Receptors

Next, I developed two different CARs to test in Jurkat T cells. First, the α-CD19 CAR was constructed *in silico* and synthesized (Fig. 2.4A). The extracellular scFv was created based on the FMC63-28Z receptor protein gene (GenBank HM852952.1) which contains the variable region sequences of the FMC63 monoclonal mouse anti-human CD19 antibody. Variable light and heavy chains were separated by a flexible 4xGGGGS linker. The extracellular hinge region was derived from the crystallizable fragment (Fc) of human immunoglobulin G (IgG). The CD28 costimulatory component included both the transmembrane and intracellular signaling domains, while the 4-1BB domain included its own costimulatory domain. Finally, the TCR CD3-zeta chain component includes immunoreceptor tyrosine-based activation motifs (ITAMs) for phosphorylation-mediated T cell activation. A membrane-localizing signaling peptide was included at the N terminus. Second, the α-CD38 CAR was constructed based on the α-CD19 CAR design (Fig. 2.4B). Variable light and heavy chains of a CD38-recognizing scFv were synthesized and substituted for those of the α-CD19 CAR. As a negative control, a "headless" CAR lacking an antigen-specific scFv altogether (though still with membrane-localizing signal peptide) was also created (Fig. 2.4C). Labeled CAR constructs were also created by attaching Ypet or mCherry after the CD3-zeta chain components with a GGSGGT linker.

Fluorescence microscopy was used to confirm appropriate membrane localization of the mCherry-tagged CARs in HEK293T cells (Fig. 2.4D), where some intracellular spots consistent

with membrane-trafficking were also seen. CAR construct plasmids were then introduced to Jurkat T cells via electroporation.

2.2.2.1 Antigen-specific binding of CAR T cells to target cells

In order to confirm the antigen specificity of the α-CD19 and α-CD38 CARs, I developed a novel flow-cytometry assay to detect binding between CAR^+ Jurkat T cells and TAA^+ Target Toledo cells. This assay relies on the assumption that CAR is expressed at a level that allows Jurkat T cells to tightly bind to at least one TAA^+ Target Toledo cell. It is also assumes that bond is strong enough to withstand the forces exerted by the flow cytometer during measurement at slow speed. After labeling or marking CAR^+ Jurkat T cells and Target Toledo cells with spectrally-distinguishable fluorescent markers or proteins, flow cytometry was used to calculate the fraction of CAR^+ Jurkat T cells that were also bound to at least one Target cell (i.e. an event positive for both markers). In this proof of concept experiment, I was able to demonstrate that Jurkat T cells expressing α-CD19 or α-CD38 CAR both exhibited a high percentage of cells that were bound to $CD19^+CD38^+$ Target cells (64.7% and 40.9%, respectively)—an order of magnitude higher than either the untransfected (dyed) or headless CAR^+ Jurkat groups (1.0% and 4.5%, respectively) that served as non-binding controls (Table 2.1). Furthermore, the percentage of Jurkat T cells expressing both α-$CD19^+$ and α-$CD38^+$ CARs that bound to Target cells reflected the average between either CAR alone (54.6%). Likewise, co-expression of α-CD19 CAR and headless CAR also dampened the overall binding affinity of those cells expressing only α-CD19 CAR (48.7%). Taken together, this data suggests that co-expressed CARs do not work cooperatively to further improve overall Target cell binding. Instead, CAR proteins compete with

one another for limited space at the immunological synapse between the cells. Therefore, I decided to focus on the strongly-binding α-CD19 CAR alone.

Other methods for determining CAR antigen-specificity were also considered, including using labeled or epitope-tagged antigens or antigen-coated beads as markers of cell-surface binding. Although these methods may allow for precise calculations of saturating antigen concentration (using free antigen) or minimum antigen density for sufficient adherence to Target cells (using antigen-coated beads), the high cost of purchasing or creating sufficient amounts of purified antigen was ultimately limiting. However, CAR T cells do indeed bind to Target cells in an antigen-specific manner, as can be seen in Supplementary File 3, a time-lapse fluorescence microscopy video with merged pseudo-colored channels (100x). This video shows an α-CD19 CAR^+ Jurkat T cell (green) actively binding to two separate $CD19^+$ Target cells (red). Together with the CAR Binding Assay results, this showed that the recognition domains of the tested CARs were indeed functional.

2.2.2.2 CAR-mediated T cell activation

Next, I tested the α-CD19CAR-Ypet construct in Jurkat T cells to ensure that binding to $CD19^+$ Target cells also triggered T cell activation. Upregulated expression of cell surface protein CD69 was used to determine T cell activation. α-CD19 CAR^+ Jurkat T cells were (or were not) co-incubated with $CD19^+$ Target cells at a 1:1 live cell ratio for 24h, after which CD69 expression was measured with fluorescently tagged α-human CD69 antibodies, read via flow cytometry (Fig. 2.5A). Gating for the $Ypet^+$ Jurkat T cells, CD69 expression was clearly upregulated only in response to co-incubation with Target cell. By contrast, headless CAR^+ Jurkat T cells did not show any significant change in CD69 expression whether or not they were

co-incubated with Target cells (Fig. 2.5B). Therefore, α-CD19 CAR can trigger antigen-specific activation in Jurkat T cells. I further noted that in all groups, CD69 expression increased in logarithmic fashion with increasing levels of CAR expression (Fig. 2.5C), likely due to limited space on the cell surface. Higher concentrations of transmembrane CARs are more at risk of forming spontaneous protein clusters which mimic the immunological synapse necessary for T cell activation. Therefore, to avoid non-specific T cell activation, CARs should be expressed at low levels to avoid non-specific T cell activation.

Overall, I found that the reliability of the CAR Binding Assay largely depends on the consistency of cell samples. For example, electroporated Jurkat T cells express varying copy numbers of the introduced plasmid(s) in a process that kills the majority of cells. Such variability in gene expression and transfection efficiency results in highly heterogenous CAR^+ Jurkat T cell populations, and thus variable TAA^+ Target cell binding dynamics. To achieve consistent results, I created stable CAR^+ Jurkat T cell lines which were useful in optimizing experimental parameters, such as the effector to target cell mixture ratio (Chapter 3). However, the CAR Binding Assay may not be able to detect weak CAR-mediated Target cell binding events since the forces introduced by the measurement process itself may exceed the strength of cell-cell binding, but more testing would be needed to confirm this hypothesis. Nevertheless, the CAR Binding Assay can be used to measure relative CAR-mediated binding affinities between dynamic living cells.

2.2.3 Biosensor detection of CAR-mediated T cell activation

Finally, the R-GECO1.2 calcium biosensor was used to monitor α-CD19 CAR-mediated T cell activation. The α-CD19 CAR-Ypet construct was transfected into the $R\text{-}GECO1^+$ Jurkat T cell line via electroporation. Twenty-four hours post-transfection, cells were added and attached

to a PLL-coated glass bottom dish 5 minutes before starting microscope time-lapse imaging. α-CD19 CAR-Ypet$^+$ R-GECO1.2$^+$ Jurkat T cells were imaged for at least 10 minutes to establish biosensor baseline dynamics. Next, CellTracker dyed CD19$^+$ Target Toledo cells were gently added and allowed to settle to the bottom of the dish as imaging continued. Due to poor transfection efficiency, each imaging field included at least one other R-GECO1.2$^+$ α-CD19 CAR$^-$ Jurkat T cell which served as a no-CAR control sample. The time at which a Target Toledo cell landed next to and touched the Jurkat cell (as evaluated by the bright field images) was considered to be t = 0 (Fig. 2.6). Analysis of R-GECO1.2 calcium biosensor intensity was conducted on both CAR$^+$ and CAR$^-$ Jurkat T cells.

On average, α-CD19CAR-Ypet$^+$ R-GECO1.2$^+$ Jurkat T cells stimulated by binding to CD19$^+$ Target cells exhibited a sustained modest 1.74-fold increase in calcium ion concentration (Fig. 2.6A) compared to the average 2.3-fold response from CD3-CD28 antibody stimulation (Fig. 2.3C, S2.1E). The R-GECO1.2 biosensor reported clear responses to Target cell binding in all but one of the ten measured cells (Fig. 2.6B). However, the kinetics and magnitude of biosensor responses varied greatly from cell to cell, reminiscent of cells stimulated by CD3-CD28 antibody clusters (Fig. S2.1E). Fluctuations in ERK activity during CD3/CD28 antibody cluster stimulation were also heterogeneous with only about 63% of cells exhibiting a change in FRET/ECFP ratio (Fig. 2.3D, Fig. S2.1F). By contrast, such changes were not seen in R-GECO1.2$^+$ α-CD19 CAR-Ypet$^-$ cells (Fig. 2.6 C,D) suggesting that the average sustained increase in intracellular calcium ions reported by R-GECO1.2 was indeed CAR-mediated.

Because of the lower sustained R-GECO1.2 biosensor response to CAR-mediated stimulation with target cells (1.74), the sustained response measured by the EKAREV biosensor would likely be insufficient for accurate analysis (already only a 1.17-fold increase on average

with CD3-CD28 antibody cluster stimulation). Furthermore, the experimental procedure for stimulating CAR T cells with TAA^+ Target cells is extremely tedious and inefficient. In an effort to streamline the procedure and decrease cell-to-cell variability, I attempted to create $Biosensor^+$ CAR^+ Jurkat T cell lines. CAR and Biosensor CDSs separated by a 2xP2A peptide self-cleavage site were introduced into the pSin lentiviral transfer vector. However, the large size of the combined constructs greatly limited viral production efficiency, resulting in poor Jurkat T cell transduction efficiencies (data not shown).

While lentiviral size restrictions can be avoided by splitting large constructs into separate viral vectors (as is done in Chapters 3 and 4), I ultimately chose not to pursue this project for several reasons. First, the current common methods for detecting CAR T cell activation (e.g. changes in endogenous gene expression, cytokine release, etc.) are not easily amenable to the rapid response time (seconds to minutes) of the tested biosensors. Individual CAR T cells would require single cell tracking over many hours, if not days, in order for T cell activation to be confirmed using standard methods. For example, detecting T cell activation by CD69 expression in CAR T cells involves immunostaining—an endpoint assay consisting of multiple washing and incubation steps which may disrupt any concurrent biosensor readings. Second, while fluorescent reporters under the control of, for example, the NFAT or IL-2 promoter can be introduced to monitor changes in gene expression related to T cell activation in real time, this technique is currently only feasible in immortalized cell lines like Jurkat T cells. The same is true of introducing genetically encoded biosensors, which renders CAR screening assays in primary T cells out of reach. Calcium responsive dyes might prove a good alternative, but the spontaneous short-lived spikes in intracellular calcium ions makes the data difficult to interpret. Third, current biosensors provide only relative changes in intensity or FRET ratio measurements. Deciphering

biosensor dynamics in cells with heterogeneous responses measured for the R-GECO1.2 and EKAREV biosensors requires further development of data analysis techniques. The relatively small dynamic range of most biosensors further compounds the detection of biosensor response in cells. Fourth, extended frequent exposure to the various excitation wavelengths used to read the biosensors can cause photobleaching and phototoxicity in cells if not carefully calibrated (discussed further in Chapter 3).

2.2.4 Future Directions

While I was able show that the R-GECO1.2 calcium biosensor was capable of detecting CAR-mediated T cell activation, significant improvements in high throughput single cell imaging, biosensor dynamic range, data analysis, and primary T cell gene delivery efficiency are likely necessary before biosensors could help streamline CAR T cell screening. As it stands, biosensors are currently best suited for studying sub-cellular molecular events and pathways.

However, since moving on from this project, it appears that perhaps Jurkat T cell reporter cell lines may be an acceptable stand-in for primary T cells to screen for functional novel CAR designs. Published only a few months ago in November 2018, a paper by Rydzek et al. describes how fluorescent protein reporters expressed under the control of minimal promoters sensitive to NF-κB and NFAT transcription factors in Jurkat T cells had been used to successfully screen a library of candidate CARs.[69] They claim to cut the required time for CAR screening from 21 days in primary T cells to only 6 days in Jurkat T cells, with reporters measured 24 hours after stimulation. However, upregulation of other endogenous genes like CD69 are also detectable 24 hours after co-incubation with targeted TAA^+ cells. Biosensors like R-GECO1.2 and EKAREV respond within seconds to minutes and could therefore decrease the process to only 5 days. Still, data analysis techniques would likely need to be developed to interpret complex, heterogenous

biosensor outputs. It will be exciting to see whether this Jurkat T cell-based CAR screening platform will prove an acceptable alternative to current methods. If so, the detection of CAR-mediated T cell activation with biosensors may warrant further exploration.

2.3 Materials and Methods

Genetic Constructs

R-GECO1.2 (Addgene #45494), YC3.6[30] (kindly gifted from the Matsuda Lab, Kyoto University), and EKAREV[29] genetic constructs were transferred into mammalian expression vectors pCDNA3.1 (Invitrogen) or pCAGGS (Addgene #41583), or were inserted into a self-inactivating second generation pSin (Addgene #16579) or pHR (Addgene #79125) lentiviral transfer plasmids. In YC3.6, the ECFP CDS was replaced by mTurquoise, and the Ypet CDS in EKAREV was replaced by the codon-diversified dYpet CDS (Addgene #78302) using SpeI/XhoI restriction sites.

The third-generation α-CD19 CAR was designed *in silico* based on a CDS kindly shared with us by Daofeng Liu of Baylor College of Medicine, TX, and was synthesized (Integrated DNA Technologies). The α-CD19 scFv was based on the FMC63-28Z receptor CDS (GenBank HM852952.1) where the variable light and heavy chains are separated by a flexible 4xGGGGS linker. The extracellular hinge region was derived from the crystallizable fragment (Fc) of human IgG, followed by the CD28 transmembrane and intracellular costimulatory signaling domains, the 4-1BB costimulatory domain, and finally the T cell activating CD3-zeta domain of the T cell receptor (TCR). An IgG-derived membrane localization signaling peptide was also included at the N terminus of the scFv. The third generation α-CD38 CAR was similarly designed. The α-CD38 scFv (synthesized by Integrated DNA Technologies) was developed based on US patent application US20100267145A1. Both constructs were linked to a C-terminal

Ypet and/or mCherry FP (with GGSGGT linker) in order to identify transfected cells. Sanger sequencing was used to confirm all genetic constructs (GeneWiz). See Supplementary File 1 for details.

Cells and Reagents

Human embryonic kidney cells (HEK293T, ATCC CRL-3216), Jurkat T cells (Clone E6-1, ATCC TIB-152), and Toledo B lymphocytes (ATCC CRL-2631) were purchased from ATCC. HEK293T cells were cultured in Dulbecco's modified eagle medium (DMEM) (Gibco #11995065) supplemented with 2 mM L-glutamine, 1 mM sodium pyruvate, 100 units/ml penicillin, 100 µg/ml streptomycin (Gibco #15140122), and 10% (v/v) fetal bovine serum (FBS) (Thermo Fischer Scientific #10438026) in standard tissue-culture-treated dishes or plates. Jurkat and Toledo cells were cultured in RPMI-1640 medium with L-glutamine, supplemented with 10% (v/v) FBS, 1x penicillin, and streptomycin in non-tissue-culture-treated plates or flasks. Biosensor^{+} Jurkat T cell lines were maintained in puromycin (Sigma #P8833-100MG). CAR constructs were introduced into Jurkat T cells via electroporation at (BioRad Gene Pulser Xcell).

Lentiviral Production

HEK293T cells were used to produce antropic VSV-G pseudotyped lentivirus with a second-generation lentiviral system. Genes of interest were cloned into transfer plasmid pPKm-145 (pSin, Addgene #90505), which was co-transfected into Lenti-X-293T cells with envelope plasmid pCMV-VSV-G (Addgene #8454) and packaging plasmid pCMVΔR8.2 (Addgene #12263) at a 2:1:1 molar ratio using the ProFection Mammalian Transfection System (Promega, Madison, WI #E1200). Viral supernatant was collected and filtered (0.22 micron) 48h after transfection and used directly to transduce other cells. Transduced cell populations were enriched (>95%) via puromycin selection to generate heterogeneous cell lines.

Fluorescence Microscopy

Images were acquired on a Nikon Eclipse Ti inverted microscope with a cooled charge-coupled device (CCD) camera. The following filters were used to image the indicated fluorophores: ECFP and mTurquoise (420DF40 excitation filter, 480DF40 emission filter, 455DCXRU dichroic mirror), mApple (580/10 nm excitation, 630/20 nm emission, 595 LP dichroic mirror), and Ypet (420DF40 excitation filter, 535DF35 emission filter, 455DCXRU dichroic mirror). Analysis was conducted using MetaFluor 7.8 or MetaMorph 7.8 software (Molecular Devices, San Jose, CA).

Non-specific Stimulation of Biosensors in Jurkat T cells

Prior to imaging, cells were plated on 35mm #0 glass bottom dishes (Cell E&G, San Diego, CA) coated with either 20 μg/mL fibronectin or 10 μg/mL poly-L-Lysine for adherent and suspension cells, respectively (Sigma, St. Louis, MO). After ~5 min to allow cells to attach to the glass bottom dish, cells were either directly imaged or were gently washed with pre-warmed cell culture medium to remove unattached cells. Alternately, glass bottom dishes were coated in Goat anti-Rabbit IgG (H+L), highly cross-adsorbed (CiteAB #SAB3700883) (1:200 dilution in PBS). Jurkat T cells expressing R-GECO1.2 or YC3.6 biosensors were stimulated with 1μM ionomycin (Sigma-Aldrich #I3909) during time-lapse fluorescence microscopy to monitor intensity and ratiometric FRET changes. Jurkat T cells expressing R-GECO1.2, YC3.6, or EKAREV biosensors were stimulated with CD3/CD28 antibody clusters, prepared by mixing mouse-derived antibodies against human CD3 (10μg/ml) and CD28 (5μg/ml) with biotinylated goat anti-mouse antibody (30μg/ml) and streptavidin (2.6μg/ml) (Fisher #555337, #556620, #31800, #434301, respectively).

Flow cytometry measurements

Fluorescent and immunostained cells were measured using a BD Accuri C6 flow cytometer equipped with 488 and 640 nm excitation lasers. Ypet and FRET fluorescence was measured using the 488 nm excitation laser with a 533/30 nm emission filter. Cell dyed or labeled with antibodies conjugated with far-red dyes were measured using the 640 nm excitation laser with a 675/25 nm emission filter. Before measuring, live cells were trypsinized (if adherent), washed three times with FACS wash buffer (filter-sterilized 0.5% BSA in PBS or autoMACS Running Buffer (Miltenyi Biotec, Germany)), then either measured directly, or immunostained for 20 minutes at 37°C, washed thrice, and then measured. Data was analyzed using FlowJo software (TreeStar). Samples of plain HEK293T, Jurkat, and Toledo cells were included with each experiment as negative controls for gating purposes.

CAR Binding Assay

Jurkat T cells were either dyed with MitoTracker Green FM (Thermofisher, #M7514) or transfected with either Ypet-tagged α-CD19 CAR, α-CD38 CAR, or headless CAR via electroporation and allowed to recover for 24h. Immediately before experiments, all target Toledo cells were stained with CellTracker Deep Red (Thermofisher, #C34565). Cells were then counted by hemocytometer and mixed at a 1:1 live Jurkat T cell:Target cell ratio (150,000 cells each) in 1 mL of culture medium. After rotating at 37°C for 45 minutes to allow for mixing and binding, samples were read on the lowest speed of a flow cytometer (BD Accuri C6) set to measure MitoTracker (Ex/Em: 490/516), Ypet (Ex/Em: 488/533nm), and Deep Red (Ex/Em: 640/675nm) events. Of the MitoTracker Dye^+ or $Ypet^+$ events, those that were also CellTracker Dye^+ were considered to represent a Jurkat T cell that had bound to at least one Target cell.

CAR-mediated T Cell Activation

Cells were prepared as described in the CAR Binding Assay, except that Target Toledo cells were not dyed and mixtures of cells were co-cultured for 24 hours. Cells were then immunostained with α-CD69 APC-conjugated antibody against early T cell activation marker CD69 BioLegend #310910) and measured via flow cytometry. Gating for Ypet^{+} or Mitotracker^{+} cells, those expressing greater amounts of CD69 were considered to have undergone CAR-mediated T cell activation.

R-GECO1.2^{+} Jurkat T cells transiently expressing α-CD19CAR-Ypet attached to a PLL-coated dish were imaged using time-lapse fluorescence microscopy (100x, every 30s) for at least 10 min to establish a baseline. Then, CD19^{+} Target Toledo cells stained with CellTracker Deep Red (Thermofisher, #C34565) were gently added to the dish and allowed to settle to bottom of the dish and interact with T cells. If no cells happened to fall next to the imaged T cell, more Target cells were added while imaging continues. From bright field images, interaction between cells was set as t = 0 and imaging was continued for at least 15 minutes.

2.4 Figures and Tables

A.

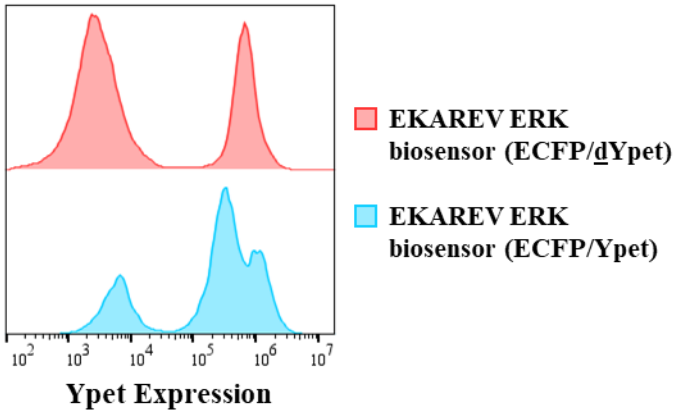

B.

```
Alignment of Ypet CDS with ECFP CDS (original EKAREV Biosensor)
Similarity : 689/714 (96.50 %)
             M  V  S  K  G  E  E  L  F  T  G  V  V  P  I  L  V  E  L  D
Ypet   1     ATGGTGAGCAAGGGCGAGGAGCTGTTCACCGGGGTGGTGCCCATCCTGGTCGAGCTGGAC  60
             ||||||||||||||||||||||||||||||||||||||||||||||||||||||||||||
ECFP   1     ATGGTGAGCAAGGGCGAGGAGCTGTTCACCGGGGTGGTGCCCATCCTGGTCGAGCTGGAC  60
             M  V  S  K  G  E  E  L  F  T  G  V  V  P  I  L  V  E  L  D
             G  D  V  N  G  H  K  F  S  V  S  G  E  G  E  G  D  A  T  Y
Ypet   61    GGCGACGTAAACGGCCACAAGTTCAGCGTGTCCGGCGAGGGCGAGGGCGATGCCACCTAC  120
             ||||||||||||||||||||||||||||||||||||||||||||||||||||||||||||
ECFP   61    GGCGACGTAAACGGCCACAAGTTCAGCGTGTCCGGCGAGGGCGAGGGCGATGCCACCTAC  120
             G  D  V  N  G  H  K  F  S  V  S  G  E  G  E  G  D  A  T  Y
             G  K  L  T  L  K  L  L   C  T  T  G  K  L  P  V  P  W  P  T
Ypet   121   GGCAAGCTGACCCTGAAGCTTCTA-TGCACCACCGGCAAGCTGCCCGTGCCCTGGCCCAC  179
             ||||||||||||||||||#|||###||||||||||||||||||||||||||||||||||||
ECFP   121   GGCAAGCTGACCCTGAAG-TTCATCTGCACCACCGGCAAGCTGCCCGTGCCCTGGCCCAC  179
             G  K  L  T  L  K   F  I  C  T  T  G  K  L  P  V  P  W  P  T
              L  V  T  T  L  G   Y  G  L  Q  C  F  A  R  Y  P  D  H  M  K
Ypet   180   CCTCGTGACCACCCTGGG-CTACGGCCTGCAGTGCTTCGCCCGCTACCCCGACCACATGA  238
             ||||||||||||||||###||##|||#||||||||||##||||||||||||||||||||||
ECFP   180   CCTCGTGACCACCCTG-ACCTGGGGCGTGCAGTGCTTCAGCCGCTACCCCGACCACATGA  238
              L  V  T  T  L   T  W  G  V  Q  C  F  S  R  Y  P  D  H  M  K
```

Figure 2.1: Fixing recombination introduced by the lentiviral gene transfer of the original EKAREV (Ypet-ECFP) ERK biosensor with Ypet CDS codon diversification. (A) Histograms of Jurkat T cells transduced via lentivirus with EKAREV ERK biosensor constructs either with (top) or without (bottom) codon-diversified dYpet. Ypet expression (right peak(s)) was used to monitor the transduced population during cell line selection (puromycin). When lentivirus was made from the original EKAREV (Ypet/ECFP) biosensor CDS, at least two populations emerged indicating recombination between the similar Ypet and ECFP CDS. Reduced sequence similarity with codon-diversified dYpet helped prevent recombination introduced by lentiviral gene transfer.[68] (B) DNA sequence alignment of Ypet with ECFP from the original EKAREV biosensor.[29] (C) DNA sequence alignment of codon-diversified dYpet[54] with ECFP from the modified EKAREV biosensor. (Serial Cloner 2.6.1)

```
                Q  H  D  F  F  K  S  A  M  P  E  G  Y  V  Q  E  R  T  I  F
Ypet   239   AGCAGCACGACTTCTTCAAGTCCGCCATGCCCGAAGGCTACGTCCAGGAGCGCACCATCT  298
              ||||||||||||||||||||||||||||||||||||||||||||||||||||||||||||
ECFP   239   AGCAGCACGACTTCTTCAAGTCCGCCATGCCCGAAGGCTACGTCCAGGAGCGCACCATCT  298
                Q  H  D  F  F  K  S  A  M  P  E  G  Y  V  Q  E  R  T  I  F
                F  K  D  D  G  N  Y  K  T  R  A  E  V  K  F  E  G  D  T  L
Ypet   299   TCTTCAAGGACGACGGCAACTACAAGACCCGCGCCGAGGTGAAGTTCGAGGGCGACACCC  358
              ||||||||||||||||||||||||||||||||||||||||||||||||||||||||||||
ECFP   299   TCTTCAAGGACGACGGCAACTACAAGACCCGCGCCGAGGTGAAGTTCGAGGGCGACACCC  358
                F  K  D  D  G  N  Y  K  T  R  A  E  V  K  F  E  G  D  T  L
                V  N  R  I  E  L  K  G  I  D  F  K  E  D  G  N  I  L  G  H
Ypet   359   TGGTGAACCGCATCGAGCTGAAGGGCATCGACTTCAAGGAGGACGGCAACATCCTGGGGC  418
              ||||||||||||||||||||||||||||||||||||||||||||||||||||||||||||
ECFP   359   TGGTGAACCGCATCGAGCTGAAGGGCATCGACTTCAAGGAGGACGGCAACATCCTGGGGC  418
                V  N  R  I  E  L  K  G  I  D  F  K  E  D  G  N  I  L  G  H
                K  L  E  Y  N  Y  N  S  H  N  V  Y  I  T  A  D  K  Q  K  N
Ypet   419   ACAAGCTGGAGTACAACTACAACAGCCACAACGTCTATATCACCGCCGACAAGCAGAAGA  478
              ||||||||||||||||||||#|||||||||||||||||||||||||||||||||||||||
ECFP   419   ACAAGCTGGAGTACAACTACATCAGCCACAACGTCTATATCACCGCCGACAAGCAGAAGA  478
                K  L  E  Y  N  Y  I  S  H  N  V  Y  I  T  A  D  K  Q  K  N
                G  I  K  A  N  F  K  I  R  H  N  I  E  D  G  G  V  Q  L  A
Ypet   479   ACGGCATCAAGGCCAACTTCAAGATCCGCCACAACATCGAGGACGGCGGCGTGCAGCTCG  538
              ||||||||||||||||||||||||||||||||||||||||||||||||#|||||||||||||
ECFP   479   ACGGCATCAAGGCCAACTTCAAGATCCGCCACAACATCGAGGACGGCAGCGTGCAGCTCG  538
                G  I  K  A  N  F  K  I  R  H  N  I  E  D  G  S  V  Q  L  A
                D  H  Y  Q  Q  N  T  P  I  G  D  G  P  V  L  L  P  D  N  H
Ypet   539   CCGACCACTACCAGCAGAACACCCCCATCGGCGACGGCCCCGTGCTGCTGCCCGACAACC  598
              ||||||||||||||||||||||||||||||||||||||||||||||||||||||||||||
ECFP   539   CCGACCACTACCAGCAGAACACCCCCATCGGCGACGGCCCCGTGCTGCTGCCCGACAACC  598
                D  H  Y  Q  Q  N  T  P  I  G  D  G  P  V  L  L  P  D  N  H
                Y  L  S  Y  Q  S  A  L  F  K  D  P  N  E  K  R  D  H  M  V
Ypet   599   ACTACCTGAGCTACCAGTCCGCCCTGTTCAAAGACCCCAACGAGAAGCGCGATCACATGG  658
              |||||#||||||##|||||||||||||##|||||||||||||||||||||||||||||||
ECFP   599   ACTACtTGAGCACCCAGTCCGCCCTGAGCAAAGACCCCAACGAGAAGCGCGATCACATGG  658
                Y  L  S  T  Q  S  A  L  S  K  D  P  N  E  K  R  D  H  M  V
                L  L  E  F  L  T  A  A  G  I  T   E  G  M  N  E  L  Y
Ypet   659   TCCTGCTGGAGTTCCTGACCGCCGCCGGGATCACT-GAGGGCATGAACGAGCTGTAC  714
              ||||||||||||||#||||||||||||||||||||####||||||#||||||||###
ECFP   659   TCCTGCTGGAGTTCGTGACCGCCGCCGGGATCACTCTC-GGCATGGACGAGCTG---  711
                L  L  E  F  V  T  A  A  G  I  T  L   G  M  D  E  L  X
```

C.

```
Alignment of dYpet with ECFP (modified EKAREV biosensor)
Similarity : 485/714 (67.93 %)
                  M  S  K  G  E  E  L  F  T  G  V  V  P  I  L  V  E  L  D
dYpet  1      ---atgtctaaaggtgaagaattattcactggtgttgtcccaattttggttgaattagat  57
              ####||###||#||#||#||##|#|||||#||#||#||#||#||##||||#||##|#||#
ECFP   1      ATGGTGAGCAAGGGCGAGGAGCTGTTCACCGGGGTGGTGCCCATCCTGGTCGAGCTGGAC  60
              M  V  S  K  G  E  E  L  F  T  G  V  V  P  I  L  V  E  L  D
              G  D  V  N  G  H  K  F  S  V  S  G  E  G  E  G  D  A  T  Y
dYpet  58     ggtgatgttaatggtcacaaattttctgtctccggtgaaggtgaaggtgatgctacgtac  117
              ||#||#||#||#||#|||||#||####||#|||||#||#||#||#||#|||||#||#|||
ECFP   61     GGCGACGTAAACGGCCACAAGTTCAGCGTGTCCGGCGAGGGCGAGGGCGATGCCACCTAC  120
              G  D  V  N  G  H  K  F  S  V  S  G  E  G  E  G  D  A  T  Y
              G  K  L  T  L  K  L  L  C  T  T  G  K  L  P  V  P  W  P  T
dYpet  118    ggtaaattgaccttaaaattactctgtactactggtaaattgccagttccatggccaaccc  177
              ||#||##|||||#|#||#||##|||||#||#||#||#||##|||||#||#||#|||||#|||
ECFP   121    GGCAAGCTGACCCTGAAGTTCATCTGCACCACCGGCAAGCTGCCCGTGCCCTGGCCCACC  180
              G  K  L  T  L  K  F  I  C  T  T  G  K  L  P  V  P  W  P  T
```

Figure 2.1: Fixing recombination introduced by the lentiviral gene transfer of the original EKAREV (Ypet-ECFP) ERK biosensor with Ypet CDS codon diversification, Continued.

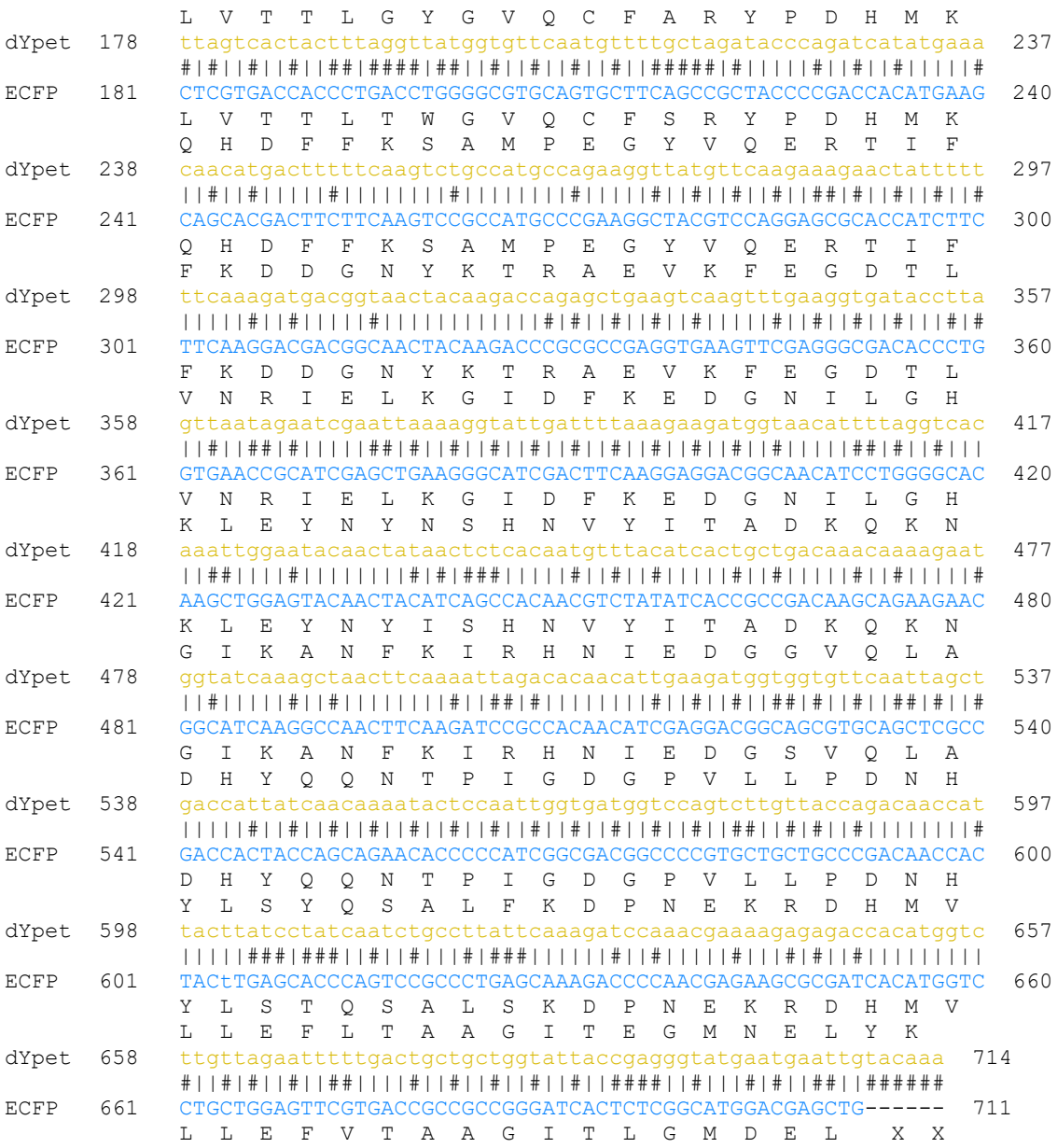

Figure 2.1: Fixing recombination introduced by the lentiviral gene transfer of the original EKAREV (Ypet-ECFP) ERK biosensor with Ypet CDS codon diversification, Continued.

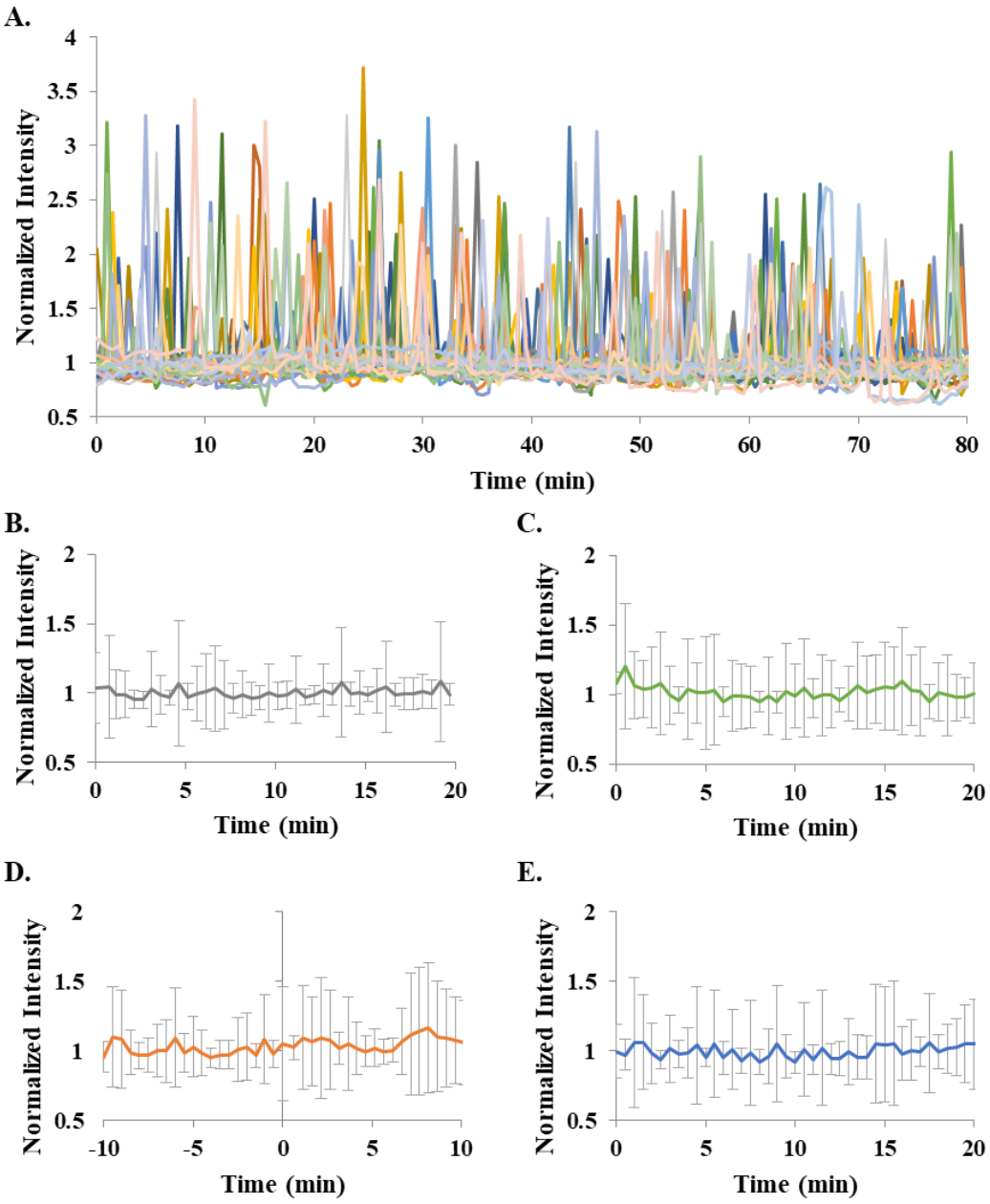

Figure 2.2: Baseline intracellular calcium ion dynamics in the R-GECO1.2 Jurkat T cell line. R-GECO1.2 biosensor fluorescent intensity (AU) is normalized to the mean intensity taken 10 minutes prior to plotted data. (A) Intracellular calcium ion spikes vary in magnitude and frequency from cell to cell (represented by different colors). Mean baseline intracellular calcium ion concentration tracked via R-GECO1.2 over time in Jurkat T cells imaged on glass surface coated (or not) poly-L-lysine before and after the addition of cell culture medium, with or without a washing step to remove unattached cells prior to imaging. (B) PLL-coated dish, no washing, cell culture medium added. (C) IgG-coated dish, no washing, no cell culture medium added. (D) PLL-coated dish, no washing, cell culture medium added (t = 0). (E) PLL-coated dish, with washing, no cell culture medium added. Mean ± standard deviation, imaged 40x every 30s.

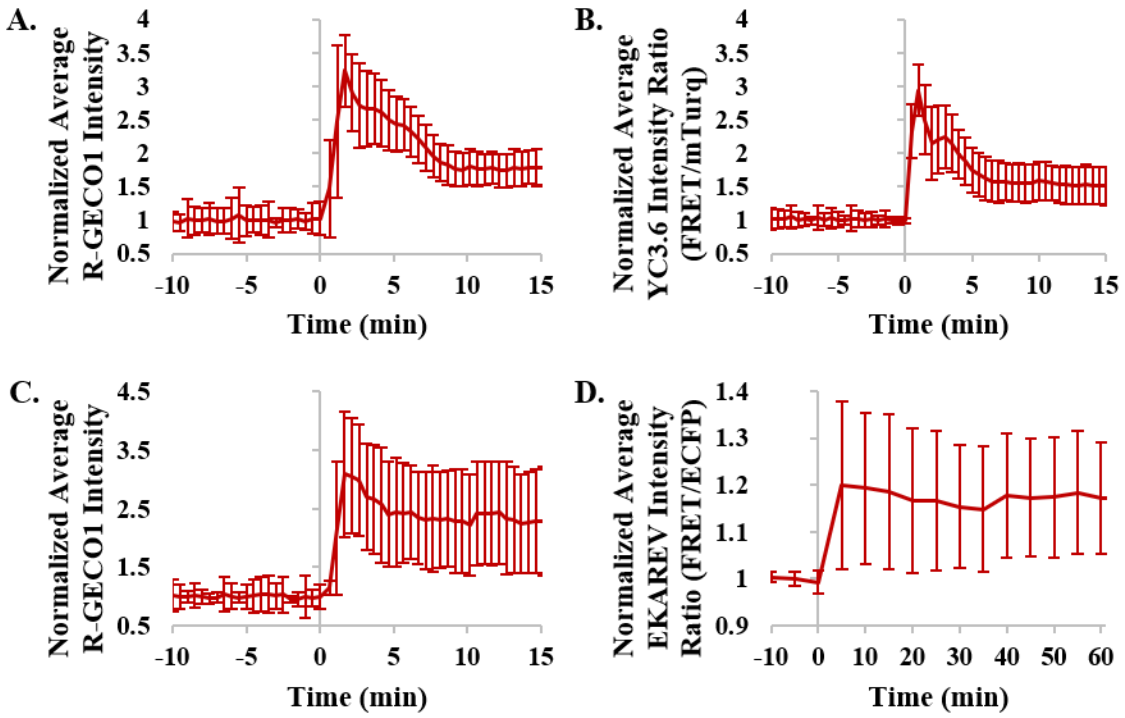

Figure 2.3: Calcium and ERK biosensors respond to stimulation in Jurkat T cells. Jurkat cell lines stably expressing each biosensor were stimulated (or not) at t = 0. (A) R-GECO1.2 with ionomycin stimulation (1μM, n = 71) or not (n=42). (B) YC3.6 intensity ratio (FRET/mTurq) with ionomycin stimulation (1μM, n = 80) or not (n = 36). (C) R-GECO1.2 with CD3/CD28 antibody cluster stimulation (n = 78) or not (n = 42). (D) EKAREV with CD3/CD28 antibody cluster stimulation (n = 27). n = independently measured cells. Mean ± standard deviation, imaged under 40x magnification every 30 s (A-C) or every 5 min (D).

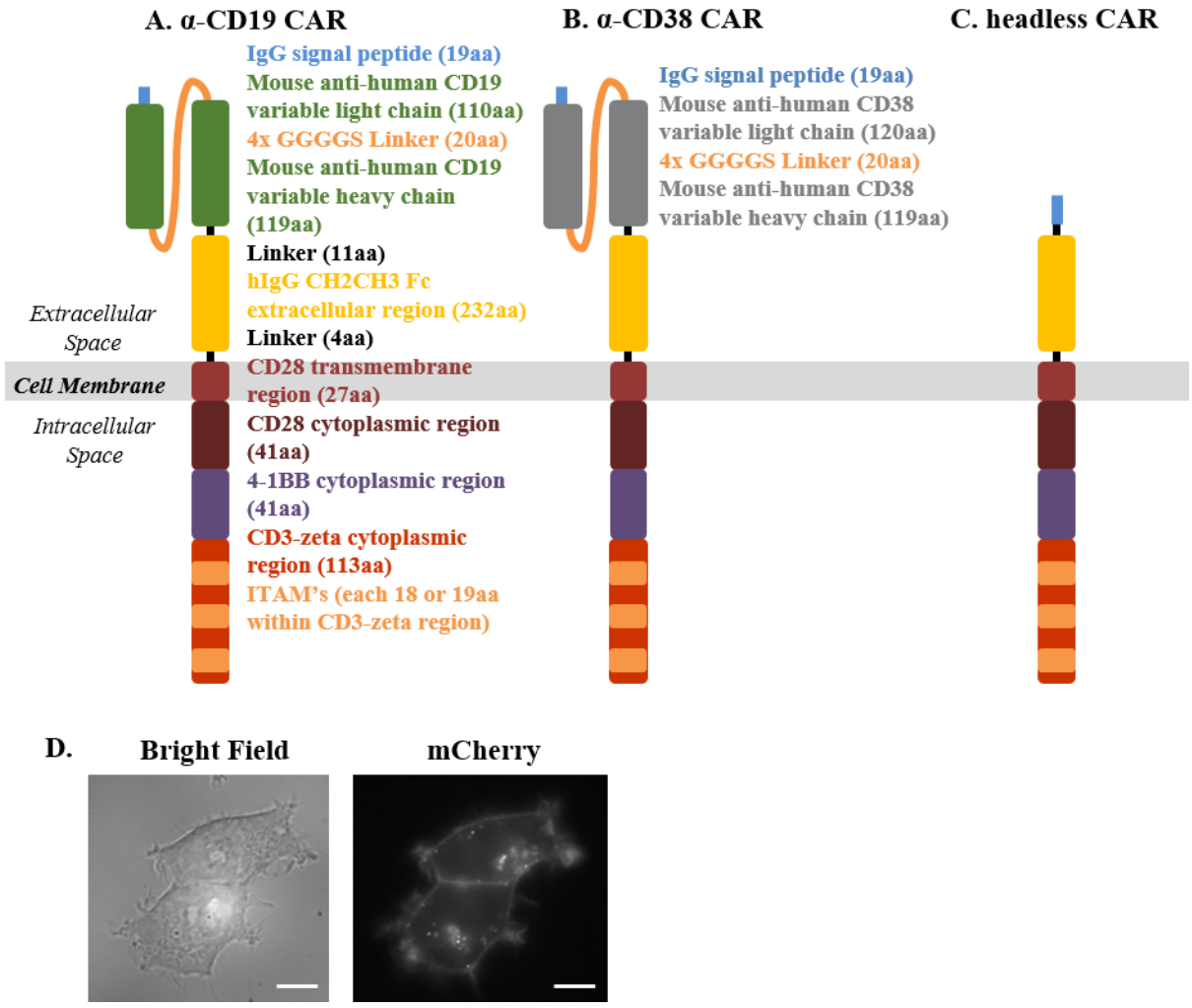

Figure 2.4: A schematic representation of the developed α-CD19, α-CD38, and headless CAR transmembrane proteins. (A) α-CD19 CAR, (B) α-CD38 CAR, and (C) headless CAR proteins with color-corresponding labels that describe each domain and its amino acid size (aa). Redundant labels are omitted. (D) Representative bright field and fluorescence microscope images showing the appropriate membrane localization of mCherry-tagged α-CD19CAR in HEK293T cells. Scale bar = 10μm.

Table 2.1: CARs allow Jurkat T cells to bind to TAA$^+$ Target cells. At a 1:1 live Jurkat to Target cell mixture, Jurkat T cells expressing α-CD19 or α-CD38 CARs both exhibited a higher fraction of cells that were bound to CD19$^+$CD38$^+$ Target cells, an order of magnitude higher than either the dyed or headless CAR$^+$ Jurkat groups that served as non-binding controls, indicating that both α-CD19 or α-CD38 scFv domains are functional. α-CD19 CAR had a higher antigen binding affinity relative to α-CD38 CAR. When equal amounts of DNA coding for α-CD19 and α-CD38 CARs were transfected into Jurkat T cells, the percentage bound to Target cells reflected an average between either CAR alone, indicating α-CD19 and α-CD38 CARs were competing rather than cooperating. Likewise, co-expression of α-CD19 CAR and headless CAR also dampened α-CD19 CAR binding affinity when expressed alone.

Jurkat T Cell Dye or Transfected Construct	Target Toledo Cell Dye (CD19$^+$CD38$^+$)	% of Jurkat T Cells Bound to Target Cells
MitoTracker Dye	CellTracker Dye	1%
Headless CAR-Ypet	CellTracker Dye	4.5%
α-CD19 CAR-Ypet	CellTracker Dye	64.7%
α-CD38 CAR-Ypet	CellTracker Dye	40.9%
α-CD19 CAR-Ypet & α-CD38 CAR-Ypet	CellTracker Dye	54.6%
α-CD19 CAR-Ypet & Headless CAR-Ypet	CellTracker Dye	48.7%

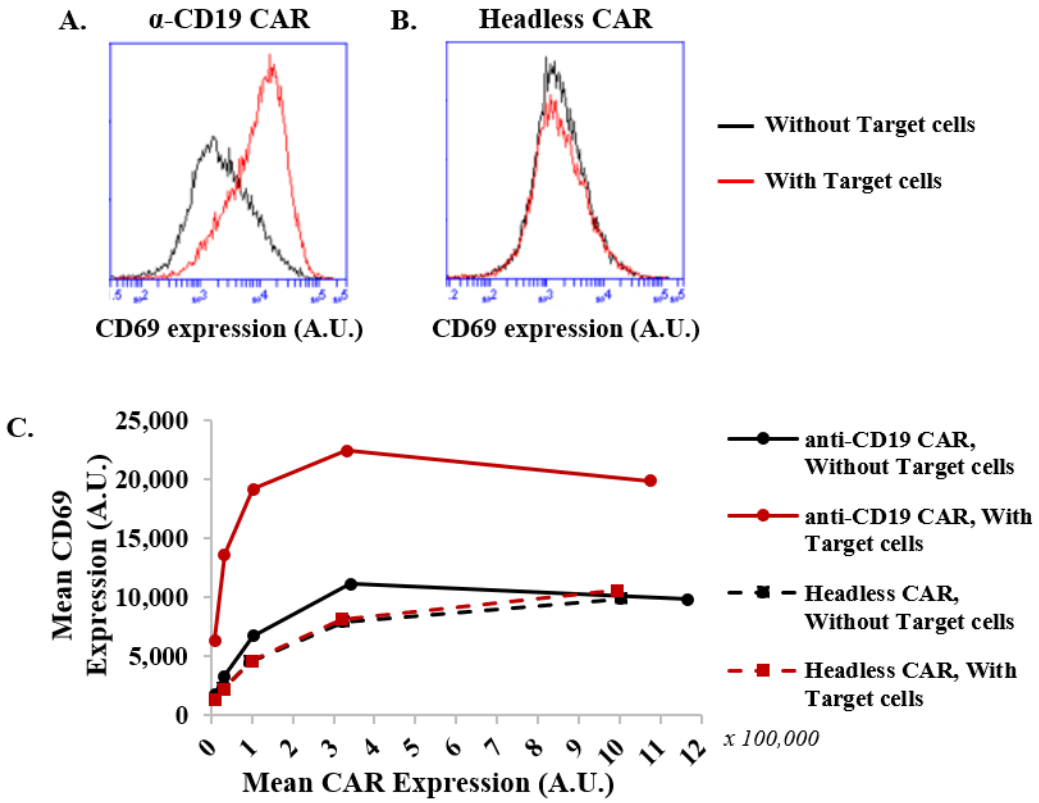

Figure 2.5: Jurkat T cells undergo CAR-mediated T cell activation. Jurkat T cells transiently expressing (A) α-CD19 CAR or (B) headless CAR either were (red) or were not (black) co-cultured with $CD19^+$ Target Toledo cells after which CAR-mediated Jurkat T cell activation is determined by an increase in CD69 expression. Only α-CD19 CAR^+ Jurkat T cells co-cultured with Target cells are activated. Without an scFv binding domain, headless CAR^+ Jurkat T cells remain inactive with or without Target cell co-culture. (C) T cell activation ($CD69^+$) as a function of CAR expression for each plot in (A) and (B). At increasing levels of CAR expression, activation increases logarithmically before plateauing, indicating that high levels of CAR expression alone can trigger T cell activation.

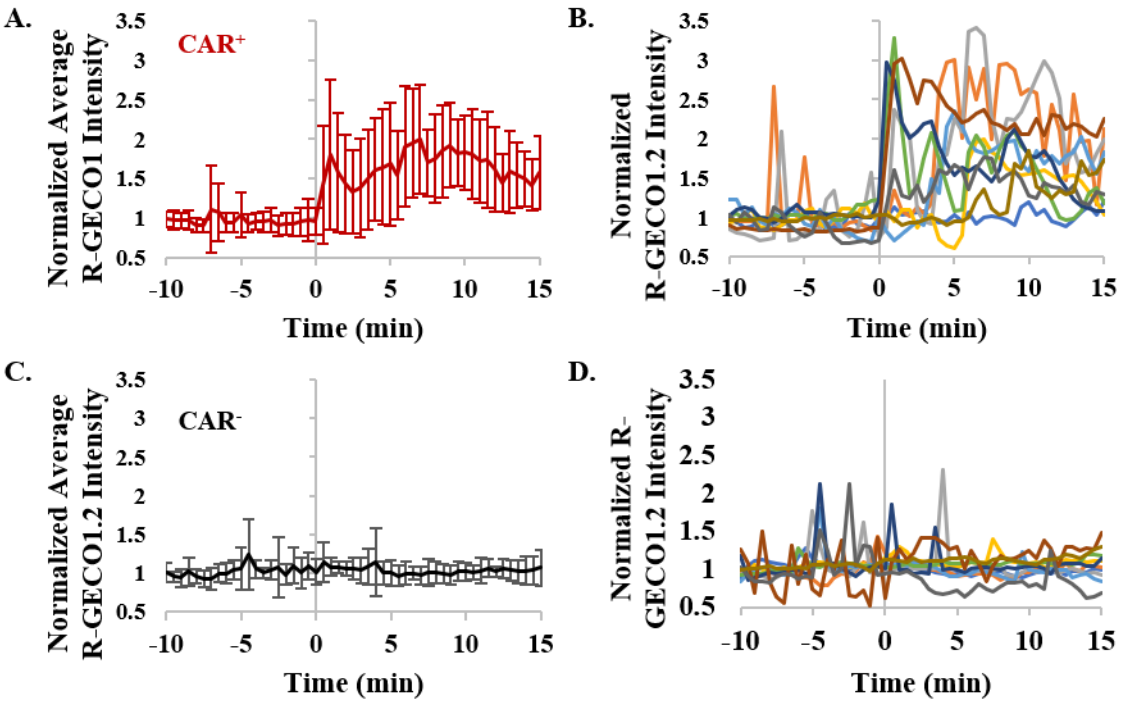

Figure 2.6: Biosensor detection of CAR-mediated T cell activation. (A) On average, R-GECO1.2^{+} α-CD19CAR^{+} Jurkat T cells that bind to CD19^{+} Target cells (t = 0) show elevated concentrations of intracellular calcium ions, an early molecular event in the T cell activation pathway. (B) However, calcium ion response, magnitude, and kinetics vary widely from cell to cell. (C) In contrast, R-GECO1.2^{+} α-CD19CAR^{-} Jurkat T cells within close proximity to CD19^{+} Target cells (t = 0) , showed no significant change in intracellular levels of calcium ions on average, (D) aside from the common spontaneous spikes seen in all Jurkat T cells. n = 10 independently measured cells for each group. Mean ± standard deviation normalized to average baseline R-GECO1.2 fluorescent intensity. Cells imaged every 30s at 100x magnification.

2.4 Supplementary Figures

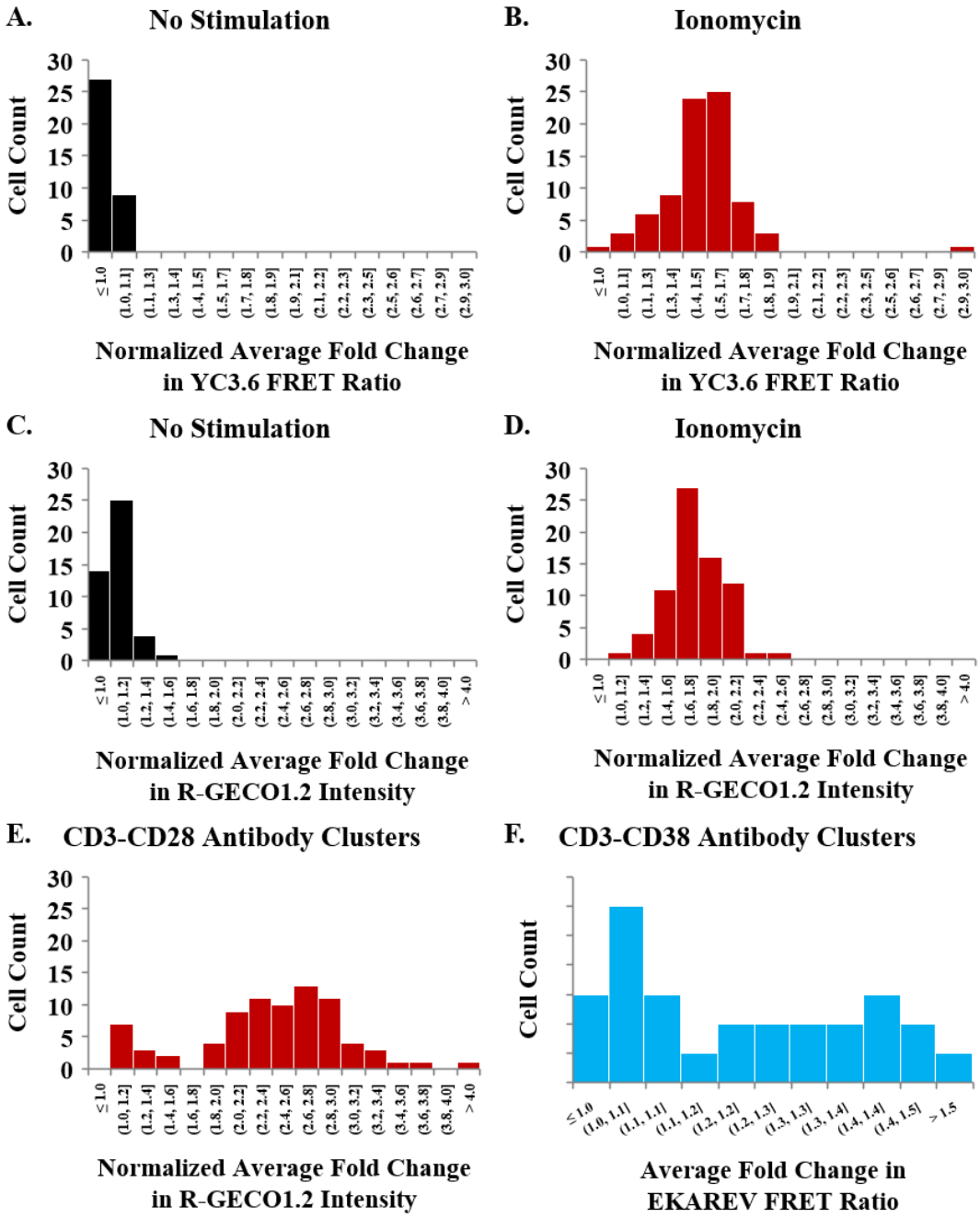

Supplementary Figure S2.1: Fold change in Biosensors before and after stimulation.
YC3.6^{+} Jurkat T cells were (A) not stimulated (n=36) or were stimulated with (B) 1µM ionomycin (n=80). R-GECO1.2^{+} Jurkat T cells were (C) not stimulated or were stimulated with (D) 1µM ionomycin or (E) CD3-CD28 antibody clusters (n=42, 71, 78, respectively). (F) EKAREV^{+} Jurkat T cells were stimulated with CD3-CD28 antibody clusters (n=27). Fold change was calculated by dividing the plateaued normalized average biosensor response after stimulation by the normalized average baseline biosensor response for each cell.

CHAPTER 3:

Optogenetic Transcriptional Regulation of CAR Expression and T Cell Activation

3.1 Introduction

One of the biggest challenges to overcome in CAR T cell therapy is on-target off-tumor toxicity.[8-11] While many TAA candidates have been identified, few have turned out to be truly tumor specific. It is exceedingly difficult to screen all cells in the human body to identify possible tumor specific antigen targets, a challenge further compounded by variability between patients. This has led CAR T cells to attack often vital TAA^+ healthy tissues elsewhere in the body.[12-14] While small molecules and drugs have been used to gain some degree of temporal control over CAR activation,[35] these substrates diffuse throughout the body making spatial regulation difficult. Even approaches targeting two or more unique antigens must be carefully tuned and balanced.[15] I therefore proposed using an external light stimulus to help limit CAR-mediated T cell activation to a specific tumor site within the body.

Many optogenetic tools have been developed to transcriptionally regulate gene expression. I decided to test the new blue light-inducible nuclear translocation and dimerization (LINTAD) system, developed in house by postdoctoral fellow Ziliang Huang (Fig. 3.1A-D). The LINTAD system merges light-inducible transcriptional effectors (LITEs)[70] with the bipartite light-inducible nuclear localization signal (biLINuS2) domain.[71] In the absence of light, LexA-DNA-Binding-Domain-CIB1-biLINuS2 (hereafter referred to as LCB) protein is expressed in the cytosol, whereas its binding partner NLS-CRY2PHR-NLS-VPR (hereafter referred to as CV) is expressed in the nucleus. Upon blue light stimulation, the biLINuS2 domain reveals a nuclear localization sequence (NLS) which drives LCB into the nucleus where blue light further drives

heterodimerization between the CIB1 and CRY2PHR domain of LCB and CV, respectively. This LCB-CV complex localizes to 4xLexAO sites upstream of a minimal promoter (hereafter referred to as P_L) where the VP69-p65-Rta (VPR) domain is positioned to drive transcription of the downstream gene of interest. The light-independent LexA-DNA-Binding-Domain-Stuffer-VPR-mCherry-biLINuS(I539) (hereafter referred to as LVB) protein was used as a positive control for transcriptional activation of P_L.

In order to locally stimulate engineered T cells with blue light at the site of the tumor, the Dual-19-38 genetic reporter construct was designed to constitutively express the myc-tagged α-CD38 Receptor. Upstream of the Receptor's hEF1α promoter, α-CD19v2-CAR-EGFP expression is controlled by the light-inducible promoter P_L (Fig. 3.1F). Note that while the myc-α-CD8 Receptor may also localize T cells to other TAA^+ healthy tissues, this receptor lacks all CAR effector function. It is, however, required that any healthy TAA^+ be spatially separate from the tumor site such that they will be out of range of the targeted blue light stimulation.

3.2 Results and Discussion

3.2.1 New CAR and Receptor Design and Characterization

When splitting costimulatory and activation domains into two transmembrane proteins, each with a unique scFv, it is important to balance the expression level and binding affinity of each.[15] For example, the 19z1 (first generation CAR with only the CD3-zeta activation domain) was shown to alone be capable of triggering some degree of activation in T cells. Inspired by this split CAR system, I further developed a new EGFP-tagged α-CD19v2 CAR (Fig. 3.2A) and a c-myc-tagged α-CD38 Receptor (Fig. 3.2B) based on the split CAR 19z1 and P28BB components.[15]

The new α-CD19v2 CAR-EGFP constructs was smaller, with a CD8α signaling peptide and CD28-based extracellular neck and hinge region supporting an effective medium affinity α-CD19v2 scFv. The α-CD38 Receptor scFv was likewise supported by a codon-diversified CD28 extracellular and transmembrane region, with a truncated (4aa) non-functional intracellular CD28 co-stimulatory domain. A c-myc tag was added after the N-terminal IgG signaling peptide of the α-CD38 Receptor to detect expression and distinguish the Receptor and CAR constructs. As described in Chapter 2, the individual α-CD19v2 CAR-EGFP and myc-α-CD38 Receptor constructs were both tested to confirm antigen-specific binding and CAR-specific T cell activation (Fig. 3.2C). A low-expression-level α-CD19v2-CAR-EGFP^{+} Jurkat T cell line was also developed to determine that the ideal 1:1 co-incubation ratio of CAR T cells to Target cell to trigger activation as determined by CD69 expression (Fig. 3.2D).

Both CAR and Receptor genetic constructs were expressed in the same Dual-19-38 construct to minimize the lentiviruses needed to establish a Jurkat cell line. Receptor protein was constitutively expressed under the hEF1α promoter, while CAR-EGFP expression was controlled by the blue light-inducible promoter. The light inducible CAR CDS was placed upstream of the constitutively expressed Receptor to avoid background levels of CAR expression due to translational readthrough. No polyadenylation (polyA) terminating sequence was included after the CAR CDS to avoid gene recombination during lentivirus production. Additional P_L-driven genetic constructs were also evaluated, including Dual-EGFP-38, in which CAR-EGFP was replaced by EGFP alone, P_L-α-CD19CAR-mNeonGreen, and P_L-mNeonGreen (mNG) (Fig. 3.1).

3.2.2 Blue light transcriptional regulation experiments in HEK293T cells

We first established that the blue light-inducible LINTAD system could drive mNG expression (all HEK293T experiments summarized in Table 3.1). HEK293T cells were transiently transfected with P_L-mNG, LCB and CV constructs and either were (Light) or were not (Dark) stimulated with blue light. In the Light group, we expected to see an increase in both the percentage of mNG^+ cells and in the mean fluorescence intensity (i.e. expression level) of mNG. Indeed, the light-stimulated LINTAD group was able to drive mNG expression in 31.9% of cells at an expression level of 1.43 million (A.U.), compared to 17.5% and 131k in the Dark group. Likewise, with the P_L-19v1-mNG construct, light-stimulated $LINTAD^+$ HEK293T cells drove α-CD19 CAR-mNG expression in 46.3% of cells at a level of 137.8k, compared to 38.5% at 69.4k in the Dark group. Unfortunately, cells showed a significant level of mNG and CAR expression without blue light stimulation, indicating that the light inducible promoter and/or LINTAD itself was not strictly gated by light stimulation.

Next, $LINTAD^+$ HEK293T cells were transfected with the Dual-19-38 construct. While in some cases light stimulation increased the percentage of α-CD19v2 CAR-$EGFP^+$ cells and the CAR expression level, results were inconsistent. Figure 3.3 shows an experiment in which the percentage of light-stimulated α-CD19v2 CAR-$EGFP^+$ cells decreased with light stimulation, but the mean CAR-EGFP expression level increased, as compared to the dark group. As a light-independent positive control, HEK29T cells were transfected with the LVB construct in place of LINTAD. Confirming the function of Dual-19-38, both the percentage of CAR^+ cells (18.4%) and the mean CAR expression level (131.9k) were higher than in $LINTAD^+$ groups. Furthermore, $LINTAD^+$ HEK293T cells transfected with Dual-E-38 expressed at least double the level of EGFP with light stimulation (128k and 145k) than without (51k and 61.5k), although the percentage of $EGFP^+$ cells remained similar.

Taken together, this data suggests that light-inducible gene expression is impeded by both gene length and the design of Dual promoter system. Shorter gene CDSs (i.e. EGFP, 0.7 kb) are naturally transcribed faster than longer gene CDSs (i.e. α-CD19v2 CAR-EGFP, 2.4 kb), resulting in higher levels of overall protein expression. However, in the Dual-19-38 construct, the lack of a polyA terminator sequence after *α-CD19v2 CAR-EGFP* necessitates that RNA polymerase must transcribe *α-CD19v2-CAR-EGFP-*P_{EF1a}*-cmyc-α-CD38-Receptor* (4.7kb) in order to express α-CD19v2-CAR-EGFP protein. Along this line of reasoning, had P_L*-α-CD19v2-CAR-EGFP* been placed downstream of the $P_{EF1\alpha}$*-myc-α-CD38Receptor*, this construct would produce high levels of background CAR expression. Splitting these constructs onto two different vectors may have improved light-inducible CAR expression levels, but prohibitively increases the number of individual constructs needed to be transduced into primary T cells. Ideas for circumventing this issue are further discussed in the Future Directions section, though were not pursued on account of non-light-induced protein expression under the light inducible promoter.

3.2.3 Blue light transcriptional regulation experiments in Jurkat T cells

The LINTAD system was also used to transcriptionally regulate mNG and CAR expression in Jurkat T cells (all Jurkat experiments summarized in Table 3.2). Similar to HEK293T cells, a higher fraction of light-stimulated Jurkat T cells transfected with the P_L*-mNG* and LINTAD *CV* and *LCB* constructs expressed mNG (16.9%) at higher expression levels (200.2k) than non-light-stimulated cells (9.0% at 45.9k, Fig. 3.4B-C). However, even without LINTAD, the leaky P_L*-mNG* construct alone drove mNG expression in 2.3% of cells at a level of 17.6k (Fig. 3.4A). Likewise, light-stimulated Jurkat T cells transfected with the P_L*-19v1-mNG* and LINTAD *CV* and *LCB* constructs also drove higher levels of α-CD19CAR-mNG expression

in a greater fraction of cells compared to the non-light-stimulated counterpart group (Light-induced: 1.45% at 26.6k, Dark: 0.6% at 14.9k). While Jurkat T cells were expected to express protein at lower levels than HEK293T cells, the LINTAD system drove CAR expression in only 1.45% of cells—an unacceptably low efficiency.

Having already experienced difficulty in HEK293T cells, the LINTAD system predictably failed to drive significant α-CD19CAR-EGFP expression from the Dual-19-38 construct in Jurkat T cells. In fact, even the light-independent LVB transcriptional activator drove CAR-EGFP expression in less than 0.5% of cells, and only 1.52% in Jurkat T cells transfected with the shorter Dual-E-38 construct. As discussed for HEK293T cell experiments, the lack of a polyA terminator sequence after *α-CD19v2 CAR-EGFP* in the Dual-19-38 construct also hampered light-induced CAR-EGFP protein expression in Jurkat T cells. Also, Jurkat T cells naturally express transgenes at a lower level than HEK293T cells, which may explain the low percentage of light-induced CAR-EGFP$^+$ Jurkat T cells.

However, we discovered that the greatest differences in α-CD19v2-CAR-EGFP expression level between Light and Dark groups occurred in Jurkat T cells that expressed low levels of Dual-19-38 (Fig. 3.4D). At high levels of Dual-19-38 expression, the CAR-EGFP expression level actually decreased in the light-stimulated cells, until eventually converging with the behavior of non-stimulated cells. Therefore, we created a Jurkat cell line that stably expressed Dual-19-38 at low expression levels. Unfortunately, Dual-19-38$^+$ Jurkat T cells transiently transfected with the LINTAD constructs were only able to drive light-induced α-CD19v2-CAR-EGFP expression in a maximum of 0.45% of cells—too few to detect an increase in CAR-mediated T cell activation (measured with antibody staining against CD69 expression,

data not shown). Therefore, within the tested experimental parameters, the LINTAD system was unable to induce significant CAR-EGFP expression in Dual-19-38^{+} Jurkat T cells.

In searching for methods to improve light-induced CAR-EGFP expression, I stimulated the Dual-19-38^{+} Jurkat T cells with lower intensities of blue light. After 18h of blue light stimulation, cells were directly measured in the flow cytometer to determine the percent of viable cells. Surprisingly, even blue light intensities below 1 mW/cm^2 were highly phototoxic to Jurkat T cells (Fig. 3.4E-H). Such phototoxicity in previous experiments was likely masked by the several washing steps conducted prior to measuring groups of cells via flow cytometry. Nevertheless, lower cell viability in light-stimulated groups introduced an additional variable between Light and Dark groups, making their comparison less reliable.

3.2.4 Future Directions

Considering light-induced CAR expression in primary T cells was my ultimate goal, I concluded that the LINTAD system was ultimately not worth pursuing for several reasons. First, more fragile primary T cells are likely more susceptible to phototoxicity, and are certainly more limited in transgene expression levels. With upwards of four separate constructs to deliver into primary T cells, poor transduction efficiency and high variability in construct delivery between cells would likely render blue light stimulation experiments unrepeatable, if not altogether impossible. Second, the LINTAD system proved to be far too leaky in the non-stimulated state to be trusted for regulating CAR expression. Even low levels of non-stimulated CAR expression would put patients at risk for on-target off-tumor toxicity. Third, light-induced CAR expression was highly inefficient (low percentage of induced cells) and expression levels were far too weak compared to the non-stimulated Dark condition. Although the design of the Dual-19-38 construct

most likely did inhibit CAR-EGFP expression, LINTAD-mediated CAR expression in the P_L-CAR-mNG construct only induced CAR expression in 1.45% of Jurkat T cells.

Having learned from the shortcoming of the LINTAD system, I elected to develop a completely different blue light photoactivatable system that would: 1) avoid phototoxicity by requiring minimal blue light energy for induction, 2) suppress non-light-stimulated background induction using an orthogonal gating system, and 3) produce robust and lasting CAR expression through permanent genetic recombination (see Chapter 4).

Nonetheless, as light-induced transcription systems become more efficient and less leaky without light stimulation, the Dual-19-38 design could benefit from future improvements. First, lentiviral gene delivery of Dual-19-38 construct could be replaced by CRISPR-Cas9-mediated genome insertion, allowing for a polyA terminator to be placed just after *α-CD19v2-EGFP* to shorten transcript size. While one copy of the Dual-19-38 construct would likely be sufficient to drive CAR expression, current low integration efficiency in primary T cells still remains a challenge. Second, the light inducible and constitutive promoters could be designed to drive expression in opposite directions by encoding, for example, $P_{EF1\alpha}$*-myc-α-CD38Receptor* backwards on the antisense strand upstream of P_L*-α-CD19v2-CAR-EGFP* (Fig. 3.5). With the nearby downstream HIV 3'LTR (long terminal repeat) of the pSin transfer vector acting as a terminator, CAR expression levels would significantly improve, though background levels of transcriptional activation by LINTAD would likely still prove challenging. In addition, experiments to confirm sufficient Receptor expression would be necessary since the long antisense transcript (~4 kb) would be terminated by the distant HIV 5'LTR. Third, the size of the CAR construct could be shorted by replacing the EGFP tag with, for example, a FLAG tag, or by replacing it with shorter second-generation CAR containing only one costimulatory domain.

Finally, while CD38 and CD19 blood cancer antigens were used in our proof of principle experiments, eventually the CAR and Receptor should be replaced with versions that recognize antigens on solid tumors.

3.3 Materials and Methods

Genetic Constructs

CV, tBFP-CV, LCB, LCB-mCh, LVB-mCh, Dual-19-38, Dual-E-38, mNeonGreen, and α-CD19 CAR-mNeonGreen genetic constructs were transferred into mammalian expression vectors pcDNA3.1 (+) (Invitrogen), pDN100,[72] or pCAGGS (Addgene #41583), or the self-inactivating second generation pSin (Addgene #16579) lentiviral transfer plasmid. Gibson assembly (New England Biolabs) was used to generate LexA-CIB1-biLINuS constructs using LexA (pDN100[72]), CIB1 (pLITE2.0-CIB1[70]) and biLINuS (pDN92[72]) templates. CRY2-VPR constructs were likewise generated by Gibson assembly of amplified DNA fragments from CRY2 (pLITE2.0-TALE-CRY2PHR-VP64[70, 73]) and VPR (Addgene #63798). Light-inducible reporter constructs were made in or from pDN100[72] and contained mNeonGreen[74] (Allele Biotechnology), or α-CD19 CAR-mNeonGreen (see below). The Dual-19-38 construct was assembled in pSin using Gibson assembly (with P_L from pDN100[72]).

α-CD19v2 CAR-EGFP and myc-α-CD38 Receptor constructs were assembled using Gibson assembly from templates of first-generation α-CD19v2 CAR (19z1) and α-PSMA chimeric costimulatory receptor (P28BB) templates[15] kindly provided by the Sadelain Lab (Memorial Sloan-Kettering Cancer Center, NY). The α-CD38 scFv domain was synthesized (Integrated DNA Technologies), based on US patent application US20100267145A1, with IgG signaling peptide and the linker between variable light and heavy chains was inspired by a third

generation α-CD19 CAR sequence shared with us by Daofeng Liu (Baylor College of Medicine, TX). The α-CD19v2-CAR-EGFP construct consisted of the N-terminal CD8α signaling peptide, α-CD19 scFv, CD28 hinge, transmembrane, and intracellular domain, 4-1BB domain, CD3-zeta domain, and GGSGGT linker, followed by EGFP. The α-CD38-Receptor construct consists of an IgG signaling peptide, c-Myc tag (EQKLISEEDL), α-CD38 scFv, and a codon-diversified CD28 hinge, transmembrane, and truncated (4aa) intracellular domain. CAR and receptor constructs were assembled in pCDNA3.1-CMV and transferred to pSin-EF1α vector via SpeI/SalI restriction enzyme cutting sites. Sanger sequencing was used to confirm all genetic constructs (GeneWiz). See Supplementary File 1 for details.

Cells and Reagents

Human embryonic kidney cells (HEK293T, ATCC CRL-3216), Jurkat T cells (Clone E6-1, ATCC TIB-152), and Toledo B lymphocytes (ATCC CRL-2631) were purchased from ATCC. HEK293T cells were cultured in Dulbecco's modified eagle medium (DMEM) (Gibco #11995065) supplemented with 2 mM L-glutamine, 1 mM sodium pyruvate, 100 units/ml penicillin, 100 μg/ml streptomycin (Gibco #15140122), and 10% (v/v) fetal bovine serum (FBS) (Thermo Fischer Scientific #10438026) in standard tissue-culture-treated dishes or plates. Toledo and Jurkat T cells were cultured in RPMI-1640 medium with L-glutamine, supplemented with 10% (v/v) FBS, 1x penicillin, and streptomycin in non-tissue-culture-treated plates or flasks. Plasmids were introduced into HEK293T cells using Lipofectamine 3000 (Thermo Fisher Scientific #L3000008), or into Jurkat T cells via electroporation at (BioRad Gene Pulser Xcell).

Blue Light Stimulation

Cells were stimulated in a standard humidified 37°C, 5% CO_2 cell culture incubator equipped with a customized blue LED lamp (460 nm, 3 mW/cm^2). Typically, 18 hours after

transfection, cells were split into two groups (Dark and Light), with the Light group exposed to continuous blue light starting 24h after transfection began. Expression was measured via flow cytometry 48h after the start of transfection (unless otherwise specified). For viability experiments, different blue light stimulation intensities were tested by increasing the distance of cells from the light source and by placing cell dishes into a larger secondary dish which limited the light as follows: covered with aluminum foil (0 mW/cm^2), opaque white tape (0.13-0.14 mW/cm^2), tissue paper (0.34-0.35 mW/cm^2), or left uncovered (0.79-0.81 mW/cm^2). After 18h of blue light stimulation, the percentage of viable cells were determined directly by flow cytometry. Light intensity was measured using a power meter (Newport, Model 843-R) before each experiment to ensure the plate wells farthest from the light source were receiving the intended irradiance flux density.

Lentiviral Production

HEK293T cells were used to produce antropic VSV-G pseudotyped lentivirus with a second-generation lentiviral system. Genes of interest were cloned into transfer plasmid pPKm-145 (pSin, Addgene #90505), which was co-transfected into Lenti-X-293T cells with envelope plasmid pCMV-VSV-G (Addgene #8454) and packaging plasmid pCMVΔR8.2 (Addgene #12263) at a 2:1:1 molar ratio using the ProFection Mammalian Transfection System (Promega, Madison, WI #E1200). Viral supernatant was collected and filtered (0.22 micron) 48h after transfection and was used directly to transduce other cells. Transduced cell populations were selected via myc-tag antibody staining using the FACSAria II Sorter at UCSD Human Embryonic Stem Cell Core Facility (La Jolla, CA).

Flow cytometry measurements

Fluorescent and immunostained cells were measured using a BD Accuri C6 flow cytometer equipped with 488 and 640 nm excitation lasers. EGFP and mNG FPs were measured using the 488 nm excitation laser with a 533/30 nm emission filter. Cell labeling antibodies conjugated with far-red dyes were measured using the 640 nm excitation laser with a 675/25 nm emission filter. Before measuring, live cells were trypsinized (if adherent), washed three times with FACS wash buffer (filter-sterilized 0.5% BSA in PBS or autoMACS Running Buffer (Miltenyi Biotec, Germany)), then either measured directly or immunostained for 20 minutes at 37°C, washed thrice, and then measured. Data was analyzed using FlowJo software (TreeStar). Samples of plain HEK293T, Jurkat, and Toledo cells were included with each experiment for gating purposes.

CAR Binding Assay

Jurkat T cells were transfected with either EGFP-tagged α-CD19v2 CAR or α-CD38 Receptor via electroporation (15-20 μg/1x10^7 cells, 4mm cuvette, 250V, 960μF, one pulse, BioRad Gene Pulser Xcell) and allowed to recover for 24h. Immediately before experiments, all target Toledo cells were stained with CellTracker Deep Red (Thermofisher, #C34565). Cells were then counted by hemocytometer and mixed at a 1:1 live Jurkat T cell:Target cell ratio (150,000 cells each) in 1 mL of culture medium. After rotating at 37°C for 45 minutes to allow for mixing and binding, samples were read on the lowest speed of a BD Accuri C6 flow cytometer set to measure MitoTracker (Ex/Em: 490/516), Ypet (Ex/Em: 488/533nm), and Deep Red (Ex/Em: 640/675nm) events. Of the MitoTracker Dye^+ or $Ypet^+$ events, those that were also CellTracker Dye^+ were considered to represent a Jurkat T cell that had bound to at least one Target cell.

CAR-mediated T Cell Activation

Cells were prepared as described in the CAR Binding Assay, except that Target Toledo cells were not dyed and mixtures of cells were co-cultured for 24 hours. Cells were then immunostained with α-CD69 APC-conjugated antibody against early T cell activation marker CD69 BioLegend #310910) and measured via flow cytometry. Gating for $EGFP^+$ or $mNeonGreen^+$ cells, those expressing greater amounts of CD69 were considered to have undergone CAR-mediated T cell activation.

3.4 Figures

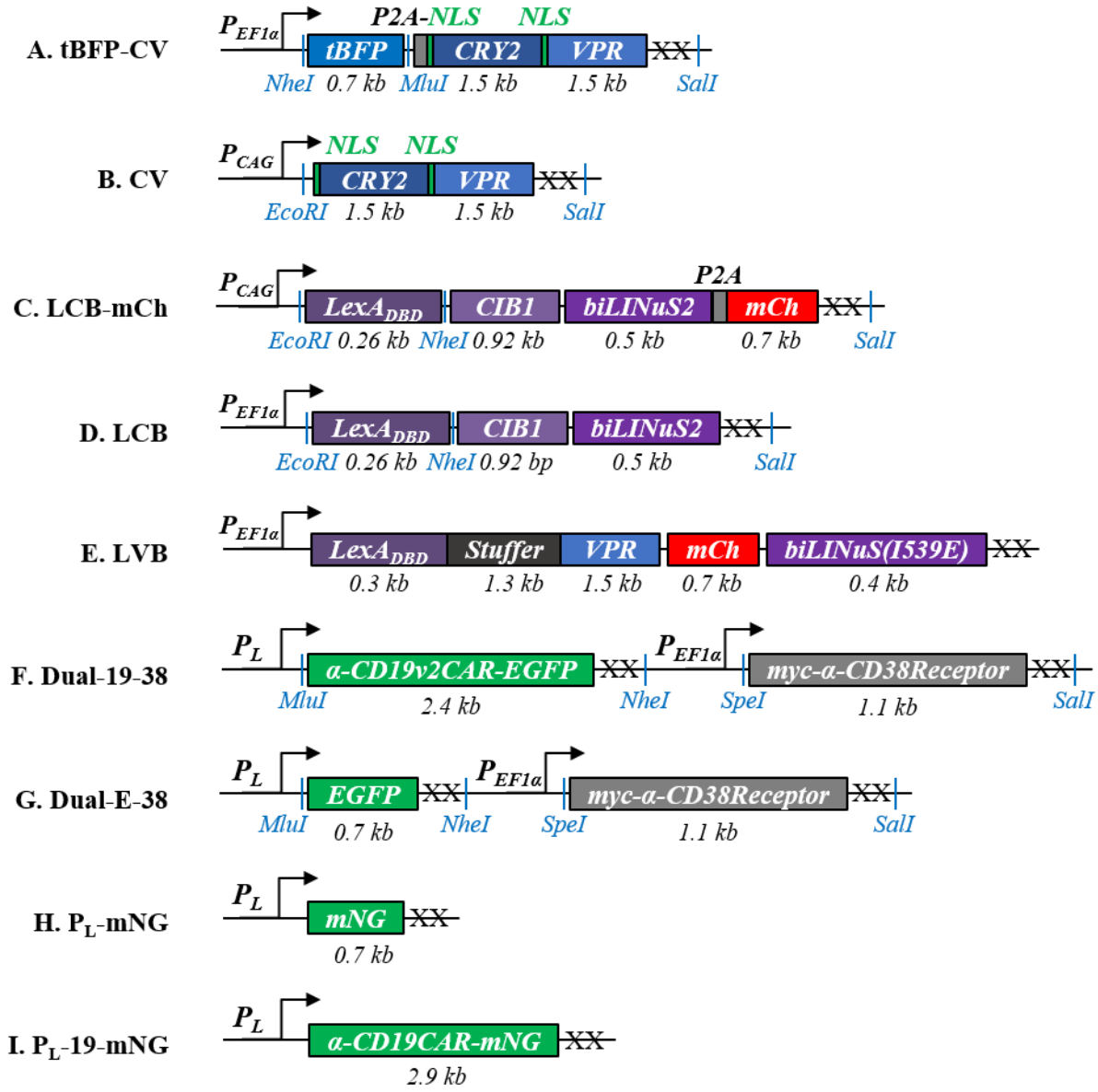

Figure 3.1: Schematic representations of different genetic constructs used in Chapter 3. (A) tBFP-CV: *pCAGGS_tBFP_P2A_NLS_CRY2_NLS_VPR*, (B) CV: *pCAGGS_LexA-DNA-Binding-Domain_Stuffer_VPR_mCherry_BiLINuS(I539E)*, (C) LCB-mCh: *pCAGGS_LexA-DNA-Binding-Domain_CIB1_biLINuS2_P2A_mCherry*, (D) LCB: *pCAGGS_LexA-DNA-Binding-Domain_CIB1_biLINuS2*, (E) LVB-mCh: *pSin_EF1α_LexA-DNA-Binding-Domain_Stuffer_VPR_mCherry_biLINuS(I539E)*, (F) Dual-19-38: *P_L_α-CD19v2CAR_EGFP_PEF1α_myc-α-CD38Receptor*, (G) Dual-E-38: *P_L_EGFP_PEF1α_myc-α-CD38Receptor*, (H) P_L-mNG: *P_L_mNeonGreen*, (I) P_L-19-mNG: *P_L_α-CD19CAR_mNeonGreen*. "XX" symbolizes 2 stop codons. P_L = minimal promoter with 4xLexAO sites.

Figure 3.2: Design and function of α-CD19v2 CAR and myc-α-CD38Receptor transmembrane proteins. A schematic representation of (A) α-CD19v2 CAR and (B) myc-α-CD38 Receptor proteins and their domains. Color-corresponding labels describe each domain and its amino acid size (aa). (C) Histograms of Jurkat T cells expressing α-CD19v2CAR-EGFP that (I) bind to and (II) are activated ($CD69^+$) by $CD19^+$ Target cells. Jurkat T cells expressing myc-α-CD38Receptor (III) bind to, but are (IV) not activated by, $CD38^+$ Target cells. (D) α-CD19v2CAR-$EGFP^+$ Jurkat T cells were co-incubated with $CD19^+$ Target cells at varying ratios, and measured for CAR-mediated T cell activation ($CD69^+$) 24 later. The 1:1 co-incubation ratio was found to maximize the number of activated α-CD19v2CAR-$EGFP^+$ Jurkat T cells. Histograms are scaled as a percentage of the maximum count and are representative of n = 3 independent experiments.

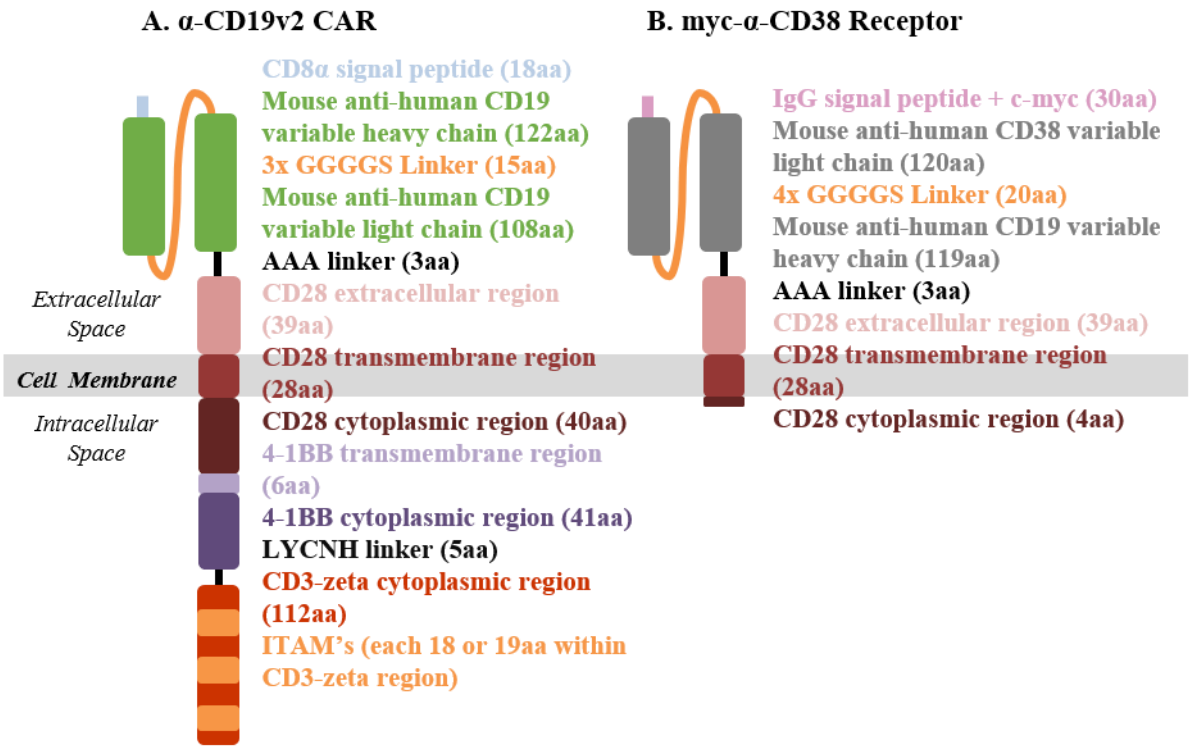
A. α-CD19v2 CAR
B. myc-α-CD38 Receptor
CD8α signal peptide (18aa)
Mouse anti-human CD19 variable heavy chain (122aa)
3x GGGGS Linker (15aa)
Mouse anti-human CD19 variable light chain (108aa)
AAA linker (3aa)
CD28 extracellular region (39aa)
CD28 transmembrane region (28aa)
CD28 cytoplasmic region (40aa)
4-1BB transmembrane region (6aa)
4-1BB cytoplasmic region (41aa)
LYCNH linker (5aa)
CD3-zeta cytoplasmic region (112aa)
ITAM's (each 18 or 19aa within CD3-zeta region)
Extracellular Space
Cell Membrane
Intracellular Space
IgG signal peptide + c-myc (30aa)
Mouse anti-human CD38 variable light chain (120aa)
4x GGGGS Linker (20aa)
Mouse anti-human CD19 variable heavy chain (119aa)
AAA linker (3aa)
CD28 extracellular region (39aa)
CD28 transmembrane region (28aa)
CD28 cytoplasmic region (4aa)

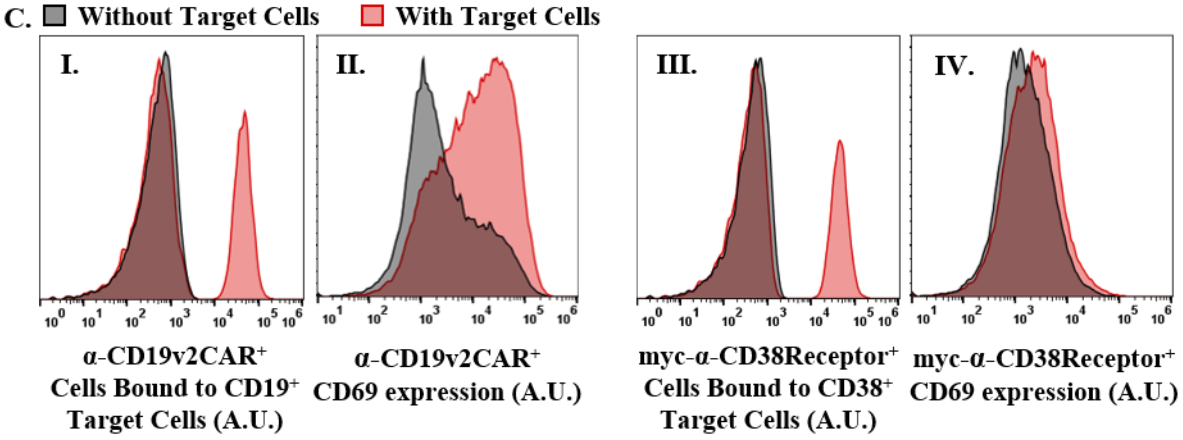
C.
Without Target Cells
With Target Cells
I.
II.
III.
IV.
α-CD19v2CAR+ Cells Bound to CD19+ Target Cells (A.U.)
α-CD19v2CAR+ CD69 expression (A.U.)
myc-α-CD38Receptor+ Cells Bound to CD38+ Target Cells (A.U.)
myc-α-CD38Receptor+ CD69 expression (A.U.)

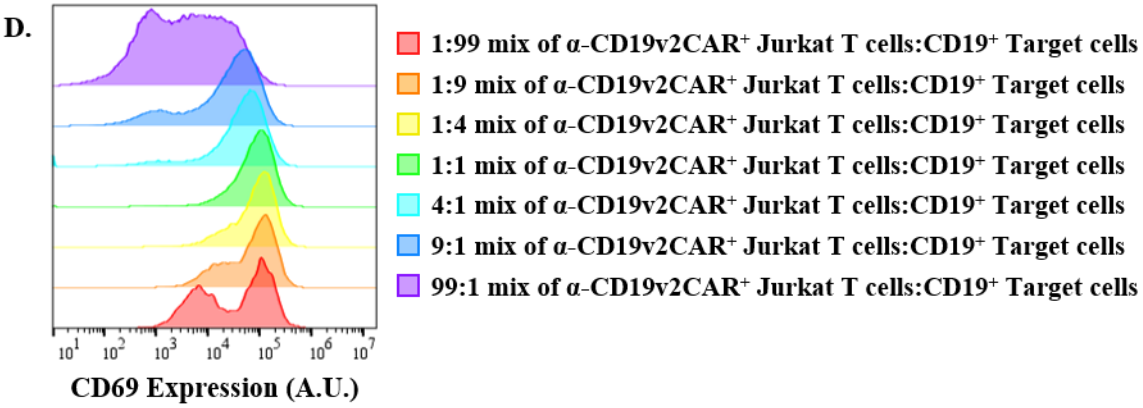
D.
1:99 mix of α-CD19v2CAR+ Jurkat T cells:CD19+ Target cells
1:9 mix of α-CD19v2CAR+ Jurkat T cells:CD19+ Target cells
1:4 mix of α-CD19v2CAR+ Jurkat T cells:CD19+ Target cells
1:1 mix of α-CD19v2CAR+ Jurkat T cells:CD19+ Target cells
4:1 mix of α-CD19v2CAR+ Jurkat T cells:CD19+ Target cells
9:1 mix of α-CD19v2CAR+ Jurkat T cells:CD19+ Target cells
99:1 mix of α-CD19v2CAR+ Jurkat T cells:CD19+ Target cells
CD69 Expression (A.U.)

Table 3.1: Summary of blue light stimulation experiments in HEK293T cells. In experiment 2, n = 2 and 3 for dark and light groups, respectively. t_1 = time after transfection that blue light stimulation began. t_2 = duration of blue light exposure (460nm, 3mW/cm^2, continuous), t_3 = time after transfection when measurements were taken. Plasmid DNA amount (μg) transfected into 200,000 HEK293T cells. Mean ± S.D in arbitrary units. FP = fluorescent protein. P_L = P_{light} = 4xLexAO-minimal promoter. 19v1 = α-CD19v1CAR (Chapter 2). mNG = mNeonGreen. Dual-19-38 = P_L-α-CD19v2-CAR-EGFP-$P_{EF1α}$-myc-α-CD38-Receptor. Dual-E-38 = P_L-EGFP-$P_{EF1α}$-myc-α-CD38-Receptor. LVB = LexA-VPR-mCh-biLINuS2.

Experiment	Reporter Construct (μg)	CV Construct (μg)	LCB Construct (μg)	t_1 (hours)	t_2 (hours)	t_3 (hours)	Dark & **Light** % FP$^+$	**Light** / Dark % FP$^+$	Dark & **Light** FP$^+$ Mean Intensity	**Light** / Dark FP$^+$ Mean Intensity
1	Dual-19-38 (1)	tBFP-CV (0.5)	LCB-mCh (0.5)	24	18	48	10.2% **11.0%**	1.08	26.6k **94.5k**	3.55
2	Dual-19-38 (1)	tBFP-CV (0.75)	LCB-mCh (0.75)	12	12	30	33.7% ± 0.6% **15.2% ± 3.0%**	0.45	66.2k ± 1.7k **57.6 ± 10.6k**	0.87
3	Dual-19-38 (1)	CV (0.5)	LCB (0.5)	24	16	48	9.7% **4.1%**	0.42	50.3k **75.5k**	1.50
4	Dual-19-38 (1)	tBFP-CV (0.5)	LCB-mCh (0.5)	24	18	48	6.4% **4.9%**	0.44	43.3k **84.1k**	1.92
5	Dual-19-38 (1)	CV (0.5)	LCB (0.5)	24	18	48	7.8% **10.3%**	1.32	42.7k **71.9k**	1.69
6	Dual-19-38 (0.5)	CV (0.5)	LCB (0.5)	24	18	48	17.5% **12.2%**	0.70	60.1k **46.5k**	0.77
7	Dual-19-38 (0.5)	tBFP-CV (0.5)	LCB-mCh (0.5)	24	18	48	17.8% **14.7%**	0.83	65.3k **47.8k**	0.73
8	Dual-19-E (0.5)	CV (0.5)	LCB (0.5)	24	18	48	16.9% **13.9%**	0.82	51.0k **128k**	2.51
9	Dual-19-E (0.5)	tBFP-CV (0.5)	LCB-mCh (0.5)	24	18	48	15.6% **16.3%**	1.04	61.5k **145.1k**	2.36
10	P_L-19v1-mNG (0.5)	tBFP-CV (0.5)	LCB-mCh (0.5)	24	18	48	38.5% **46.3%**	1.20	69.4k **137.8k**	1.99
11	P_L-mNG (0.5)	CV (0.5)	LCB (0.5)	24	18	48	17.5% **31.9%**	1.82	131.0k **1.43M**	10.95
12	P_L-mNG (0.5)	LVB (0.5)		-	-	24	28.9%	-	2.46M	-
13	Dual-19-38 (0.5)	LVB (0.5)		-	-	24	18.4%	-	131.9k	-

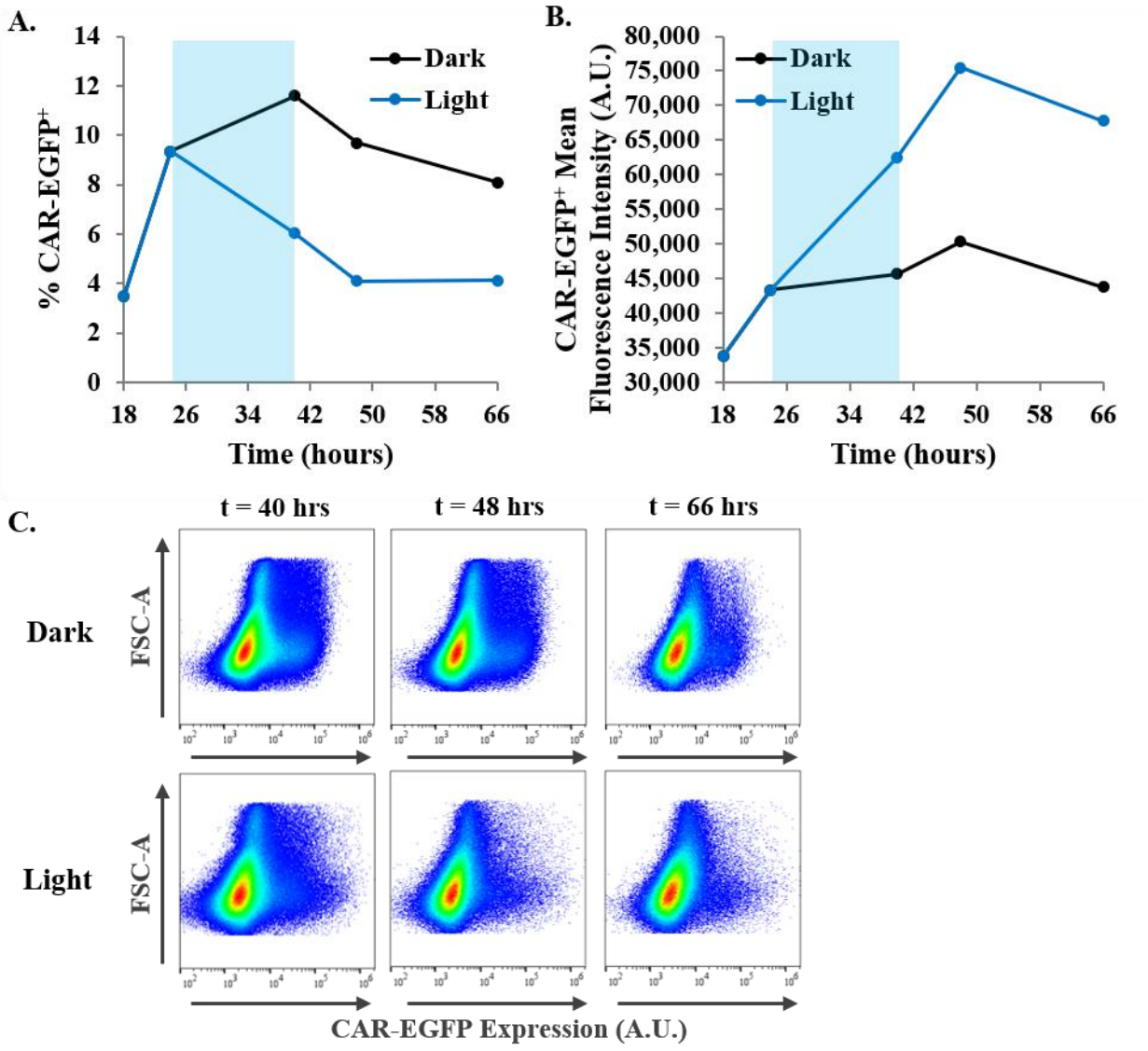

Figure 3.3: Figure 3.3: Blue light stimulation and LINTAD-driven α-CD19v2-CAR-EGFP expression from Dual-19-38 over time in HEK293T cells. HEK293T cells transiently expressing Dual-19-38 and LINTAD either are (Light) or are not (Dark) exposed to 16h continuous 3 mW/cm^2 blue light (460nm). (A) Compared to the Dark group, a lower percentage of CAR-EGFP$^+$ cells were present after light exposure, yet (B) the average expression level of CAR-EGFP$^+$ cells increased. (C) Forward scatter plots of CAR-EGFP expression (EGFP) at timepoints t = 40, 48, 66 hrs. The blue shaded box on plots A and B indicate when blue light exposure took place (t = 24h - 40h) and transfection began at t = 0. Plots are from a single experiment, but representative of trends observed across several experiments.

Table 3.2: Summary of Blue Light Stimulation experiments in Jurkat T cells. t_1 = time after transfection that blue light stimulation began. t_2 = duration of blue light exposure (473nm, 3mW/cm^2, continuous), t_3 = time after transfection when measurements were taken. FP = fluorescent protein. Plasmid DNA amount (μg) electroporated into 10M Jurkat T cells. If no amount is given, the construct has been stably integrated into the genome. Mean ± S.D. FP = fluorescent protein. Mean intensity in arbitrary units. Dual-19-38 = P_L-α-CD19v2CAR-EGFP-$P_{EF1α}$-myc-α-CD38-Receptor, Dual-E-38: P_L-EGFP-$P_{EF1α}$-myc-α-CD38-Receptor. P_L = P_{light} = 4xLexAO-minimal promoter. 19v1 = α-CD19v1CAR. mNG = mNeonGreen. LVB = LexA-VPR-mCh-biLINuS2.

Exper-iment	Reporter Construct (μg)	CV Construct (μg)	LCB Construct (μg)	t_1 (hours)	t_2 (hours)	t_3 (hours)	Dark & **Light** % FP$^+$	Dark & **Light** FP$^+$ Mean Intensity	**Light** / Dark % FP$^+$	**Light** / Dark FP$^+$ Mean Intensity
1	Dual-19-38 (5)	tBFP-CV (5)	LCB-mCh (5)	12	12	30	2.0% **1.3%**	0.65	12.5k **15.3k**	1.23
2	Dual-19-38 (10)	tBFP-CV (5)	LCB (5)	24	12	45	0.7% **0.7%**	1.00	11.9k **15.5k**	1.30
3	Dual-19-38 (5)	CV (5)	LCB (5)	12	12	24	2.5% **2.2%**	0.88	11.0k **9.5k**	0.86
4	Dual-19-38	CV (2.5)	LCB (2.5)	6	18	24	0.03% **0.06%**	2.00	8.3k **7.0k**	0.84
4	same experiment as above					30	0.03% **0.13%**	4.33	7.6k **6.3k**	0.83
5	Dual-19-38	CV (5)	LCB (5)	6	18	24	0.2% **0.35%**	1.75	8.9k **8.4k**	0.94
5	same experiment as above					30	0.14% **0.45%**	3.21	8.3k **7.1k**	0.86
6	Dual-19-38	tBFP-CV (5)	LCB-mCh (5)	24	12	48	0.07% **0.08%**	1.14	9.7k **8.4k**	0.87
7	Dual-E-38 (5)	tBFP-CV (5)	LCB-mCh (5)	24	12	48	0.14% **0.16%**	1.14	10.3k **20.8k**	2.02
8	P_L-19v1-mNG (5)	tBFP-CV (5)	LCB-mCh (5)	24	18	48	0.6% **1.45%**	2.42	14.9k **26.6k**	1.79
9	P_L-mNG (5)	CV (5)	LCB (5)	24	18	48	9.0% **16.9%**	1.88	49.5k **200.2k**	4.04
10	Dual-19-38	LVB (5)		-	-	20	0.49%	-	7.6k	-
11	Dual-E-38 (5)	LVB (5)		-	-	20	1.52%	-	48.8k	-

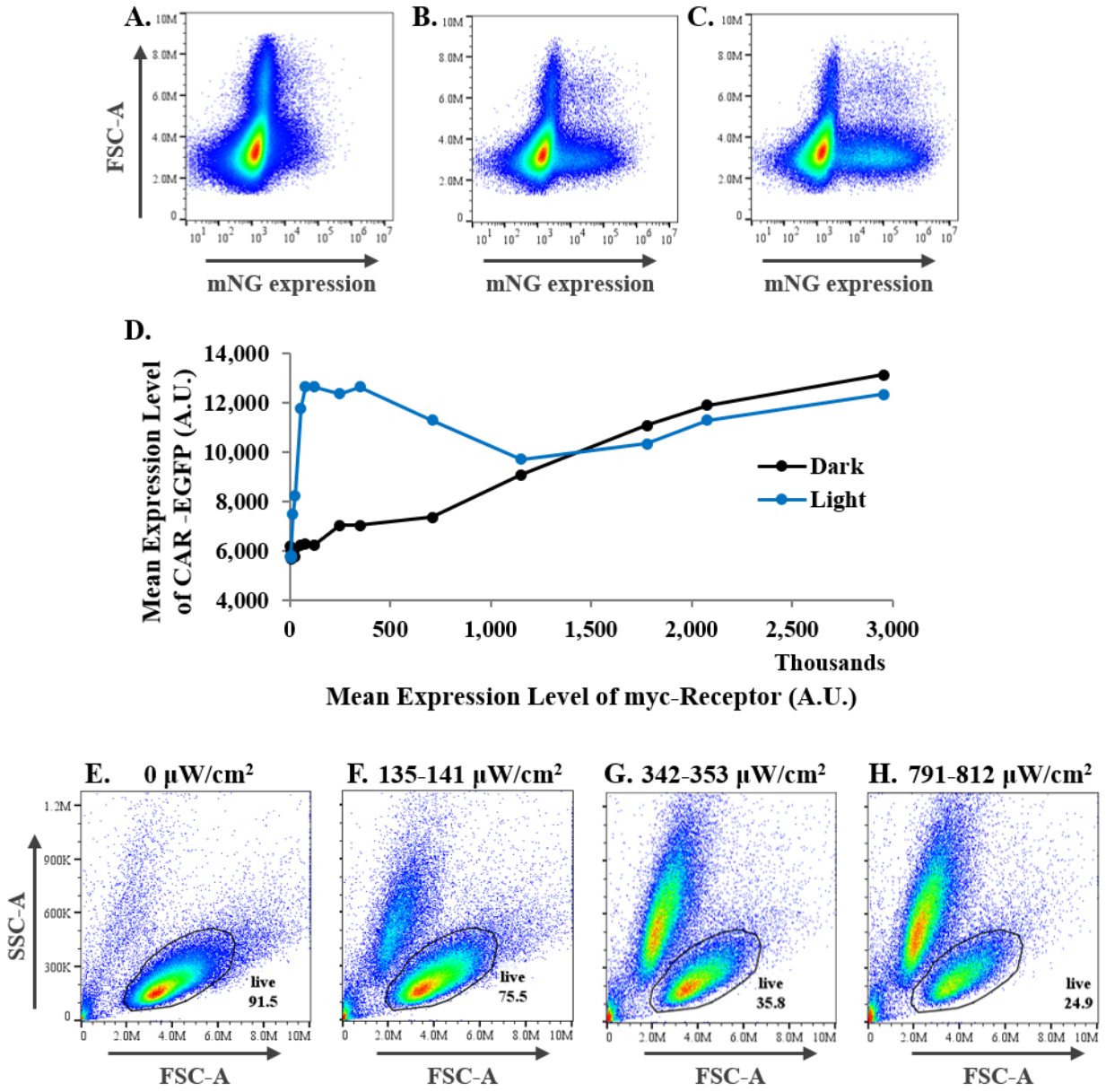

Figure 3.4: Blue light experiments in Jurkat T cells. Jurkat T cells transiently transfected with the (A) P_L-*mNG* construct alone or with (B-C) LINTAD constructs *CV* and *LCB* either were (A,C) or were not (B) exposed to 18h of blue light (460nm, 3 mW/cm^2) 24h post-transfection. Jurkat T cell mNG protein expression was evaluated via flow cytometry 48h post-transfection. The percentage of mNG$^+$ Jurkat T cells and average mNG expression levels were as follows: (A) 2.3% and 17.6, (B) 9.0% and 45.9k, (C) 16.9% and 200.2k. (D) Representative plot (Table 3.2, Experiment 2) showing that the LINTAD system produced the greatest difference in CAR-EGFP expression level between light-stimulated (Light) and non-stimulated (Dark) when the Dual-19-38 construct was expressed at low levels (as measured by myc-Receptor expression). (E-H) Dual-19-38$^+$ Jurkat T cells were exposed to 460 nm blue light for 18h, after which they were directly measured via flow cytometry. The live cell population gate in forward and side scatter plots measures the percentage of viable cells for each different exposure intensity ranges: (E) 91.5% at 0 µW/cm^2, (F) 75.5% at 135-141 µW/cm^2, (G) 35.8% at 342-353 µW/cm^2, and (H) 24.9% at 791-812 µW/cm^2.

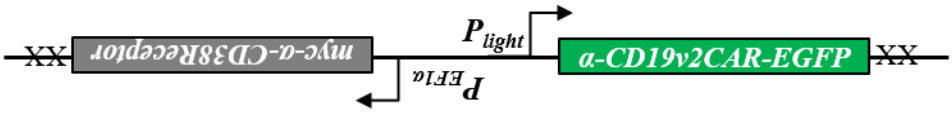

Figure 3.5: Future improvements to the Dual-19-38 construct. The Dual-19-38 construct was designed to omit highly repetitive polyA terminator sequences that can cause undesirable recombination during lentiviral gene transfer.[68] However, this design significantly impeded light-inducible CAR expression due, in part, to the long transcript size necessary for translation. By encoding $P_{EF1\alpha}$*-myc-α-CD38Receptor* on the antisense DNA strand upstream of P_L*-α-CD19v2-CAR-EGFP*, light-induced CAR expression levels should improve without interference or transcriptional readthrough from $P_{EF1\alpha}$*-myc-α-CD38Receptor*. XX = 2 stop codons.

CHAPTER 4:

A logic-gated drug and photoactivatable Cre-loxp system for spatiotemporal control of cell-based therapeutics

4.1 Introduction

Although synthetic biologists have developed a variety of genetically-encoded Boolean logic gates to allowed CAR T cells to interpreting more complex signals *in vivo*, finding a perfectly unique combination of antigens for a particular patient is currently difficult, especially considering heterogeneity between patients. However, when cancerous and healthy tissues both expressing target antigen(s) are spatially distinct *in vivo*, an external stimulus with high spatiotemporal control can limit CAR T cell activity to the tumor site. Light is an ideal stimulus in that it can be quickly and reversibly applied with unparalleled control over the dosage, duration, and location of stimulation. This spatial confinement also narrows the search area for identifying a set of tumor-specific antigens. Therefore, CAR T cells equipped with optogenetic logic gates have the potential to limit CAR T cell activation to the tumor site, thus protecting healthy tissues elsewhere in the body from on-target off-tumor toxicity (Fig. 4.1, Table 4.1).

In this Chapter, I introduce a new robust optogenetic split-Cre system called TamPA-Cre which is gated by the drug **tam**oxifen and utilizes the blue light **p**hoto**a**ctivatable Magnet dimerizing pair, nMag-pMag, to strictly regulate CAR expression with high spatiotemporal resolution. By gating CAR expression with both tamoxifen and blue light, the TamPA-Cre system exhibits significantly suppressed background Cre-loxP recombinase activity compared to the blue-light-gated PA-Cre system.[48] Furthermore, the TamPA-Cre system is just as sensitive to low intensity, short-duration blue light exposure as the PA-Cre system and is also compatible with the mutant loxP sites lox66 and lox71. We use human embryonic kidney (HEK) 293T cells

to optimize tamoxifen- and blue light stimulation protocols, and to show that TamPA-Cre can efficiently alter gene expression through Cre-loxP recombination. In Jurkat T cells, we show that CAR expression is highly dependent on cells receiving both tamoxifen- and blue light stimulation, and that TamPA-Cre drives CAR-mediated T cell activation against antigen$^+$ target cells. Additionally, we demonstrate that our photoactivatable Cre system is more practical to work with than the PA-Cre system in shared laboratory and clinical settings where it is difficult to eliminate all sources of blue light. Finally, we integrated approaches that improve tumor site specificity via multi-antigen recognition with our drug-and-light-inducible system to allow for high spatiotemporal control of T cell activation. TamPA-Cre can thus be helpful in locally regulating CAR expression in T cells that might otherwise cause on-target off-tumor toxicity in healthy tissues elsewhere in the body.

4.2 Results and Discussion

4.2.1 Testing Photoactivatable Split-Cre Systems

Before deciding which genetically encoded photo-sensitive proteins to use in our own system, we tested the two most recently developed blue light photoactivatable split-Cre systems. The first, PA-Cre 2.0, relies on the blue-light-driven heterodimerization between CIB1 and CRY2(L348F) domains (*Arabidopsis thaliano*, heterodimer half-life: 24 minutes) to reconstruct functional Cre recombinase from the split CreN(19-104) and CreC(106-343) components.[49] PA-Cre was the second system tested. It utilizes the *Neurospora Crassa*-derived Vivid photoreceptor mutant heterodimers negative Magnet (nMag) and positive Magnet (pMag) to reconstitute its split CreN(19-59) and CreC(60-343) components into functional Cre with blue light (heterodimer half-life: 1.8h).[48] To compare these two systems (Fig. 4.2), we developed a

puromycin-selected HEK293T cell line that stably expresses the deletion-based Cre-loxP EGFP Reporter construct (Fig. 4.3A), as well as a novel controllable blue light stimulation apparatus (Fig. 4.4).

EGFP Reporter HEK293T cells were transiently transfected with either PA-Cre2.0, PA-Cre, or Cre constructs. After 24 hours, these groups either were (Light) or were not (Dark) exposed to blue light stimulation (30 W/m^2, continuous, 30s). 24 hours after blue light stimulation, cells were measured for EGFP expression via flow cytometry. In PA-Cre2.0 and PA-Cre groups, the percentage of Cre-loxP recombined ($EGFP^+$) cells were normalized to that of corresponding Cre groups (Fig. 4.3B). Cells in both Light PA-Cre2.0 and PA-Cre groups exhibited more Cre-loxP recombination compared to their respective Dark counterparts (2.1- and 3.4-fold increases, respectively), indicating that both systems were responding as expected to blue light stimulation. The Light PA-Cre group exhibited robust levels of Cre-loxP recombination (0.92 ± 0.09), whereas the Light PA-Cre2.0 group showed only a fraction of that (0.12 ± 0.02). While different blue light intensities and patterns of exposure may have improved Cre-loxP recombination levels in the Light PA-Cre2.0 group, we highly prioritized robust recombination efficiency driven by minimal blue light energy. Furthermore, we anticipated that the recombination efficiency of any system may be further impeded by lower levels of protein expression in primary human T cells used for future therapeutic CAR T cell applications. Therefore, we decided to pursue the sensitive, efficient, and robust nMag-CreN59 and pMag-CreC60 heterodimerizing domains of the PA-Cre system.

Despite robust recombination efficiency in the Light PA-Cre group, the Dark PA-Cre group suffered from high background levels of spontaneous Cre-loxP recombination (0.27 ± 0.02), which was found to be proportional to PA-Cre protein expression levels (Fig. 4.5A).

Furthermore, while testing the PA-Cre system in EGFP Reporter HEK293T cells using a pulsatile blue light protocol (15 W/m^2, pulsatile: [1s on, 59s off], 24h), we found it necessary to actively protect non-blue light-stimulated cells from all light using aluminum foil (Dark PA-Cre group, 0.204 ± 0.024). Otherwise, an additional small but significant percentage of cells underwent Cre-loxP recombination (Ambient PA-Cre group, 0.289 ± 0.048), presumably driven by incidental exposure to the laboratory's ambient white room lighting (0.34-0.78 W/m^2) while in the incubator (Fig. 4.3C). While this increase was not always statistically significant across all experiments (due to the inherently variable nature of ambient light exposure), these results nonetheless indicated that the highly photo-sensitive PA-Cre system was susceptible to additional Cre-loxP recombination unless precautions are taken to filter out all sources of blue light. Considering higher percentages of recombined cells would later translate into premature CAR expression in engineered T cells, it was essential for us to develop an easier to handle photoactivatable split-Cre system that minimized background Cre-loxP recombination without sacrificing the robust recombination efficiency of the PA-Cre system.

4.2.2 Testing Cre-ERT2 Systems

We focused on suppressing background Cre-loxP recombination in non-stimulated cells by spatially segregating the PA-Cre heterodimers within the cell. Both CreN-nMag-NLS and NLS-pMag-CreC are necessary and sufficient to drive Cre-loxp recombination (Fig. 4.5B). In separating these proteins, so we hoped to prevent spontaneous heterodimerization and thus background Cre recombinase activity within the nucleus. Although this could be achieved in a number of ways (e.g. using the *As*LOV2-based blue light-inducible nuclear localization signal system),[71] it was preferable to find an orthogonally-inducible, well-gated, robust system

compatible with use *in vivo*. The US Food and Drug Administration-approved drug tamoxifen and its active metabolites have been widely used to induce nuclear translocation of proteins (including Cre) which are fused to the T2 mutant Estrogen Receptor ligand binding domain (ERT2)[50-52]. These tamoxifen-inducible Cre systems are widely used in transgenic mouse models to conditionally induce genomic changes *in vivo*.[75] However, tamoxifen and its active metabolites are also photosensitive.[42]

Therefore, we tested whether or not blue light stimulation would affect the tamoxifen-induced Cre recombinase activity of the tightly-gated ERT2-Cre-ERT2 system (Fig. 4.3D).[76] Using the same light stimulation protocol as in Figure 4.3C, we found that EGFP Reporter HEK293T cells transiently expressing ERT2-Cre-ERT2 showed no significant difference in the percentage of cells that had undergone Cre-loxP recombination between Dark, Ambient, or Light groups. Without stimulation with 4-hydroxytamoxifen (500nM, 4-OHT), ERT2-Cre-ERT2 groups exhibited low amounts of background Cre-loxP recombination (Dark: 0.061 ± 0.004, Ambient: 0.065 ± 0.007, Light: 0.0646 ± 0.008). With 4-OHT stimulation, all ERT2-Cre-ERT2 groups similarly showed a robust, significant increase in Cre-loxP recombination (Dark: 1.27 ± 0.156, Ambient: 1.32 ± 0.124, Light: 1.16 ± 0.090).

Reassured that 4-OHT stimulation was not significantly impacted by relevant levels of blue light stimulation, we further investigated tamoxifen-induced nuclear translocation dynamics of the ERT2-mCherry fusion protein (Fig. 4.2F) in HEK293T cells. Using time-lapse fluorescence microscopy, we discovered that nuclear translocation driven by 4-OHT (500nM) occurred on the order of hours. ERT2-mCherry protein was only clearly nuclear-localized (with a nuclear-to-cytosolic ratio of mean fluorescence intensity of at least 2) after approximately three hours (Fig. 4.3E), after which blue light stimulation would be more effective.

4.2.3 Design and Function of TamPA-Cre

We integrated both Tamoxifen-ERT2 and Photoactivatable-Cre systems to create a genetically-encoded AND-gate which requires both tamoxifen- and blue light stimulation to drive Cre-loxP recombination (Fig. 4.6A). In our system, called TamPA-Cre, we chose to fuse *ERT2* to the smaller *CreN59-nMag* rather than to *pMag-CreC60* to avoid potentially competitive native nuclear localization sequences (NLS) in CreC60. The PA-Cre system's heterodimers were designed to be expressed at relatively equal levels, with both proteins translated from a single transcript and separated by the P2A self-cleaving peptide. The TamPA-Cre system was similarly designed using two tandem repeats of P2A to improve protein cleavage. The *ERT2-CreN(2-59)* sequence from *ERT2-Cre-ERT2* was fused to the N-terminus of *nMag* (without *NLS*), and fluorescent marker *P2A-mCherry* was added to the C-terminus of *NLS-pMag-CreC60* to confirm expression. Our design also includes a codon-diversified *pMag* coding sequence (CDS) to prevent potential recombination introduced by lentiviral gene transfer between the nearly identical *nMag* and *pMag* sequences (Fig. 4.7).[68] However, although this construct worked well for transient expression, its large single transcript size significantly impeded lentivirus production efficiency. We therefore separated *ERT2-CreN-nMag* and *NLS-pMag-CreC* into separate vectors, each with a unique fluorescent marker. An added benefit of fusing the ERT2 domain to CreN rather than CreC was that it balanced the size of both *ERT2-CreN-nMag* and *NLS-nMag-CreC* (approximately 1.6 and 1.4kb, respectively), resulting in similar protein expression levels and comparable efficiency in lentivirus production (data not shown). We also created *ERT2-CreN-nMagHigh1*, which expresses the mutated nMag variant nMagHigh1 (M135I/M165I), previously shown to improve light-induced heterodimerization with pMag.[77] Along with *NLS-pMag-CreC*, this system is referred to as TamPA-Cre-nH1 (Fig. 4.2I).

The mechanism of TamPA-Cre activation is illustrated in Figure 4.6B. In the absence of tamoxifen- or blue light stimulation, TamPA-Cre is inactive with ERT2-CreN-nMag and NLS-pMag-CreC proteins spatially segregated to the cytosol and nucleus, respectively. This physical separation is intended to prevent spontaneous, concentration-dependent nMag-pMag dimerization and subsequent background Cre-loxP recombination, as seen in the PA-Cre system (Fig. 4.5B). Unlike PA-Cre, inactive TamPA-Cre is designed to be invulnerable to light stimulation, meaning cells expressing TamPA-Cre are not at risk of undergoing premature Cre-loxP recombination driven by, for example, the ambient white fluorescent lighting found in a typical lab or clinical environment. Before Cre-loxP recombination can occur, TamPA-Cre must first be primed by 4-OHT, which binds to ERT2-CreN-nMag and drives nuclear translocation. At this point, TamPA-Cre is again vulnerable to spontaneous nMag-pMag dimerization until 4-OHT is removed or degraded and ERT2-CreN-nMag returns to the cytosol. However, with both ERT2-CreN-nMag and NLS-pMag-CreC inside the nucleus, primed TamPA-Cre can be activated by blue light stimulation. Active TamPA-Cre has undergone blue light-induced dimerization of nMag-pMag, bringing CreN and CreC protein halves together to reconstitute Cre recombinase activity.

4.2.4 Optimizing tamoxifen and blue light stimulation

We tested the TamPA-Cre system in EGFP Reporter HEK293T cells with a variety of tamoxifen- and blue light stimulation protocols to optimize Cre-loxP recombination. Two parameters were found to be particularly important: the blue light stimulation pattern (pulsatile versus continuous), and the time at which light was started relative to 4-OHT addition. Figure 4.3C illustrates two such protocols, each calling for a total three hours of 5 W/m^2 blue light

stimulation, delivered either continuously with concurrent 4-OHT addition (Protocol A), or in a pulsatile pattern started three hours after 4-OHT addition (Protocol B).

Under Protocol A, TamPA-Cre drives only minor blue light-induced recombination (0.17 ± 0.01) compared to its cognate group without tamoxifen (0.14 ± 0.02). Considering tamoxifen-induced ERT2-mCh nuclear localization in HEK293T takes approximately three hours (Fig. 4.3E), during this time, there is likely little primed TamPA-Cre in the nucleus to activate with blue light. Indeed, delaying light stimulation by eight hours after 4-OHT addition improved the levels of Cre-loxP recombination (0.246 ± 0.051) (Fig. 4.8A). However, we also found that a 24-hour pulsatile blue light protocol (started concurrently with tamoxifen stimulation) also similarly improved TamPA-Cre-driven recombination levels (0.254 ± 0.035), despite providing cells with less than half of Protocol A's total blue light energy. (Fig. 4.8B) Assuming NLS-pMag-CreC heterodimerized with either CreN-nMag-NLS or ERT2-CreN-nMag proteins dissociate similarly after blue light stimulation is removed (exponential decay, half-life: 1.8h),[77] less than 1% of those dimers will have dissociated during the 59s of darkness between blue light pulses (Fig. 4.9). Essentially, this pulsatile blue light stimulation is sufficient to sustain a nearly maximal level of active TamPA-Cre in tamoxifen-treated EGFP Reporter HEK293T cells over 24 hours.

By providing 24-hours of pulsatile blue light stimulation (7.5s on, 52.5s off) started three hours post-tamoxifen stimulation (Protocol B), TamPA-Cre drove robust Cre-loxP recombination (0.80 ± 0.10) in EGFP Reporter HEK29T cells, on par with PA-Cre (0.85 ± 0.03) (Fig. 4.8C). Without blue light stimulation, cells in the Dark and Ambient PA-Cre groups still exhibited significant background Cre-loxP recombination (0.36 ± 0.08, 0.46 ± 0.07, respectively). However, even in tamoxifen-primed TamPA-Cre groups, cells in Dark and Ambient groups exhibited significantly suppressed levels of background Cre-loxP recombination

(both 0.10 ± 0.03). Furthermore, this low background is maintained in TamPA-Cre groups that did not receive tamoxifen—even when subjected to blue light stimulation (0.15 ± 0.02). Taken together, these experiments indicate that the TamPA-Cre system works best given pulsatile blue light stimulation started after significant tamoxifen-induced nuclear localization of ERT2-CreN-nMag protein (as suggested in Fig. 4.3E). Given this optimized tamoxifen- and blue light stimulation protocol, the TamPA-Cre system drives Cre-loxP recombination just as robustly as the PA-Cre system, while significantly suppressing background Cre-loxP recombination.

We also tested whether replacing nMag with the nMagHigh1 would improve the robustness of our TamPA-Cre system. With a reported 13-fold increase in heterodimerization between pMag and nMagHigh1,[77] we predicted that this feature might help to counteract any loss in robustness caused by incomplete nuclear translocation of ERT2-CreN-nMag in the TamPA-Cre system. Following Protocol B, we found that without tamoxifen-stimulation, the TamPA-Cre-nH1 system already drove Cre-loxP recombination in a significant fraction of EGFP Reporter HEK293T cells (0.51 ± 0.06) (Fig. 4.6E). This indicates that tamoxifen-gating does not prevent all ERT2-CreN-nMag or ERT2-CreN-nMagHigh1 proteins from entering the nucleus. However, these low nuclear protein concentrations were sufficient to elicit significant Cre-loxP recombination in Light TamPA-Cre-nH1 groups, but not in Light TamPA-Cre groups (Fig. 4.6D). However, without tamoxifen or blue light stimulation, the TamPA-Cre-nH1 system was just as capable of dampening background Cre-loxP recombination (Dark: 0.13 ± 0.02, Ambient: 0.14 ± 0.01). On the other hand, with tamoxifen-stimulation, background Cre-loxP recombination was significantly increased for cells in the Dark and Ambient TamPA-Cre-nH1 groups (0.22 ± 0.02 and 0.35 ± 0.03, respectively) compared to their counterparts without tamoxifen-stimulation (0.12 ± 0.02, and 0.13 ± 0.01, respectively), highlighting the

concentration-dependent nature of background recombination as well as the primed TamPA-Cre-nH1 system extreme sensitivity to ambient light. Finally, tamoxifen- and blue light-stimulated cells in the Light TamPA-Cre-nH1 group exhibited extremely robust recombination (1.25 ± 0.13), comparable to the ERT2-Cre-ERT2 system (Fig. 4.3D). All in all, given both tamoxifen- and blue light stimulation, the TamPA-Cre-nH1 system was more robust than the PA-Cre system, with significantly repressed levels of background Cre-loxp recombination in the unstimulated state. However, tamoxifen or blue light stimulation alone was sufficient to drive significant increases in recombination in the TamPA-Cre-nH1 system, highlighting a less-stringent AND-gate than the TamPA-Cre system. Therefore, TamPA-Cre is a safer choice to strictly regulate CAR expression in T cells to avoid on-tumor off-target toxicities.

4.2.5 Design and function of CAR Reporter

We first established that Jurkat T cells constitutively expressing low levels of α-CD19CAR-EGFP underwent antigen-specific CAR-mediated T cell activation (measured as the percentage of $CD69^+$ Jurkat T cells) upon co-incubation with $CD19^+$ Toledo Target cells (81.1 ± 0.35%) (Fig. 4.10A-B). Co-incubation with $CD19^-$ K562 Target cells showed no activation beyond baseline levels of CAR-expressing Jurkat T cells alone (3.18 ± 0.09% and 4.9 ± 0.16%, respectively). Likewise, Jurkat T cells constitutively expressing myc-α-CD38 Receptor did not undergo CAR-mediated T cell activation despite binding to $CD38^+$ Toledo Target cells[78] (Fig. 3.2C).

Having shown that the tamoxifen- and photo-activatable TamPA-Cre system drives robust Cre-loxP recombination with minimal background activity, we next tested whether it could be used to selectively induce CAR expression. After much testing of reporter

configurations (Fig. 4.11), we decided to use the deletion-based CAR Reporter consisting of a floxed *myc-α-CD38Receptor* (with stop codons) followed by *α-CD19CAR-EGFP*, all driven by the hEF1α promoter (Fig. 4.7A). In cells, only the myc-tagged α-CD38 homing receptor is initially translated and expressed on the T cell surface, allowing T cells to bind to both $CD38^+$ cancerous and healthy cells. During Cre-loxP recombination, *myc-α-CD38Receptor* is excised along with its stop codons, allowing for constitutive expression of α-CD19CAR-EGFP. Over-expression of CAR can lead to spontaneous T cell activation (Fig. 4.10C), so only 1-2 copies (on average) of the CAR Reporter were transduced to create CAR Reporter Jurkat T cells.

Both halves of either the PA-Cre or TamPA-Cre components were transduced into CAR Reporter Jurkat T cells sequentially to establish high expression levels of each component using puromycin selection. No recombination was seen in CAR Reporter Jurkat T cells transduced with only one of the two TamPA-Cre components, showing both halves are necessary to drive Cre-loxP recombination (Fig. 4.10D). CAR Reporter Jurkat T cells expressing complete PA-Cre or TamPA-Cre were protected from light when possible during cell line development and culture to prevent any possible premature recombination from ambient light exposure.

4.2.6 TamPA-Cre drives CAR expression and T cell activation in Jurkat T cells

We first tested whether CAR Reporter Jurkat T cells stably expressing the TamPA-Cre system could undergo Cre-loxP recombination. Three hours after incubation with 4-OHT (500nM), cells were stimulated, or not (0h), with pulsatile blue light (5 W/m^2, [5s on, 55 s off]) delivered over 0, 1, 3, 6, or 24 hours. Cre-loxP recombination levels increased exponentially with the duration of blue light stimulation, and had plateaued by 24 hours of exposure (Fig. 4.12C, 4.13, Table 4.2). Moving forward with Protocol E (Fig. 4.12B), we tracked the fraction of

cells expressing myc-α-CD38Receptor and α-CD19CAR-EGFP (normalized to the initial percentage of CAR Reporter$^+$ cells) in TamPA-Cre CAR Reporter Jurkat T cells over several days (Fig. 4.12D, Table 4.2). Without a means to replenish receptor proteins after the *myc-α-CD38Receptor* CDS is excised during Cre-loxP recombination, the fraction of cells expressing myc-α-CD38Receptor decayed exponentially over time (half-life: ~33.7h), reaching a minimum of 0.093 ± 0.013 five days after the start of blue light stimulation. Simultaneously, the fraction of cells expressing α-CD19CAR-EGFP protein increase exponentially (half-life: 13.3h) such that 24 hours after blue light stimulation began, 35.8 ± 2.57% of CAR$^+$ cells were still expressing the receptor (data not shown). Because α-CD19CAR-EGFP is more rapidly expressed than myc-α-CD38Receptor is lost, engineered TamPA-Cre CAR Reporter T cells should remain anchored to the tumor site following stimulation (Fig. 4.14A)

Next, we tested the integrity of the tamoxifen- and blue light stimulation AND-gate in the TamPA-Cre system. CAR Reporter Jurkat cell lines expressing either TamPA-Cre or PA-Cre, or not (Reporter), were (Light) or were not (Dark) subjected to Protocol E tamoxifen- and blue light stimulation, with (TamPA-Cre only) or without tamoxifen stimulation. Recombination was calculated by normalizing the % CAR-EGFP$^+$ cells to the initial % CAR-Reporter$^+$ cells. A modest but significant fraction of CAR Reporter Jurkat T cells underwent Cre-loxP recombination (0.21 ± 0.02) in the Light PA-Cre group, approximately 4-fold more than in the Dark PA-Cre group (0.052 ± 0.007) (Fig. 4.14B, 4.15A). However, consistent with HEK293T experiments, cells in the Dark PA-Cre group also exhibited significant background recombination, 3.64-fold more than in the Dark Reporter group (0.014 ± 0.006). By contrast, cells in the Dark TamPA-Cre group exhibited no significant increase in background recombination, regardless of whether or not cells received tamoxifen stimulation (0.019 ± 0.005

or 0.016 ± 0.001, respectively) (Fig. 4.14C, 4.15B). Upon tamoxifen- and blue light stimulation, the TamPA-Cre system drove Cre-loxP recombination in a significant portion of CAR Reporter Jurkat T cells (0.524 ± 0.015), 27-fold greater than in the Dark TamPA-Cre group that received tamoxifen. However, without tamoxifen, blue light stimulation alone did cause the TamPA-Cre system to drive a minor but significant 2.8-fold increase in recombination (0.044 ± 0.008) compared to its cognate Dark group. This highlights that even in the absence of tamoxifen stimulation, a small amount of ERT2-CreN-nMag protein is likely present in the nucleus where it is capable of driving recombination given optimal blue light stimulation. However, exposing TamPA-Cre CAR Reporter Jurkat T cells to ambient light over 48h did not drive any additional recombination, unlike PA-Cre CAR Reporter Jurkat T cells (Fig. 4.10E). Therefore, without tamoxifen stimulation, cells expressing the TamPA-Cre system are likely still safe from premature Cre-loxP recombination in most practical settings.

Finally, we tested whether TamPA-Cre-driven α-CD19CAR-EGFP expression in Jurkat T cells could cause CAR-mediated T cell activation upon interaction with $CD19^+$ Target cells. Two days after subjecting PA-Cre and TamPA-Cre CAR Reporter Jurkat T cells to Protocol E (Light), or not (Dark), each independent subgroup of cells either were (+Target) or were not (-Target) co-cultured with an equal number of $CD19^+$ Toledo Target cells. All groups were analyzed 24h later for expression of the early activation marker CD69 via flow cytometry. Activation was calculated by normalizing the percentage of $CD69^+$ cells to the initial percentage of CAR-$Reporter^+$ cells (Fig. 4.14D-E, 4.15C-D).

Surprisingly, nearly double the percentage of cells measured to be CAR-$EGFP^+$ were found to be $CD69^+$ (activated) by $CD19^+$ Target cells in both fully stimulated PA-Cre and TamPA-Cre groups. However, this increase was not seen in Reporter groups with or without

Target cells. Taken together, this indicates that about half of the recombined PA-Cre and TamPA-Cre cells expressing low levels CAR-EGFP likely escaped flow cytometer detection, resulting in underestimates of recombination. However, even low levels of CAR-EGFP expression can drive antigen-specific T cell activation, so the amplified functional output of CD69 expression is more accurately reflective of true recombination levels.

In co-culture with $CD19^+$ Target cells, tamoxifen- and blue light-stimulated TamPA-Cre drove nearly all CAR $Reporter^+$ Jurkat T cells to undergo CAR-mediated T cell activation (0.927 ± 0.024), 19.2-fold more than those without $CD19^+$ Target cells (0.048 ± 0.006). By comparison, Light PA-Cre groups co-cultured with $CD19^+$ Target cells exhibited activation in less than half of CAR $Reporter^+$ Jurkat T cells (0.406 ± 0.035), only 4.39-fold more than in non-stimulated PA-Cre groups (0.093 ± 0.013).

However, compared to Reporter groups, all PA-Cre and TamPA-Cre Dark groups displayed a significantly larger fraction of activated CAR $Reporter^+$ Jurkat T cells, which was further increased upon co-incubation with $CD19^+$ Target cells. While these results indicate that the presence of PA-Cre or TamPA-Cre alone is sufficient to drive some degree of T cell activation, a portion is likely driven by background levels of CAR expression which can alone non-specifically activate T cells (Fig. 4.10C), driving further activation upon incubation with $antigen^+$ Target cells. Blue light stimulation can also drive a portion of PA-Cre or TamPA-Cre CAR Reporter Jurkat T cells to express CAR via Cre-loxP recombination, due to background levels of CreN in the nucleus. Recombined cells additionally contribute to activated cell populations both non-specifically without $antigen^+$ Target cells or antigen-specifically with $antigen^+$ Target cells. However, even with Light and $antigen^+$ Target cell stimulation, the fraction of activated TamPA-Cre cells was still 12.2-fold lower without tamoxifen stimulation than with,

demonstrating that tamoxifen-gating significantly suppresses background CAR-mediated T cell activation. However, in practice, neither PA-Cre nor TamPA-Cre CAR Reporter engineered T cells would be subjected to stimulation by tamoxifen, antigen$^+$ Target cells, or blue light (beyond ambient lighting) before they would be administered to a patient. In this case, the fraction of activated PA-Cre CAR Reporter Jurkat T cells is only 9.1-fold lower than in fully stimulated PA-Cre cell groups, whereas this fraction in TamPA-Cre Jurkat T cells is 35-fold lower than in fully stimulated TamPA-Cre cell groups. With robust and well-gated tamoxifen- and light-inducible CAR expression and T cell activation, the TamPA-Cre system proves to be an effective tool for controlling local CAR-mediated T cell activation.

In contrast to previous experimental results, TamPA-Cre significantly outperformed PA-Cre in CAR Reporter Jurkat cell lines in terms of robust activation. However, this may be a consequence of trying to establish a PA-Cre CAR Reporter Jurkat cell line. Despite diligent protection from light, PA-Cre still drives a relatively high level of background recombination. Cells expressing high levels of nuclear PA-Cre are more sensitive to light stimulation (Fig. 4.5A), but are also more susceptible to spontaneous background recombination—an irreversible process that ultimately results in their removal from the population when enriching for CAR Reporter$^+$ (myc$^+$) cells via MACS. Therefore, the remaining PA-Cre$^+$ population consists of cells that are less sensitive to both spontaneous and blue-light-driven recombination. TamPA-Cre+ CAR Reporter Jurkat T cells, on the other hand, maintain a low frequency of spontaneous background recombination, allowing for high expression levels of TamPA-Cre which are, in turn, more sensitive to blue light stimulation following tamoxifen treatment.

4.2.7 Summary and future directions

We have developed a novel logic-gated optogenetic split Cre system by integrating both ERT2-fusion proteins and blue-light-inducible nMag-pMag heterodimerizing domains to drive robust Cre-loxP recombination with significantly suppressed background. Only after treatment with tamoxifen is the TamPA-Cre system primed to be activated by short pulses of low intensity blue-light-stimulation. The tamoxifen gate helps prevent premature and spontaneous Cre-loxP recombination within cells prior to specific blue-light-stimulation—a weakness of other photoactivatable Cre-loxP systems. Applying the TamPA-Cre system to our floxed CAR-Reporter construct in Jurkat T cells, we were able to precisely induced CAR expression and antigen-specific T cell activation. With its unique high spatiotemporal control over T cell activation, the TamPA-Cre system could be used to locally induced T cell effector functions against cancer cells *in vivo* while avoiding on-target off-tumor toxicity in TAA^+ healthy tissues.

The TamPA-Cre system also offers greater spatiotemporal control over other engineered CAR systems, like SynNotch[79] and SUPRA CAR.[80] Until photoactivatable transcription-based CAR expression systems become more robust with lower background expression,[81-83] suicide switches[34, 84] and iCARs[33] can further prevent on-target off-tumor toxicity by TamPA-Cre-activated CAR T cells leaving the stimulated region following tumor eradication. CRISPR-Cas9 technology can also help integrate large TamPA-Cre and engineered CAR T cell system designs into safe and effective loci in the genome.[73] Furthermore, while the highly controllable TamPA-Cre system can replace virtually any Cre-loxP system, we foresee that it will serve as a particularly useful alternative to CRE-ERT2 systems in mouse lines where spontaneous Cre-loxp background recombination in vivo is already an established problem.[85]

4.3 Materials and Methods

Cre and CAR construct design

Detailed information on cloning and constructs can be found in Supplementary Table 3, but is briefly explained here. pCDNA3.1-CMV (Thermo Fisher, #V79020), pSin-EF1α (Addgene #16579), and pHR-PGK (Addgene #79125, 79130) mammalian expression vector backbones were used. Molecular cloning was done in DH5α competent cells (Thermo Fisher #18265017) and plasmids isolated using miniprep (Sigma, #PLN350) and maxiprep (Qiagen, #12163) kits. Traditional T4 ligation with restriction enzyme digest (New England Biolabs) or Gibson Assembly (NEB #E2622L) methods were used to create constructs. Sufficient plasmid concentration (>0.5μg/ml) and purity (260/280 ≥ 1.8, 260/230 ≥ 2.0) were ensured for all experiments as measured by a Nanodrop 2000c Spectrophotometer (Thermo Fisher #ND2000C). PA-Cre2.0. Both photoactivatable Cre partners CRY2(L348F)-CreN (Addgene #75368) and CIBI-CreC(N1) (Addgene #75367) were cloned into a pSin vector separated by an IRES and preceded by a PGK promoter and mCherry marker. PA-Cre photoactivatable Cre partners CreN-nMag and pMag-CreC were cloned from a synthesized DNA template of the Sato Lab's published PA-Cre construct, a kind gift from the Wilson Wong Lab (Boston University), into pSin-EF1a with mCherry and tBFP fluorescent markers, respectively. Before both PA-Cre components were cloned into pSin-EF1a with an mCherry marker, the pMag sequence was codon-diversified and synthesized (gBlock, Integrated DNA Technologies) in an effort prevent unwanted recombination between nMag and pMag during lentiviral production. ERT2-CreN59 was cloned from a pSin-6xUAS-CMV_{min}-ERT2-Cre-ERT2 template (a generous gift from the Todd Coleman Lab, UCSD) and assembled with nMag (NLS removed) in pCDNA3.1-CMV or with nMag-P2A-mCherry in pCDNA3.1 and pSin-EF1α. The full constitutively expressed Cre

sequence (Addgene #14797) with mCherry marker was cloned into the pSin-PGK vector. Tamoxifen-dependent ERT2-Cre-ERT2 was cloned into pSin-EF1a along with a c-terminal mCherry marker to create pSin-EF1α-ERT2-Cre-ERT2-2xP2A-mCh.

CAR and receptor constructs were assembled from first-generation α-CD19 CAR (19z1) and α-PSMA chimeric costimulatory receptor (P28BB) templates kindly donated by the Sadelain Lab (Memorial Sloan-Kettering Cancer Center, NY). The α-CD38 scFv domain was synthesized (Integrated DNA Technologies), based on US patent application US20100267145A1, with IgG signaling peptide and VL-VH linker inspired by a third generation α-CD19 CAR sequence shared with us by Daofeng Liu (Baylor College of Medicine, TX). The α-CD19-CAR-EGFP construct consists of a CD8 signaling peptide, α-CD19 scFv, CD28 hinge, transmembrane, and intracellular domain, 4-1BB domain, CD3-zeta domain, GGSGGT linker, and EGFP. The α-CD38-Receptor construct consists of an IgG signaling peptide, c-Myc tag (EQKLISEEDL), α-CD38 scFv, and a codon-diversified CD28 hinge, transmembrane, and truncated/nonfunctional (4aa) intracellular domain. CAR and receptor constructs were assembled in pCDNA3.1-CMV and transferred to pSin-EF1α vector.

EGFP and CAR Reporter constructs containing floxed components were partially assembled in the pLV-CMV-LoxP-DsRed-LoxP-EGFP (Addgene #65726) vector, and were fully assembled in pSin-EF1α. Lox66 sites were generated via overlap extension PCR using MEA344 and 345 primers, while Lox71 was created by using a mutated reverse primer (MEA346) to change the LoxP of the template site into a Lox71-containing PCR product for subsequent assembly. Sanger sequencing was used to confirm all genetic constructs (GeneWiz). See Supplementary File 1 for details.

Cell culture and reagents

The following cell lines were purchased from ATCC: human embryonic kidney cells (HEK293T), Jurkat (Clone E6-1, TIB-152) T cells, K-562 lymphoblasts (CCL-243, $CD38^-$/$CD19^-$ target cells), and Toledo B lymphocytes (CRL-2631, $CD38^+$/$CD19^+$ target cells). HEK293T cells were cultured in Dulbecco's modified eagle medium (DMEM) (Gibco #11995065) supplemented with 2 mM L-glutamine, 1 mM sodium pyruvate, 100 units/ml penicillin, 100 μg/ml streptomycin (Gibco #15140122), and 10% (v/v) fetal bovine serum (FBS) (Thermo Fischer Scientific #10438026) in standard tissue-culture-treated dishes or plates. K-562, Jurkat, and Toledo cells were cultured in RPMI-1640 medium with L-glutamine, supplemented with 10% (v/v) FBS, 1x penicillin, and streptomycin in non-tissue-culture-treated plates or flasks. HEK293T EGFP Reporter and Jurkat PA-Cre and TamPA-Cre cell lines were maintained in puromycin (Sigma #P8833-100MG).

(Z)-4-Hydroxytamoxifen (Sigma #H7904-5MG) was dissolved in 200-proof ethanol with heat to make 50mM frozen stock solution aliquots (protected from light with foil). Immediately before adding 4-OHT to cells, an aliquot of stock solution was serially diluted in the appropriate fresh cell culture medium to 500 nM in experiments calling for the addition of 4-OHT.

Lentiviral production

Lenti-X 293T cells (Clontech Laboratories #632180) cultured in DMEM +10% FBS +1x Pen/Strep were used to produce VSV-G pseudotyped lentivirus with a second-generation lentiviral system. Genes of interest were cloned into transfer plasmid pPKm-145 (Addgene #90505), which was co-transfected into Lenti-X-293T cells with envelope plasmid pCMV-VSV-G (Addgene #8454) and packaging plasmid pCMVΔR8.2 (Addgene #12263) at a 2:1:1 molar ratio using the ProFection® Mammalian Transfection System (Promega, Madison, WI #E1200). Viral supernatant was collected and filtered (0.22 micron) 48h after transfection and either used

directly or concentrated 100x using PEG-it Virus Precipitation Solution (System Biosciences, Palo Alto, CA) before use. Excess virus was aliquoted and stored at -80°C for future use.

Lentiviral transduction in cell lines

The EGFP Reporter HEK293T cell line was made by lentiviral transduction. First, functional titer was determined by mCherry expression. Then, the cell line was generated from a group in which 1-20% of cells were transduced (~1-2 copied/cell) and was selected and maintained by culturing in 0.5 μg/mL puromycin.

For Jurkat T cells, unconcentrated or concentrated lentivirus supernatant was added directly to 100,000 cells/mL in culture medium and incubated 24hrs, after which the virus was removed and the cells plated in fresh culture medium. After 4-5 days, lentivirus functional titration of the CAR Reporter construct in Jurkat T cells was measured by AlexaFluor647-conjugated antibody immunostaining against the myc-tag (Cell Signaling #2233S) on constitutively-expressed myc-α-CD38Receptor. A group in which 1-20% of cells were transduced (~1-2 copies/cell) was sorted via myc-tag antibody staining using the FACSAria II Sorter at UCSD Human Embryonic Stem Cell Core Facility (La Jolla, CA). Cells were expanded in culture medium, aliquoted, and cryopreserved. Sorted CAR Reporter Jurkat T cells were likewise also transduced with PA-Cre and TamPA-Cre constructs, with nMag and pMag constructs transduced sequentially with FACS sorting between each transduction. Unless otherwise specified, cell culture plates containing cells transduced or transfected with complete PA-Cre or TamPA-Cre were handled in a room illuminated by red light (HIGROW, 36W, 660nm) and were otherwise protected from light with aluminum foil to prevent premature recombination. Functional titration of the α-CD19CAR-EGFP construct in Jurkat T cells was

measured by EGFP expression, and a group in which 1-20% of cells were transduced (~1-2 copies/cell) was selected for and maintained using puromycin.

Jurkat cell lines expressing the CAR Reporter were occasionally enriched via MACS selection using 1:10 dilution of Biotin-conjugated antibody against the myc-tag (Jackson ImmunoResearch Inc. #115-066-006) to label cells, and Anti-Biotin MicroBeads in the MidiMACS Separator with LS Columns (Miltenyi Biotec, Germany) to separate cells with the CAR Reporter.

Blue Light Stimulation

An intensity-adjustable blue light control system was made by Phillip Kyriakakis. To diffuse the light more evenly across the plate of cells, first, the blue LED (LUXEON Rebel #LXML-PB02, 472nm) was mounted with Dual Lock Reclosable Fasteners (3M) in the center of the bottom of a deep, polyester white-walled container with a clear PET plastic lid and synthetic rubber gasket (IKEA #402.574.99). Small plastic Decorating Clips (3M) were used to hold the LED wire along the inside walls of the container, keeping it out of the light path. Then, a static cling frosted window film (Beautyhero) was cut to size and placed on the inside of the lid. Closing with the lid, the container was flipped lid-side-down and centered on top of a lidless black plastic box (Hammond #1591ESBK) in which a cell culture plate would be placed for blue light exposure. The blue light intensity was adjusted and measured using a power meter (Newport, Model 843-R) before each experiment to ensure the plate wells farthest from the light source were receiving the intended irradiance flux density. For experiments, the LED container was placed on top of the black box holding the plate of cells immediately before placing in 37°C, 5% CO_2 cell culture incubator for the indicated blue light exposure patterns. The control box and computer were operated outside of the incubator. The blue LED used in this experiment was

measured using the TECAN Infinite M1000 Pro, which measured peak intensity at 473 nm with a bandwidth of 29 nm. (See Fig. 4.4 for photographs and measurement data.)

Plate(s) exposed to the Ambient light condition were placed in the frontmost position on the top shelf of a shared cell culture incubator, where the cells were intermittently exposed to approximately 0.34-0.78 W/m^2 of white fluorescent light according to normal lab use. During a typical business day between 8:00 am and 8:00 pm, we estimate that the incubator door is opened approximately 100 times per day for about 5s each. However, we purposely forwent strict control over the Ambient light condition in order to faithfully simulate light exposure in our busy shared lab environment. Therefore, we expect—and indeed find—that cells exposed to the Ambient light condition may or may not exhibit significantly higher recombination levels than those kept in the dark simply because of inherently variable day-to-day use of the incubator.

HEK 293T Experiments

With the exception of the Ambient light condition, all samples were protected from environmental light with aluminum foil immediately after transfection and throughout the duration of the experiment unless otherwise specified (e.g. blue light stimulation). All procedures outside of the incubator were conducted in red light only to minimize any effects that ambient light from the room and biosafety hood may have on photoactivation.

EGFP Reporter HEK293T cells were plated at 100,000 cells/well in a tissue-culture-treated 24-well plate. After 24h, cells were transfected with construct plasmid(s) using Lipofectamine 3000 (Thermo Fisher Scientific #L3000015). 8h after transfection, each group was split into multiple 24-well plates (10-15% confluence/well), each plate corresponding to a unique light condition (Dark, Ambient, or Light). Dark condition plate(s) remained wrapped in foil until endpoint measurements. Foil was removed from Ambient condition plate(s) at this

point until endpoint analysis to allow for exposure to the normal light of our shared lab environment. 24h post-transfection, foil was temporarily removed from Light condition plates to expose them to the specified blue light condition, after which the Light condition plate(s) were again wrapped in foil until endpoint analysis.

Jurkat Experiments

Throughout pseudo-cell line creation, culture, and experimentation, Jurkat T cells expressing the CAR Reporter along with complete PA-Cre or TamPA-Cre were protected from environmental light with aluminum foil at all times unless otherwise specified (e.g. Ambient light condition, blue light stimulation). All procedures outside of the incubator were conducted in red light only to minimize any effects that ambient light from the room and biosafety hood may have on photoactivation.

CAR Reporter Jurkat cell lines with or without PA-Cre or TamPA-Cre were plated at 100,000 cells/well in multiple non-tissue-culture-treated 24-well plates (Genesee Scientific Corp. #25-102), with one set of TamPA-Cre cells receiving 500 nM 4-OHT. Unless otherwise specified, one of the plates was moved into a separate cell culture incubator and stimulated with 6.5 W/m^2 of pulsatile blue light (5s on, 55s off) for 24h, then wrapped in foil. 48h after blue light stimulation started, each group of Jurkat T cells was passed to a round bottom non-tissue-culture-treated 96-well plate (2 wells, 100,000 cells each), one with and one without 100,000 $CD19^+$ Toledo target cells (200 μL/well). After a further 24h of incubation, Jurkat T cells were immunostained with an APC-conjugated antibody against early T cell activation marker CD69 (BioLegend #310910) and measured via flow cytometry. Recombination (% $EGFP^+$ cells) and activation (% $CD69^+$ cells) measurements were normalized to the initial percentage of cells expressing the CAR Reporter, as measured by immunostaining for the myc-tag on

CD38Receptor). Jurkat groups were not normalized to cells expressing Cre (as was done with HEK293T cells) because a stable cell lines with constitutive Cre expressed at levels comparable to PA-Cre or TamPA-Cre died over time, preventing the creation of a stable cell line (data not shown).

Jurkat T cells expressing α-CD19CAR-EGFP or myc-α-CD38Receptor-EGFP were shown to bind to $CD19^{+}CD38^{+}$ Toledo target cells via the CAR Binding Assay (described in Chapter 2). Briefly, Toledo target cells were dyed with CellTracker deep red (Ex/Em: 630/650nm, ThermoFisher), mixed 1:1 with CAR or Receptor Jurkat T cells (~150,000 cells each) in 1 mL of cell culture medium, and placed in a 37°C rotator for 30-45 min to allow for binding. Then, the mixture of cells was directly measured at slow speed by flow cytometer (BD Accuri C6) to identify the percentage of CAR^{+} or $Receptor^{+}$ Jurkat T cells ($EGFP^{+}$) that were also bound to target cells ($CellTracker^{+}$).

Microscopy

Prior to imaging, cells were plated on 35mm #0 glass bottom dishes (Cell E&G, San Diego, CA) coated with either 20 μg/mL fibronectin or 10 μg/mL poly-L-Lysine for adherent and suspension cells, respectively (Sigma, St. Louis, MO). Images were acquired on a Nikon Eclipse Ti inverted microscope with a cooled charge-coupled device (CCD) camera. The following filters were used to image the indicated fluorophores: tBFP (420/40 nm excitation, 480/40 nm emission, 455 nm LP dichroic mirror), mCherry (580/10 nm excitation, 630/20 nm emission, 595 LP dichroic mirror), and EGFP (457-487 nm excitation, 502-538 nm emission, GFP filter cube set). Analysis was conducted using MetaFluor 7.8 or MetaMorph 7.8 software (Molecular Devices, San Jose, CA).

Flow cytometry measurements

Fluorescent and immunostained cells were measured using a BD Accuri C6 flow cytometer equipped with 488 and 640 nm excitation lasers. EGFP expression was measured using the 488 nm excitation laser with a 533/30 nm emission filter. Cell labeling antibodies conjugated with far-red dyes were measured using the 640 nm excitation laser with a 675/25 nm emission filter. Before measuring, live cells were trypsinized (if adherent), washed three times with FACS wash buffer (filter-sterilized 0.5% BSA in PBS or autoMACS Running Buffer (Miltenyi Biotec, Germany)), then either measured directly, or immunostained for 20 minutes at 37°C, washed thrice, and then measured. Data was analyzed using FlowJo software (TreeStar). Samples of plain HEK293T, Jurkat, and Toledo cells were included with each experiment as negative controls for gating purposes.

Data and Statistical Analysis

For data presentation, the normalized values were shown to clearly compare the differences among the experimental groups. Statistical significance was assessed by Student's t test (two tailed, two-sample unequal variance) with p values determined as follows: not significant (n.s.) if $p > 0.05$, * if $p \leq 0.05$, ** if $p \leq 0.01$, *** if $p \leq 0.001$. Error bars represent the standard deviation.

4.4 Figures and Tables

Table 4.1: Truth table highlighting potential on-target off-tumor toxicity risks for several engineered CAR T cell system. CAR T cell systems target localized cancerous cells that express Antigen1 and/or Antigen2. Expected CAR-mediated T cell activation is given as an output for each unique combination of inputs, noting incidents of on-target on-tumor and on-target off-tumor toxicities. Note: blue light stimulation is only applied locally at the tumor site. T cells expressing the basic α-Antigen1 CAR will trigger on-target off-tumor toxicity against any Antigen1$^+$ healthy cells along with the cancer cells. The ON-Switch α-Antigen1 CAR system[35] relies on a diffusible small molecule to turn reconstitute CAR function. Small molecules, however, are at risk of diffusing throughout the body, leaving Antigen1$^+$ healthy cells susceptible to on-target off-tumor toxicity. The cytosolic costimulatory and activating domains of CAR can be split into 2 proteins, each with unique antigen recognition domains. CAR function is reconstituted upon binding to Antigen1$^+$ Antigen2$^+$ targeted cancer cells.[15] However, the split CAR will also trigger on-target off-tumor toxicity against any Antigen1$^+$ Antigen2$^+$ healthy cells. The synNotch receptor localizes T cells to all Antigen1$^+$ cells, after which α-Antigen2 CAR is automatically expressed.[79] This system similarly puts Antigen1$^+$ Antigen2$^+$ healthy cells at risk for on-target off-tumor toxicity. The TamPA-Cre system also localizes T cells to all Antigen1$^+$ cells, but α-Antigen2 CAR is only expressed after global tamoxifen administration and localized blue light stimulation. As long as Antigen1$^+$ Antigen2$^+$ healthy cells are not colocalized with cancer cells, they are not at risk for on-target off-tumor toxicity.

	Input(s)				**Output: CAR-Mediated T Cell Activation** On-target On-tumor or On-target Off-tumor				
	Antigen1$^+$ Target	**Antigen2$^+$ Target**	**Small Mol. Stimulation**	**Blue Light Stimulation**	**α-Antigen1 CAR**	**ON-Switch α-Antigen1-CAR**	**α-Antigen1, α-Antigen2 Split CAR**	**α-Antigen1 synNotch α-Antigen2 CAR**	**TamPA-Cre α-Antigen1 Receptor α-Antigen2 CAR**
Healthy Cells	0	0	0	0	0	0	0	0	0
	0	0	1	0	0	0	0	0	0
	0	1	0	0	0	0	0	0	0
	0	1	1	0	0	0	0	0	0
	1	0	0	0	1	0	0	0	0
	1	0	1	0	1	1	0	0	0
	1	1	0	0	1	0	1	1	0
	1	1	1	0	1	1	1	1	0
Cancer Cells	1	1	0	0	1	0	1	1	0
	1	1	0	1	1	0	1	1	0
	1	1	1	0	1	1	1	1	0
	1	1	1	1	1	1	1	1	1

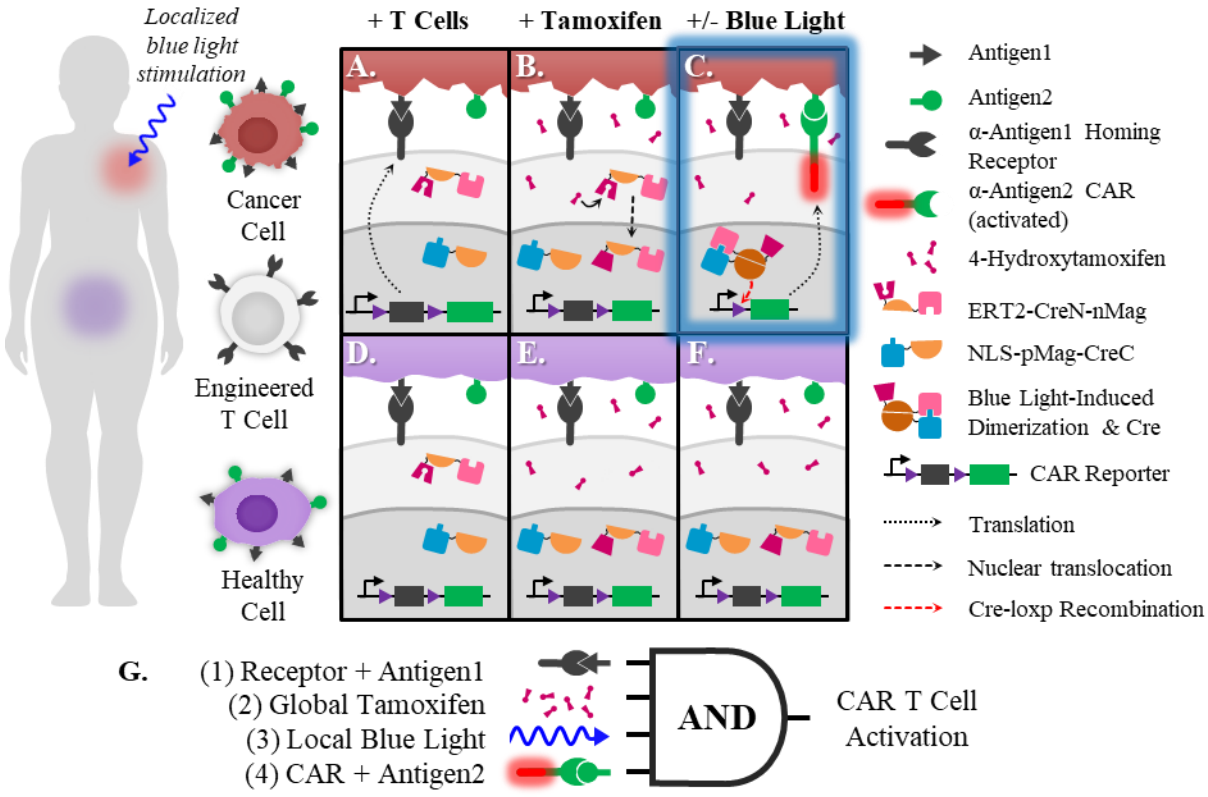

Figure 4.1: Schematic of TamPA-Cre application and molecular mechanism. (Left) Person with cancerous (red) and healthy (purple) tissue in separate regions of the body. Both tissues contain cells that express Antigen1 and Antigen2. Engineered T cells express TamPA-Cre (ERT2-CreN-nMag and NLS-pMag-CreC) and the CAR Reporter genetic construct, consisting of a constitutive promoter driving expression of the floxed (purple) *α-Antigen1 Homing Receptor* CDS with stop codons (black), followed by *α-Antigen2 CAR* (green). Upon intravenous injection, the engineered T cells bind and localize to both cancerous (A) and healthy (D) Antigen1$^+$ cells. TamPA-Cre is inactive as its NLS-pMag-CreC and ERT2-CreN-nMag protein halves are nuclear and cytosolically, respectively, to prevent spontaneous or premature background Cre-loxp recombination. After administration of tamoxifen, metabolite 4-OHT binds with ERT2-CreN-nMag to drive nuclear localization (B,E), priming TamPA-Cre. Next, blue light is applied to the cancerous tissue region only (C), inducing nMag-pMag heterodimerization which reconstitutes active TamPA-Cre recombinase activity within the nucleus. The CAR Reporter's floxed *α-Antigen1 Receptor* CDS is excised through Cre-loxP recombination along with its stop codons, thus allowing *α-Antigen2 CAR* to be expressed. The T cell is finally activated upon recognition of Antigen2. However, T cells localized to the healthy tissue region (F) are not exposed to blue light and thus do not express α-Antigen2 CAR, effectively protecting healthy cells that express both Antigen1 and Antigen2. (G) Boolean logic representation of the AND-gated TamPA-Cre system. (1) T cells must first bind to cells expressing Antigen1 via the Receptor. (2) Then, TamPA-Cre must be primed with tamoxifen before receiving localized (3) blue light stimulation in the cancerous tissue region. Next, this drives Cre-loxp recombination and CAR expression. (4) Finally, T cell activation is triggered only when Antigen2 is recognized by the CAR.

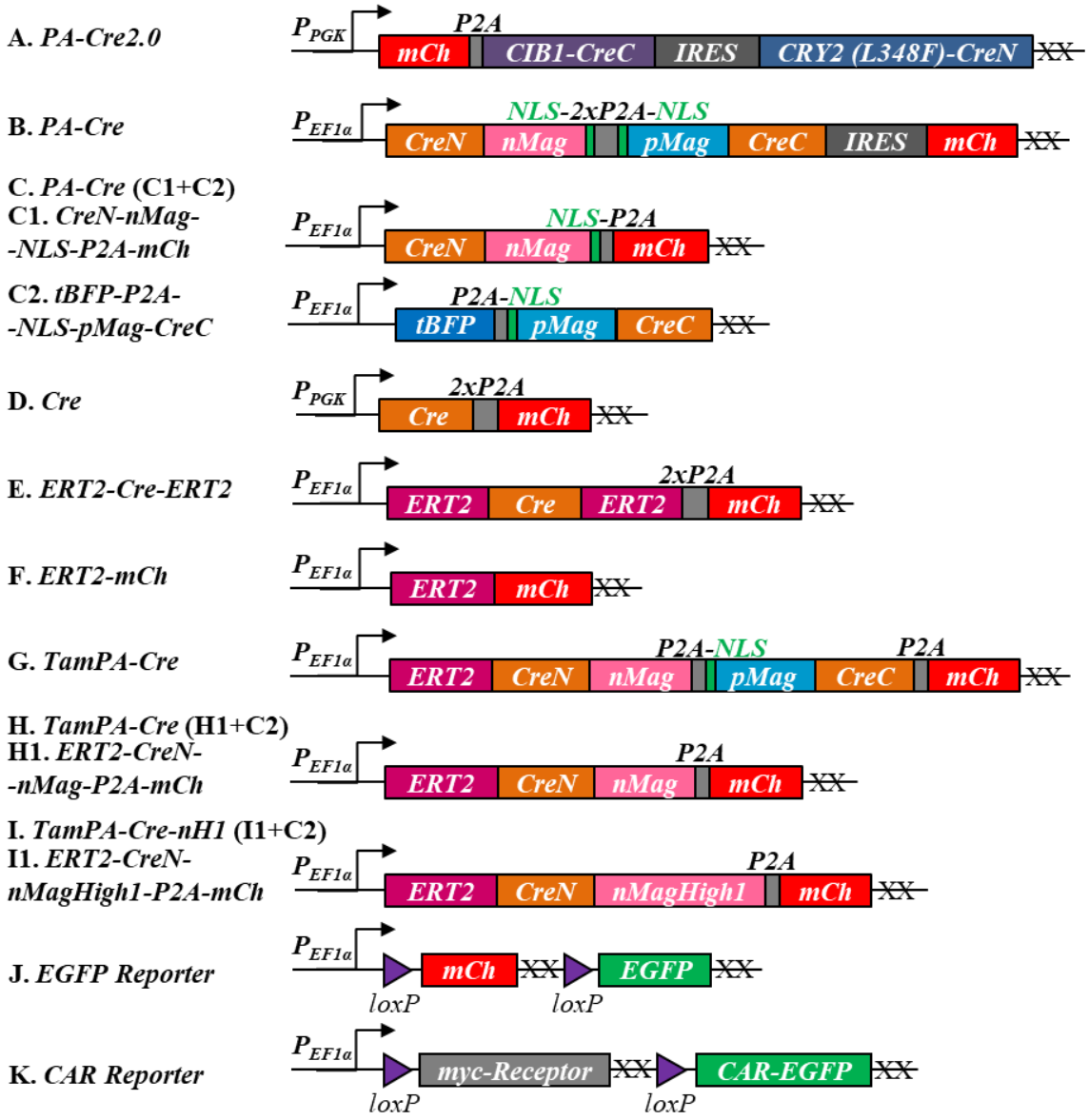

Figure 4.2: Schematic representations of different genetic constructs used in Chapter 4. The following constructs were assembled in self-inactivating vectors compatible with the second generation lentivirus packaging system: (A) PA-Cre2.0:[49] *pSin_mPGK_mCherry_P2A_CIBI-CreC(106-343)_IRES_CRY2(L348F)-CreN(19-104)*, (B) PA-Cre[48] in one vector: *pSin_hEF1α_CreN(19-59)_NLS_2xP2A_NLS_pMag_CreC(60-343)*, or (C) two vectors: (C1) *pSin_hEF1α_CreN(19-59)_nMag_NLS_P2A_mCherry_IRES_PuroR* and (C2) *pSin_hEF1α_tBFP_P2A_NLS_pMag_CreC(60-343)_IRES_PuroR*, (D) Cre: *pSin_hEF1α_Cre_2xP2A_ mCherry*, (E) ERT2-Cre-ERT2: *pSin_hEF1α_ERT2-Cre-ERT2*, (F) ERT2-mCh: *pSin_hEF1α_ERT2_ mCherry*, (G) TamPA-Cre in one vector: *pSin_hEF1α_ERT2_CreN(2-59)_nMag_P2A_NLS_pMag(codon diversified)_CreC(60-343)_P2A_mCherry*, or (H) two vectors: (H1) *pSin_hEF1α_ERT2_CreN(2-59)_nMag_P2A_mCherry_IRES_PuroR* and (C2), (I) TamPA-Cre-nH1 in two vectors: (I1) *pSin_hEF1α_ERT2_CreN(2-59)_nMagHigh1_IRES_PuroR* AND (C2), (J) EGFP Reporter: *pSin_hEF1α_loxp_mCherry_loxP_EGFP_IRES_PuroR*, and (K) CAR Reporter *pSin_hEF1α_loxp_myc-α-CD38Receptor_loxP_α-CD19CAR-EGFP_IRES_PuroR*.

Figure 4.3: Evaluation of photoactivatable and tamoxifen-dependent Cre recombinase systems. (A) Schematic representation of the EGFP Reporter genetic construct before and after Cre-loxP recombination. Expression of *mCherry* is driven under the hEF1α promoter. During Cre-loxP recombination, the floxed *mCherry* is irreversibly excised along with its stop codons (XX), thus allowing for *EGFP* expression. (B) EGFP Reporter HEK293T cells transiently transfected with PA-Cre2.0, PA-Cre, or Cre constructs did (Light) or did not (Dark) receive blue light stimulation (30 W/m^2, continuous, 30s) (n=3). (C) EGFP Reporter HEK293T cells transiently transfected with PA-Cre or Cre constructs did (Light) or did not (Ambient, Dark) receive blue light stimulation (15 W/m^2, pulsatile: [1s on, 59s off], 24h) (n=4). (D) EGFP Reporter HEK293T cells transiently transfected with ERT2-Cre-ERT2 or Cre constructs did (Light) or did not (Ambient, Dark) receive blue light stimulation (15 W/m^2, pulsatile: [1s on, 59s off], 24hrs) (n=4). (E) Representative time-lapse fluorescence microscopy images of HEK293T cells transiently expressing ERT2-mCherry before and after the addition of nuclear-localizing 4-OHT (500nM) (imaged every 2min, 100x mag., scale bar = 10μm, n=6 independently measured cells). Reporter = untransfected EGFP Reporter HEK293T cell line. Unlike cells in the Dark groups, those in Ambient groups were not protect from ambient room light with aluminum foil throughout the experiment. Blue light = 473 ± 29nm, stimulation started 24h post-transfection. Recombination = % EGFP$^+$ cells normalized to mean of corresponding Cre group, measured 96h post-transfection. Plotted mean ± s.d. of n independently tested groups, each with ≥ 10,000 cells analyzed by flow cytometry. P-values: *n.s.* $p > 0.05$, (*) $p \leq 0.05$, (**) $p \leq 0.01$, (***) $p \leq 0.001$ using heteroscedastic two-tailed Student's *t*-Test.

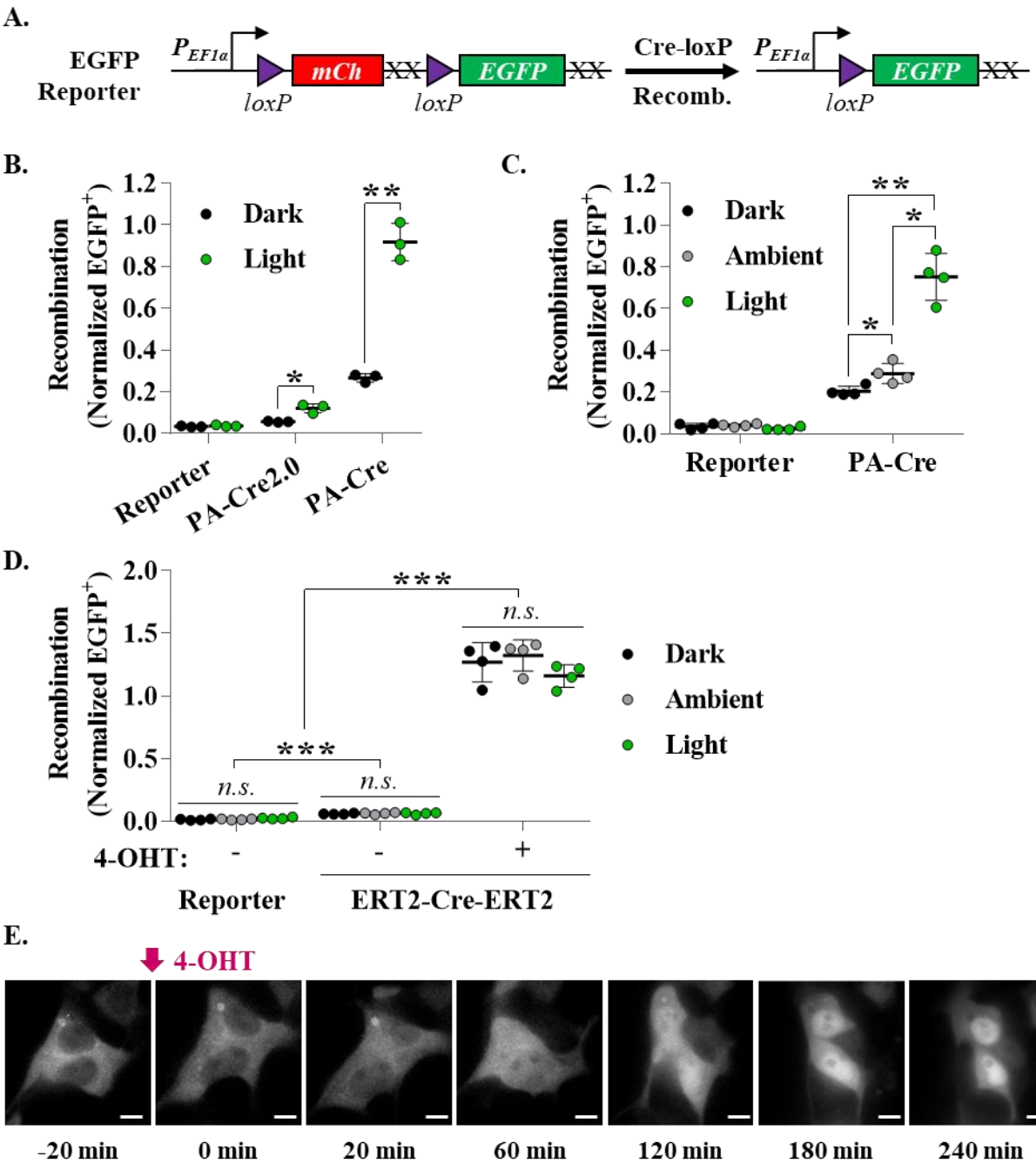
A.
EGFP Reporter
$P_{EF1\alpha}$
mCh
EGFP
loxP
loxP
Cre-loxP Recomb.
$P_{EF1\alpha}$
EGFP
loxP
B.
Recombination (Normalized EGFP+)
Dark
Light
Reporter
PA-Cre2.0
PA-Cre
C.
Recombination (Normalized EGFP+)
Dark
Ambient
Light
Reporter
PA-Cre
D.
Recombination (Normalized EGFP+)
n.s.
4-OHT:
Reporter
ERT2-Cre-ERT2
Dark
Ambient
Light
E.
4-OHT
-20 min
0 min
20 min
60 min
120 min
180 min
240 min

Figure 4.4: Design and characterization of the blue light stimulation apparatus. (A) To distribute light from a single LED evenly across a plate of cells, we built the blue light stimulation apparatus with an LED placed at a defined distance from a polypropylene light-diffusion film. (I) Close up of the mounted blue LED covered in a protective layer of transparent epoxy. (II) Dual Lock Reclosable Fasteners (yellow) were adhered to the back of the LED (not shown) and in the center of the bottom of a deep, polyester white-walled container with a clear PET plastic lid and synthetic rubber gasket. Small plastic Decorating Clips (white) were used to hold the LED wire along the inside container walls, out of the light path. A small notch was cut into the white container to minimize strain on the wire when the lid was fastened. (III) A polypropylene static-cling frosted window film was cut to size and placed on the inside of the lid to work as a light-diffusion film. (IV) The LED was mounted in the bottom center of the container and the wires secured with clips. In the background, the wire connects to the intensity-adjustable blue LED control system (Phillip Kyriakakis). (V) The lid was fastened onto the blue light box and the blue light is turned on to demonstrate function. The cell culture place was centered inside a lidless black plastic box, which is fitted to the beveled lid of the blue light box (VI) After blue light intensity was measured and adjusted using a power meter, the blue light box was flipped upside down and centered on top of the cell culture plate in the lidless black plastic box. During experiments, this configuration is assembled inside of a humidified 37°C, 5% CO_2 cell culture incubator. The air-tight lid of the blue light box helped protect the LED from environmental wear and damage inside of the incubator. Finally, blue light exposure times and patterns are entered through the LED control system's software outside of the incubator. (B) Spectral evaluation of blue LED used to stimulate photoactivatable Cre-loxP recombination. The LED was measured by mounting it onto a cell culture plate, then using a microplate reader (Infinite M1000 Pro, Tecan) to measure the intensity of the LED at different wavelengths (1 nm intervals). Peak intensity wavelength occurred at 473 nm (bandwidth = 29 nm). (C) Characterization of light distribution showing more even distribution with greater distance from the LED light and scattering from the diffusion film. The blue light box was set up shown in AVI, such that light intensity could be measured at the approximate location experience by cells in each well of a 24-well plate. The shortest distance between the light source and center of the 24-well plate cell culture plane was approximately 15.5 cm. The lid with the diffusion filter was located a minimum of 10.1 cm from the light source. Future designs will include an array of multiple LEDs to further improve light distribution.

A.

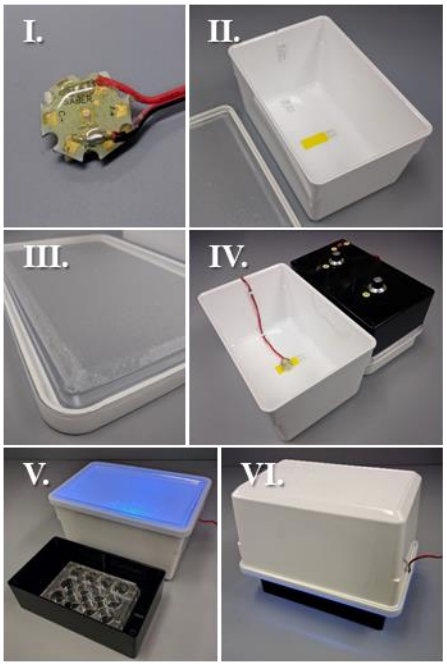
I.
II.
III.
IV.
V.
VI.

B.

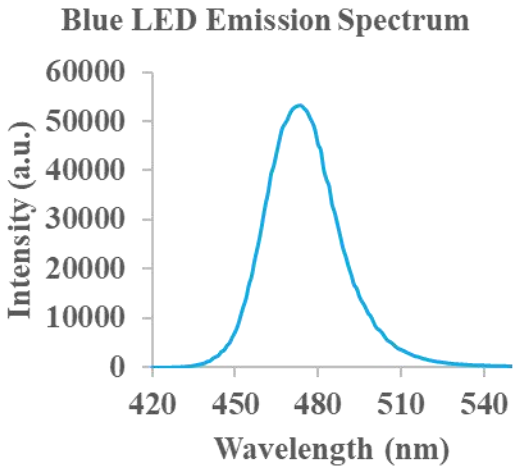
Blue LED Emission Spectrum
Intensity (a.u.)
60000
50000
40000
30000
20000
10000
0
420
450
480
510
540
Wavelength (nm)

C.

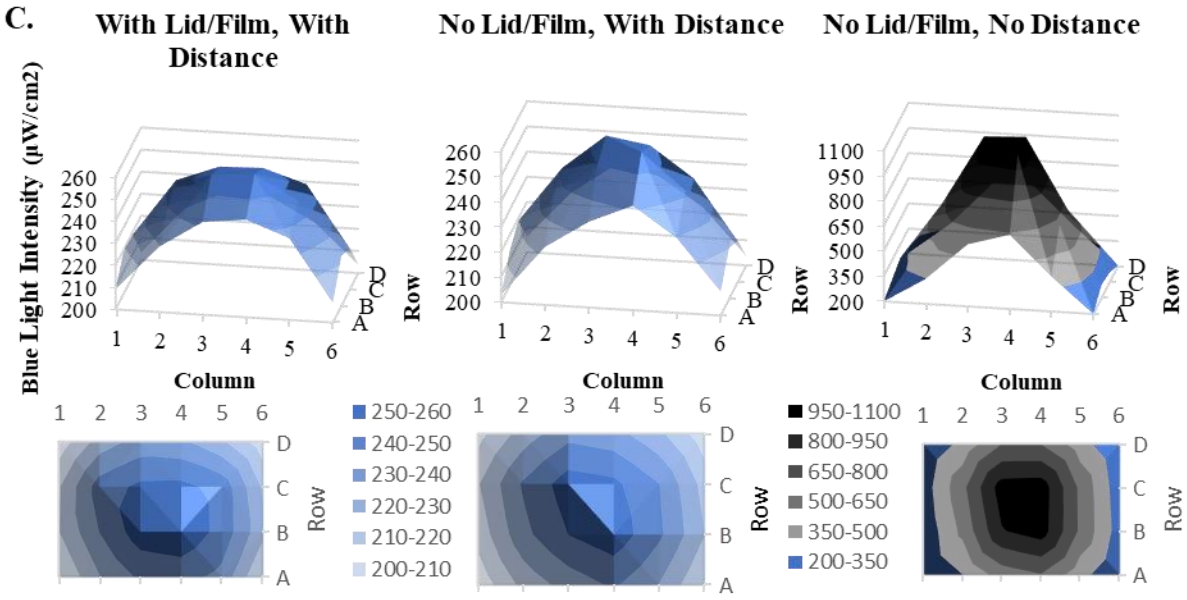
With Lid/Film, With Distance
No Lid/Film, With Distance
No Lid/Film, No Distance
Blue Light Intensity (µW/cm2)
Column
Row
250-260
240-250
230-240
220-230
210-220
200-210
950-1100
800-950
650-800
500-650
350-500
200-350

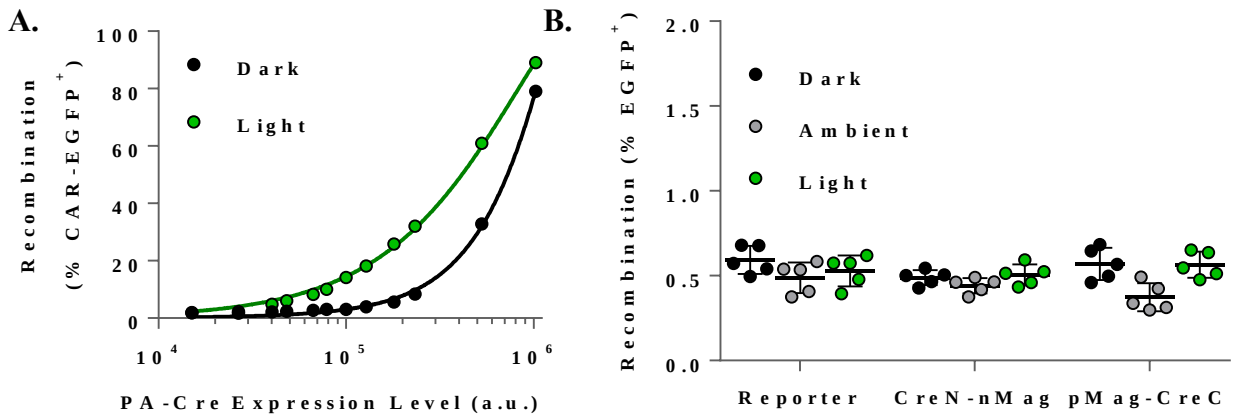

Figure 4.5: Additional characterization of the PA-Cre system. (A) Excessive expression of PA-Cre drives high levels of spontaneous recombination. CAR Reporter Jurkat T cells were transiently transfected via electroporation with PA-Cre split between two vectors (Fig. 4.2C). 24-hours post-transfection, cells were (Light) or were not (Dark) subjected to pulsatile blue light stimulation over the next 24h (50 W/m^2, [1s on 60s off]). Recombination was measured 24h after the start of blue light stimulation and is represented as % CAR-EGFP$^+$ cells as measured by flow cytometry. Trend lines fitted to Dark (black) and Light (green) groups were created using a two-phase exponential association model (GraphPad Prism7) where Y=Ymax1*(1-exp(-K1*X)) + Ymax2*(1-exp(-K2*X)) (Table S2). At low PA-Cre expression levels (as measured by the intensity of the mCherry marker), the difference between the Light and Dark groups is small. With increasing expression level, light-induced PA-Cre drives increasing levels of recombination while cells kept in the dark remain relatively low. However, at higher expression levels, the difference between Recombination in Dark and Light groups begins to narrow as dark groups become more susceptible to spontaneous background recombination. Data is from the analysis of one experiment, but represents a common trend seen across several different experiments in which PA-Cre was variably expressed. (B) Cre-loxP recombination cannot be driven by CreN-nMag-NLS or NLS-pMag-CreC alone. EGFP Reporter HEK293T cells transiently transfected with CreN-nMag-NLS-P2A-mCherry (CreN-nMag), or tBFP-P2A-NLS-pMag-CreC (pMag-CreC) constructs either were (Light) or were not (Dark, Ambient) exposed to blue light stimulation (5 W/m^2, pulsatile: [7.5s on, 52.5s off], 24h) (n=5). Across Reporter, CreN-nMag, and pMag-CreC groups, there is no significant difference within each light condition (Dark, Ambient, Light). Recombination = percent of EGFP$^+$ cells. Blue light = 473 ± 29nm. Plotted mean ± s.d. of n independently tested groups, each with ≥ 10,000 cells analyzed by flow cytometry. P-values: *n.s.* $p > 0.05$, (*) $p \leq 0.05$, (**) $p \leq 0.01$, (***) $p \leq 0.001$ using heteroscedastic two-tailed Student's *t*-Test.

Figure 4.6: Design and optimization of TamPA-Cre in HEK293T cells. (A) Schematic of *TamPA-Cre* in single genetic construct with codon-diversified *pMag* and marker *P2A-mCh* (top). Schematic of TamPA-Cre split into two genetic constructs: *ERT2-CreN-nMag* with marker *P2A-mCh* (bottom left) and *NLS-pMag-CreC* with marker *tBFP-P2A* (bottom right). (B) Schematic of mechanism of tamoxifen- AND blue-light-gated TamPA-Cre (described in manuscript). (C) Schematic illustrating two different light protocols that provide equal amounts of blue light energy (not to scale). Protocol A: 3h of continuous blue light stimulation (5 W/m^2) started together with the addition of 500 nM 4-OHT. Protocol B: 24h of pulsatile blue light stimulation (5 W/m^2, pattern: [7.5s on, 52.5s off]) started 3h after the addition of 500 nM 4-OHT. (D) EGFP Reporter HEK293T cells transiently transfected with TamPA-Cre were exposed to either light Protocol A or Protocol B. Dark (wrapped with foil) and Ambient (no foil) groups did not received blue light treatment. Recombination was measured 96h post-transfection (n=3). (E) EGFP Reporter HEK293T cells transiently transfected with TamPA-Cre-nMagHigh1 were subjected to Protocol B, as described in (C) (n=3). Unlike plates in the Dark condition, plates in the Ambient condition were not protect from ambient room light with aluminum foil post-transfection. Dot plots indicate recombination (% EGFP+ cells normalized to the initial % of cells for the corresponding Cre groups) in each of n independently tested groups of cells, including mean ± s.d. P-values: n.s. $p > 0.05$, *$p \leq 0.05$, **$p \leq 0.01$, ***$p \leq 0.001$ using heteroscedastic two-tailed Student's t-Test.

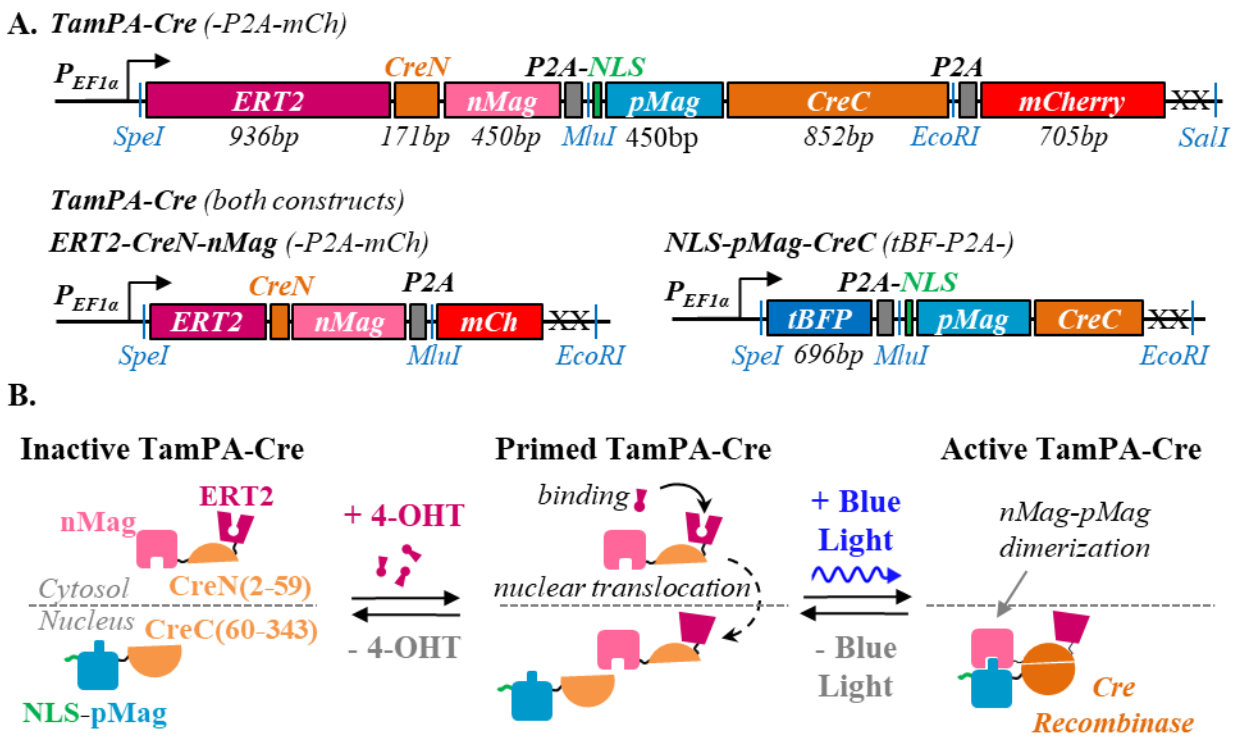
A. TamPA-Cre (-P2A-mCh)
P EF1α
CreN
P2A-NLS
P2A
ERT2
nMag
pMag
CreC
mCherry
XX
SpeI
936bp
171bp
450bp
MluI
450bp
852bp
EcoRI
705bp
SalI
TamPA-Cre (both constructs)
ERT2-CreN-nMag (-P2A-mCh)
P EF1α
CreN
P2A
ERT2
nMag
mCh
XX
SpeI
MluI
EcoRI
NLS-pMag-CreC (tBF-P2A-)
P EF1α
P2A-NLS
tBFP
pMag
CreC
XX
SpeI
696bp
MluI
EcoRI
B.
Inactive TamPA-Cre
Primed TamPA-Cre
Active TamPA-Cre
nMag
ERT2
Cytosol
CreN(2-59)
Nucleus
CreC(60-343)
NLS-pMag
+ 4-OHT
- 4-OHT
binding
nuclear translocation
+ Blue Light
- Blue Light
nMag-pMag dimerization
Cre Recombinase
C.
Protocol A:
4-OHT
-3h
0
3h
24h
Irradiance: 5 W/m²
Delay After 4-OHT: None
Pattern: Continuous
Duration of pattern: 3h
Total Time Light On: 3h
Protocol B:
4-OHT
-3h
0
24h
Irradiance: 5 W/m²
Delay After 4-OHT: 3h
Pattern: Pulsatile (7.5s on, 52.5s off)
Duration of pattern: 24h
Total Time Light On: 3h
D.
Recombination (Norm. % EGFP+)
Dark
Ambient
Light
*
n.s.
**
4-OHT:
Protocol A
Protocol B
TamPA-Cre
E.
Recombination (Norm. % EGFP+)
Dark
Ambient
Light
**
**
**
4-OHT:
Reporter
TamPA-Cre-nH1

A.

```
Alignment of nMag CDS with pMag CDS
Similarity : 446/450 (99.11 %)
                H  T  L  Y  A  P  G  G  Y  D  I  M  G  Y  L   D  Q  I  G  N
nMag    1       CATACTCTTTATGCCCCCGGTGGATATGACATTATGGGATATCTG-GACCAGATCGGCAA  59
                ||||||||||||||||||||||||||||||||||||||||||||#|##|||||||#|#||
pMag    1       CATACTCTTTATGCCCCCGGTGGATATGACATTATGGGATATCTGAGG-CAGATCAGGAA  59
                H  T  L  Y  A  P  G  G  Y  D  I  M  G  Y  L  R   Q  I  R  N
                 R  P  N  P  Q  V  E  L  G  P  V  D  T  S  C  A  L  I  L  C
nMag   60       CCGGCCAAACCCGCAGGTGGAACTGGGCCCCGTGGATACATCCTGCGCCTTGATTCTTTG  119
                ||||||||||||||||||||||||||||||||||||||||||||||||||||||||||||
pMag   60       CCGGCCAAACCCGCAGGTGGAACTGGGCCCCGTGGATACATCCTGCGCCTTGATTCTTTG  119
                 R  P  N  P  Q  V  E  L  G  P  V  D  T  S  C  A  L  I  L  C
                 D  L  K  Q  K  D  T  P  I  V  Y  A  S  E  A  F  L  Y  M  T
nMag   120      TGACCTGAAACAGAAAGACACCCCGATAGTTTACGCGAGTGAAGCCTTCCTCTACATGAC  179
                ||||||||||||||||||||||||||||||||||||||||||||||||||||||||||||
pMag   120      TGACCTGAAACAGAAAGACACCCCGATAGTTTACGCGAGTGAAGCCTTCCTCTACATGAC  179
                 D  L  K  Q  K  D  T  P  I  V  Y  A  S  E  A  F  L  Y  M  T
                 G  Y  S  N  A  E  V  L  G  R  N  C  R  F  L  Q  S  P  D  G
nMag   180      AGGTTACAGCAACGCAGAGGTGCTGGGCCGGAATTGCCGGTTTCTGCAAAGCCCTGACGG  239
                ||||||||||||||||||||||||||||||||||||||||||||||||||||||||||||
pMag   180      AGGTTACAGCAACGCAGAGGTGCTGGGCCGGAATTGCCGGTTTCTGCAAAGCCCTGACGG  239
                 G  Y  S  N  A  E  V  L  G  R  N  C  R  F  L  Q  S  P  D  G
                 M  V  K  P  K  S  T  R  K  Y  V  D  S  N  T  I  N  T  M  R
nMag   240      CATGGTGAAGCCCAAGAGCACCCGGAAGTACGTGGATAGTAACACAATCAATACTATGCG  299
                ||||||||||||||||||||||||||||||||||||||||||||||||||||||||||||
pMag   240      CATGGTGAAGCCCAAGAGCACCCGGAAGTACGTGGATAGTAACACAATCAATACTATGCG  299
                 M  V  K  P  K  S  T  R  K  Y  V  D  S  N  T  I  N  T  M  R
                 K  A  I  D  R  N  A  E  V  Q  V  E  V  V  N  F  K  K  N  G
nMag   300      CAAGGCAATCGACAGGAATGCCGAGGTGCAGGTTGAAGTAGTCAATTTTAAAAAGAATGG  359
                ||||||||||||||||||||||||||||||||||||||||||||||||||||||||||||
pMag   300      CAAGGCAATCGACAGGAATGCCGAGGTGCAGGTTGAAGTAGTCAATTTTAAAAAGAATGG  359
                 K  A  I  D  R  N  A  E  V  Q  V  E  V  V  N  F  K  K  N  G
                 Q  R  F  V  N  F  L  T  M  I  P  V  R  D  E  T  G  E  Y  R
nMag   360      ACAGCGATTTGTTAATTTCCTGACTATGATACCTGTTAGGGACGAAACAGGCGAGTATCG  419
                ||||||||||||||||||||||||||||||||||||||||||||||||||||||||||||
pMag   360      ACAGCGATTTGTTAATTTCCTGACTATGATACCTGTTAGGGACGAAACAGGCGAGTATCG  419
                 Q  R  F  V  N  F  L  T  M  I  P  V  R  D  E  T  G  E  Y  R
                 Y  S  M  G  F  Q  C  E  T  E
nMag   420      ATACTCTATGGGATTCCAGTGCGAAACAGAA  450
                ||||||||||||||||||||||||||||||
pMag   420      ATACTCTATGGGATTCCAGTGCGAAACAGAA  450
                 Y  S  M  G  F  Q  C  E  T  E
```

Figure 4.7: Diversification of the pMag CDS. (A) DNA sequence alignment of nMag and pMag (Serial Cloner 2.6.1) from PA-Cre[48] showing that the CDS for each are nearly identical and are thus susceptible potential recombination introduced by lentiviral gene transfer.[68] (B) DNA sequence alignment of pMag with codon-diversified dpMag (Serial Cloner 2.6.1). Reduced sequence similarity helps prevent potential recombination introduced by lentiviral gene transfer.[68] Codon diversification of the pMag CDS was done by hand and synthesized dpMag dsDNA (Integrated DNA Technologies, IA) was used for subsequent molecular cloning.

B.

```
Alignment of pMag CDS with dpMag CDS(codon-diversified)
Similarity : 308/450 (68.44 %)
             H  T  L  Y  A  P  G  G  Y  D  I  M  G  Y  L  R  Q  I  R  N
pMag   1     CATACTCTTTATGCCCCCGGTGGATATGACATTATGGGATATCTGAGGCAGATCAGGAAC  60
             ||#||#||#||#||#||#||#||#||#||#||#||#||##||#||#||#||#||#||#||#
dpMag  1     CACACACTGTACGCTCCAGGCGGATACGATATAATGGGCTACTTGAGGCAAATAAGGAAT  60
             H  T  L  Y  A  P  G  G  Y  D  I  M  G  Y  L  R  Q  I  R  N
             R  P  N  P  Q  V  E  L  G  P  V  D  T  S  C  A  L  I  L  C
pMag  61     CGGCCAAACCCGCAGGTGGAACTGGGCCCCGTGGATACATCCTGCGCCTTGATTCTTTGT  120
             ||#||#||#||#||#||#||#||#||#||#||#||#||#||##||#||#||#||#||#||#
dpMag 61     CGACCTAATCCTCAGGTAGAGCTTGGGCCTGTTGACACAAGCTGTGCCCTGATCCTGTGC  120
             R  P  N  P  Q  V  E  L  G  P  V  D  T  S  C  A  L  I  L  C
             D  L  K  Q  K  D  T  P  I  V  Y  A  S  E  A  F  L  Y  M  T
pMag  121    GACCTGAAACAGAAAGACACCCCGATAGTTTACGCGAGTGAAGCCTTCCTCTACATGACA  180
             ||#||#||#||#||#||#||#||#||#||#||#||#||#||#||#||#||#||#||#||#
dpMag 121    GATCTCAAGCAAAAGGATACACCAATCGTGTATGCAAGCGAGGCGTTTCTGTATATGACC  180
             D  L  K  Q  K  D  T  P  I  V  Y  A  S  E  A  F  L  Y  M  T
             G  Y  S  N  A  E  V  L  G  R  N  C  R  F  L  Q  S  P  D  G
pMag  181    GGTTACAGCAACGCAGAGGTGCTGGGCCGGAATTGCCGGTTTCTGCAAAGCCCTGACGGC  240
             ||#||#||#||#||#||#||##||||##||||#||#||#||##||||####||#||#||#
dpMag 181    GGATATAGTAATGCTGAAGTATTGGGAAGGAACTGTCGCTTCTTGCAGTCTCCCGATGGT  240
             G  Y  S  N  A  E  V  L  G  R  N  C  R  F  L  Q  S  P  D  G
             M  V  K  P  K  S  T  R  K  Y  V  D  S  N  T  I  N  T  M  R
pMag  241    ATGGTGAAGCCCAAGAGCACCCGGAAGTACGTGGATAGTAACACAATCAATACTATGCGC  300
             |||||#||#||#||###||#||#|||||#||#||#||#||#||#||#||#||#|||#|#
dpMag 241    ATGGTTAAACCAAAATCCACACGAAAGTATGTTGACAGCAATACTATTAACACCATGAGA  300
             M  V  K  P  K  S  T  R  K  Y  V  D  S  N  T  I  N  T  M  R
             K  A  I  D  R  N  A  E  V  Q  V  E  V  V  N  F  K  K  N  G
pMag  301    AAGGCAATCGACAGGAATGCCGAGGTGCAGGTTGAAGTAGTCAATTTTAAAAAGAATGGA  360
             ||#||#||#||##|||#||#||#||#||#||#||#||#||#||#||#||#||#||#||#||#
dpMag 301    AAAGCTATTGATCGGAACGCGGAAGTCCAAGTGGAGGTCGTGAACTTCAAGAAAAACGGC  360
             K  A  I  D  R  N  A  E  V  Q  V  E  V  V  N  F  K  K  N  G
             Q  R  F  V  N  F  L  T  M  I  P  V  R  D  E  T  G  E  Y  R
pMag  361    CAGCGATTTGTTAATTTCCTGACTATGATACCTGTTAGGGACGAAACAGGCGAGTATCGA  420
             ||##|||#||#||#||#||#||#|||#||#||#||#||#||#||#||#||#||#||#||#
dpMag 361    CAAAGATTCGTCAACTTTCTTACCATGATCCCAGTGAGAGATGAGACCGGAGAATACCGG  420
             Q  R  F  V  N  F  L  T  M  I  P  V  R  D  E  T  G  E  Y  R
             Y  S  M  G  F  Q  C  E  T  E
pMag  421    TACTCTATGGGATTCCAGTGCGAAACAGAA  450
             ||#||#|||||#||#||#||#||#||#||#
dpMag 421    TATTCAATGGGCTTTCAATGTGAGACCGAG  450
             Y  S  M  G  F  Q  C  E  T  E
```

Figure 4.7: Diversification of the pMag CDS, Continued.

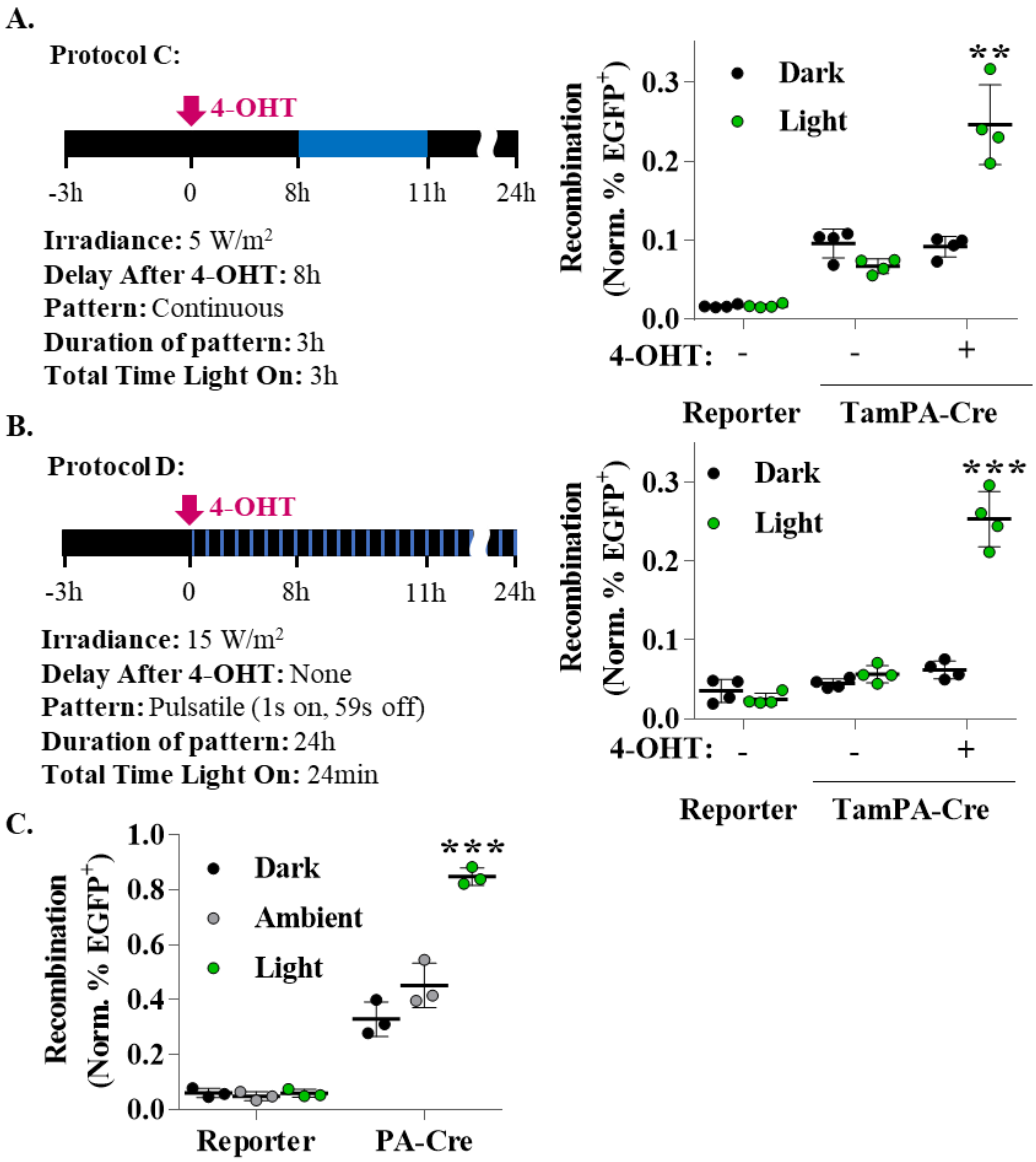

Figure 4.8: Optimizing TamPA-Cre recombination efficiency through different tamoxifen- and blue light stimulation protocols. (A,B) Schematic illustrating the tamoxifen- and blue light stimulation protocols along with the experimental results of EGFP Reporter HEK293T cells transiently transfected with TamPA-Cre or Cre constructs that were (Light) or were not (Dark) exposed to blue light stimulation outlined in (A) Protocol C: (5 W/m^2, continuous, 3h) started 8h after 4-OHT addition (n=4), or (B) Protocol D: (15 W/m^2, pulsatile: [7.5s on, 52.5s off], 24h) started with 4-OHT addition. Delaying blue light stimulation after 4-OHT addition and changing to a pulsatile blue light pattern improved TamPA-Cre performance. (C) For comparison, EGFP Reporter HEK293T cells transiently transfected with PA-Cre or Cre construct were (Light) or were not (Dark, Ambient) exposed to Protocol B: (5 W/m^2, pattern: [7.5s on, 52.5s off], 24h) started 3h after 4-OHT addition (n=3). Reporter = untransfected EGFP Reporter HEK293T cell line. Recombination = % EGFP$^+$ cells normalized to mean of corresponding Cre group, measured 96h post-transfection. Plotted mean ± s.d. of n independently tested groups, each with ≥ 10,000 cells analyzed by flow cytometry. P-values: n.s. $p > 0.05$, (*) $p \leq 0.05$, (**) $p \leq 0.01$, (***) $p \leq 0.001$ using heteroscedastic two-tailed Student's t-Test.

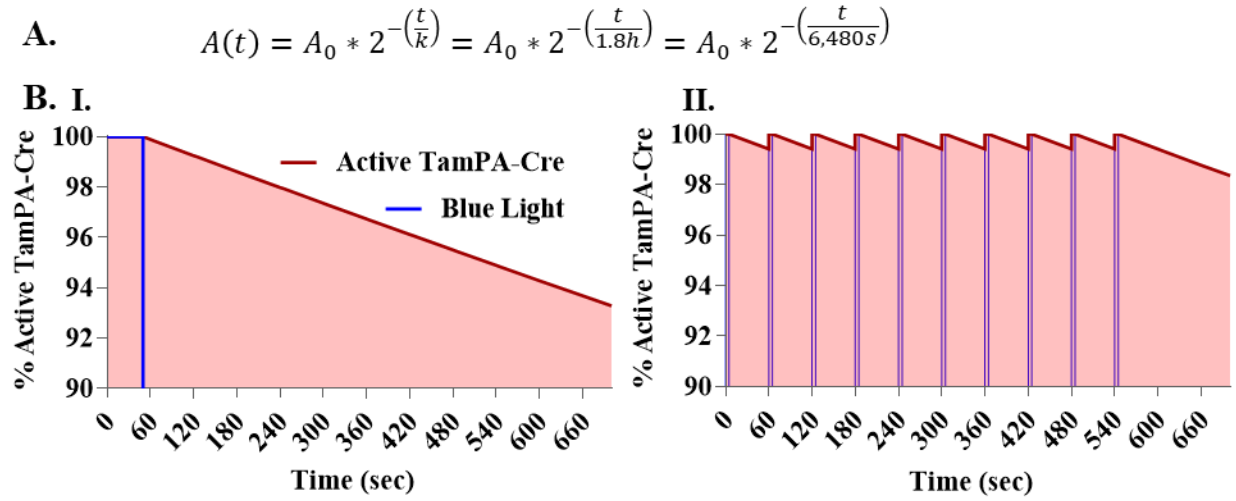

Figure 4.9: Pulsatile blue light stimulation protocols improve Cre-loxP recombination efficiency due to slow nMag-pMag degradation kinetics. (A) Blue light-induced heterodimerization between nMag and pMag proteins occurs rapidly, while nMag-pMag heterodimers dissociate exponentially with a half-life of ~1.8h upon the removal of blue light stimulation (Kawano, Suzuki et al. 2015). From an initial heterodimer concentration of A_0, the remaining heterodimer concentration after the blue light stimulus is removed can be calculated as a function of time using the exponential decay equation where the half-life k is equal to 1.8h or 6,480s. Such slow degradation kinetics maintain the percentage of active TamPA-Cre above 99.0% 93s after blue light is removed. (B) The plots track the theoretical percentage of active TamPA-Cre in tamoxifen-induced cells given 50s of continuous blue light stimulation (I) or given ten 5-second pulses of (equivalent intensity) blue light stimulation, each pulse separated by 55s of darkness (II). 700 second after the beginning of each blue light stimulation protocol, only 93.28% of maximal active TamPA-Cre levels remain given 10s of continuous light, while 98.36% of maximal active TamPA-Cre is still present to drive recombination given the pulsatile protocol. The area under the % Active TamPA-Cre curve (shaded red) is proportional to the probability that a given cell will undergo Cre-loxp recombination over a given time interval. From these graphs, it is obvious that the area under to curve for the pulsatile blue light stimulation (II) is greater than for continuous blue light stimulation (I), thus increasing the chances that a given cell will undergo TamPA-Cre mediated Cre-loxp recombination.

Figure 4.10: CAR-mediated T cell activation is antigen specific at low CAR expression levels. (A) Schematic representation of the *α-CD19CAR-EGFP* and the *myc-α-CD38Receptor-EGFP* genetic constructs. The hEF1α promoter drives constitutive expression of *α-CD19CAR* or *myc-α-CD38Receptor*. (*pSin_hEF1α_α-CD19CAR-ggsggt-EGFP_IRES_PuroR,* or *pSin_hEF1α_myc_α-CD38Receptor-ggsggt-EGFP_IRES_PuroR*). (B) Jurkat T cells and α-CD19CAR-EGFP$^+$ Jurkat T cells were co-incubated with an equal number of either CD19$^-$ K562 Target cells, CD19$^+$ Toledo Target cells, or no Target cells for 24h after which the percentage of activated (% CD69$^+$) Jurkat T cells was measured via flow cytometry (n=3). Only α-CD19CAR$^+$ Jurkat T cells co-incubated with CD19$^+$ Toledo Target cells were significantly activated (81.1 ± 0.35 %). Co-incubation with either no Target cells or CD19$^-$ K562 Target cells yielded similar results, indicating that CAR-mediated T cell activation is not affected by the presence or absence of TAA$^-$ Target cells. (C) A portion of Jurkat T cells expressing low levels of α-CD19CAR-EGFP can undergo non-specific T cell activation (blue), which increases with higher expression levels (green). Histograms show representative results from multiple experiments. (D) Representative histograms from flow cytometry measurement of CAR Reporter Jurkat cell line (red) transduced with either CreN-nMag-NLS-P2A-mCh (yellow), ERT2-CreN-nMag-P2A-mCh (green), or tBFP-P2A-pMag-CreC (blue) constructs. All CAR Reporter Jurkat T cells express myc-α-CD38Receptor (left) and do not express α-CD19 CAR-EGFP. Non-transduced Jurkat T cells (black) shown for reference. (E) PA-Cre$^+$ and TamPA-Cre$^+$ CAR Reporter Jurkat cell lines were exposed to the Ambient light condition. Recombination (% CAR-EGFP$^+$) was measured before and after via flow cytometry (n=3). After 48h, PA-Cre had driven a significant increase in recombination while no such change was seen in TamPA-Cre groups. The increase in PA-Cre groups is likely due to a combination of spontaneous and ambient light-driven recombination. Recombination = % CAR-EGFP$^+$ cells. Dot plots show mean ± s.d. of n independently tested groups, each with ≥ 10,000 cells analyzed by flow cytometry. P-values: n.s. $p > 0.05$, (*) $p \leq 0.05$, (**) $p \leq 0.01$, (***) $p \leq 0.001$ using heteroscedastic two-tailed Student's t-Test.

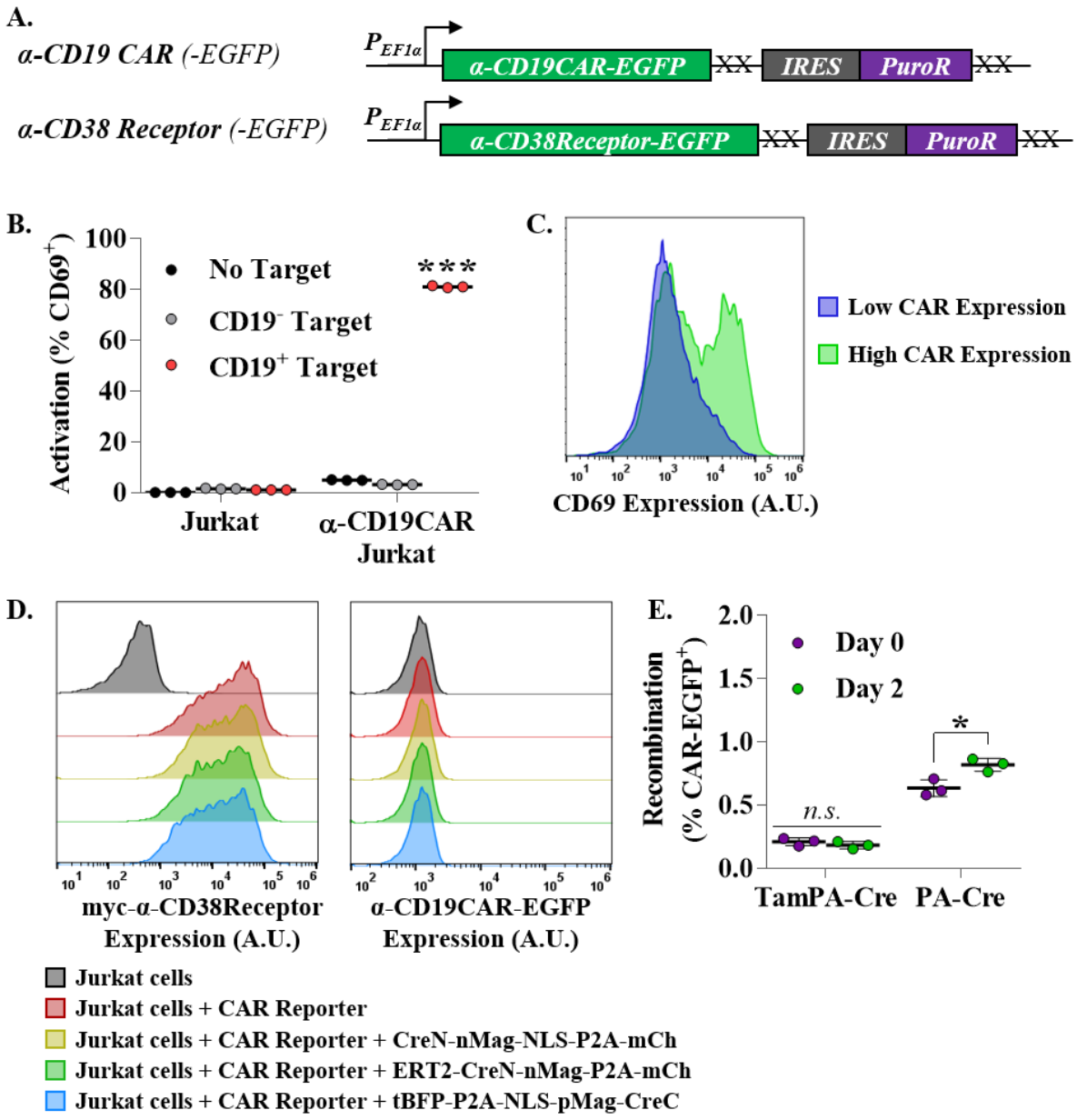
A.
α-CD19 CAR (-EGFP)
P EF1α
α-CD19CAR-EGFP
XX
IRES
PuroR
XX
α-CD38 Receptor (-EGFP)
P EF1α
α-CD38Receptor-EGFP
XX
IRES
PuroR
XX
B.
Activation (% CD69+)
100
80
60
40
20
0
No Target
CD19- Target
CD19+ Target
***
Jurkat
α-CD19CAR Jurkat
C.
Low CAR Expression
High CAR Expression
CD69 Expression (A.U.)
D.
myc-α-CD38Receptor Expression (A.U.)
α-CD19CAR-EGFP Expression (A.U.)
Jurkat cells
Jurkat cells + CAR Reporter
Jurkat cells + CAR Reporter + CreN-nMag-NLS-P2A-mCh
Jurkat cells + CAR Reporter + ERT2-CreN-nMag-P2A-mCh
Jurkat cells + CAR Reporter + tBFP-P2A-NLS-pMag-CreC
E.
Recombination (% CAR-EGFP+)
2.0
1.5
1.0
0.5
0.0
Day 0
Day 2
n.s.
*
TamPA-Cre
PA-Cre

A.

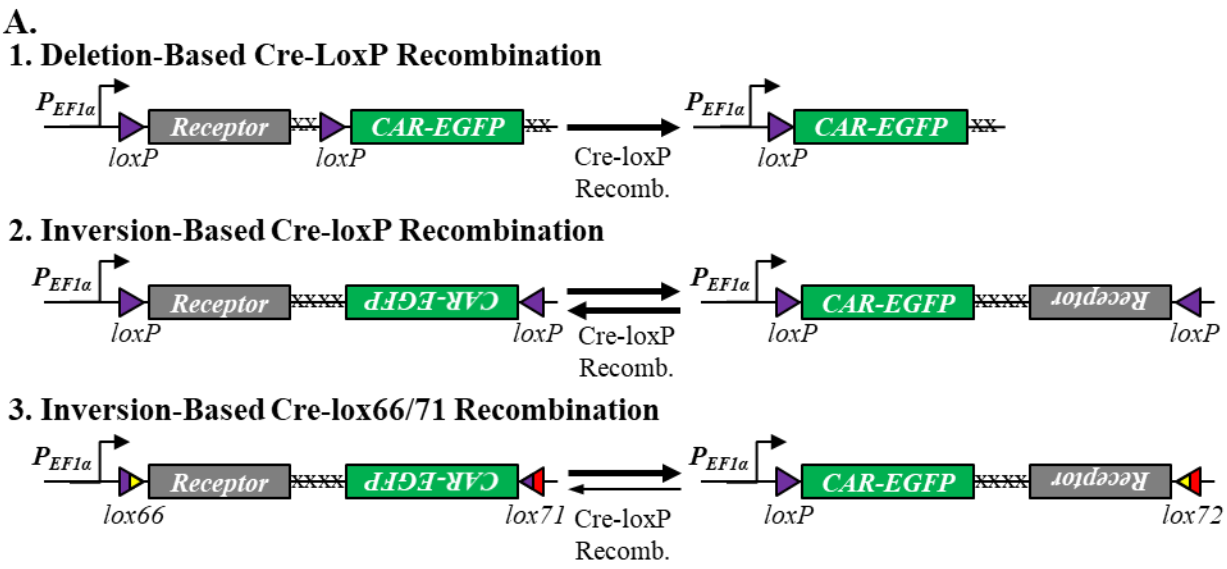

B.

	1. Cre-loxP Deletion	2. Cre-loxP Inversion	3. Cre-lox66/71 Inversion
Recombination	**Irreversible**	**Reversible**	**Mostly Irreversible**
Pre-recombination fraction of CAR⁺ cells	+ + (high copy) - (low copy)	- (high copy) - (low copy)	- (high copy) - (low copy)
Post-recombination fraction of CAR⁺ cells	+ + + + (high copy) + + + + (low copy)	+ + (high copy) + + (low copy)	+ + + (high copy) + + + (low copy)
Post-recombination CAR expression level	+ + + + (high copy) + + (low copy)	+ + (high copy) + (low copy)	+ + (high copy) + (low copy)

Figure 4.11: Testing different Cre-loxP CAR Reporter designs. (A) Three different Cre-loxP CAR Reporter constructs were evaluated: (1) deletion-based (irreversible), (2) inversion-based (reversible), and (3) inversion based with loxP mutant sites lox66 and lox71 (mostly irreversible). Ideally, receptor expression would not be turned off. However, due to lentiviral packaging size restraints, only one promoter could be used. As efficiency improves, other gene insertion methods (e.g. CRISPR-Cas9) will undoubtedly allow for larger, more complex designs. (B) Qualitative summary of Cre-, PA-Cre-, and TamPA-Cre-mediated recombination experiments that were conducted in both HEK293T and Jurkat T cells expressing high (high copy) or low (low copy) levels of each CAR Reporter construct. While inversion-based CAR Reporters had the advantage of preventing all background CAR-EGFP expression before recombination, deletion-based CAR Reporter functions similarly at low copy number while providing higher expression levels of CAR-EGFP after recombination.

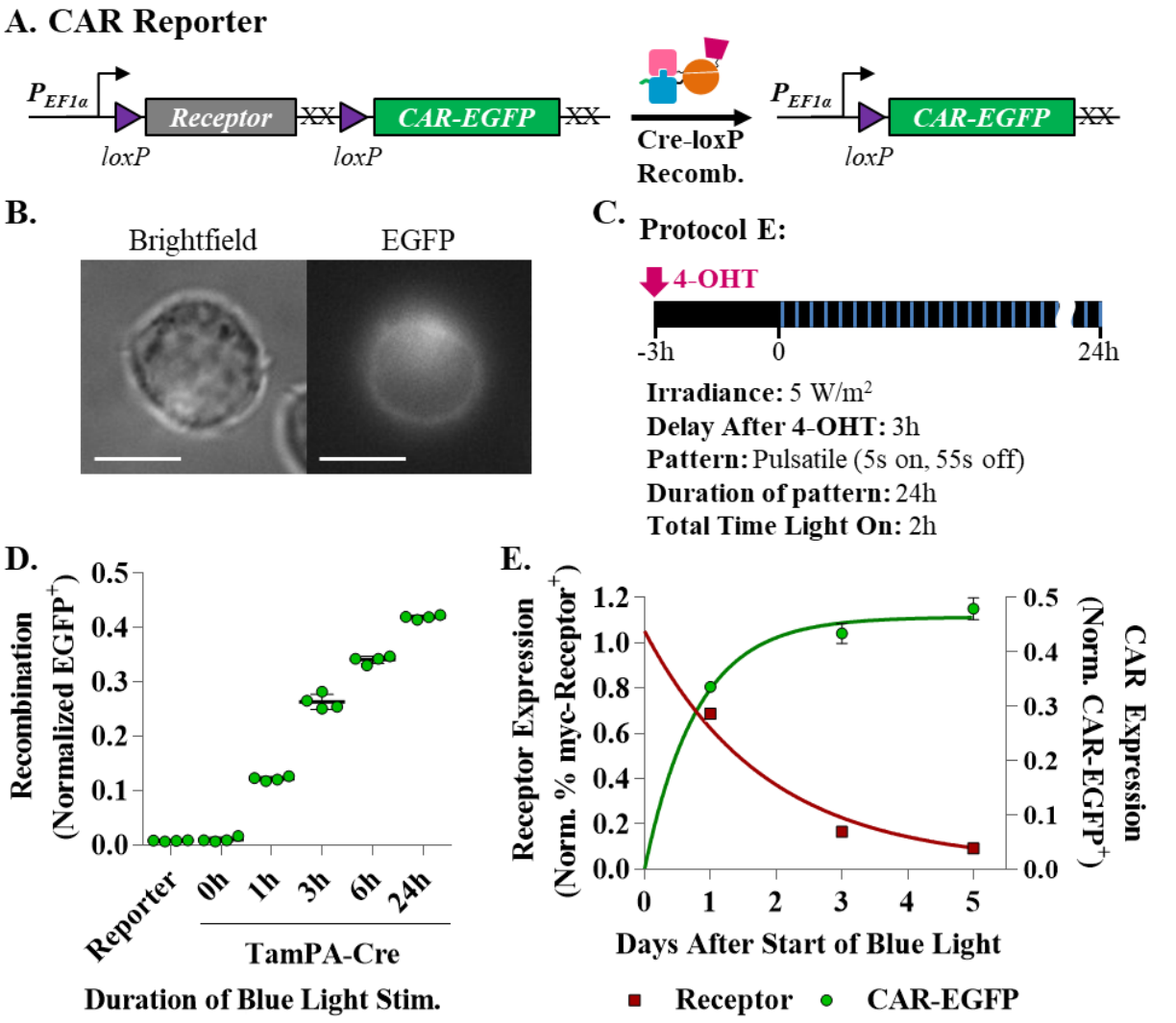

Figure 4.12: TamPA-Cre drives CAR expression with tamoxifen and blue light stimulation. (A) Schematic of CAR Reporter construct before and after Cre-loxP recombination. Expression of *myc-α-CD38Receptor* is driven under the hEF1α promoter. During Cre-loxP recombination, the floxed *myc-α-CD38Receptor* (with stop codons, XX) is irreversibly excised allowing for (B) α-CD19CAR-EGFP expression (Jurkat cell, 100x, scale bar = 10μm). (C) Schematic illustrating stimulation of Protocol E: (5 W/m^2, pulsatile: [5s on, 55s off], 24h) started 3h after 4-OHT addition. (D) TamPA-Cre$^+$ CAR Reporter Jurkat T cells exposed to Protocol E, but for a duration of 0, 1, 3, 6, or 24h (n=4). (E) TamPA-Cre$^+$ CAR Reporter Jurkat T cells exposed to Protocol E, measured for expression 1, 3, and 5 days after start of blue light stimulation, fitted with exponential decay and association trendlines (GraphPad, see Table S2 for details) (n=4). Reporter = CAR Reporter Jurkat cell line. 4-OHT (500nM). Blue light = 473 ± 29nm, stimulation started 24h post-transfection. Recombination = percentage of α-CD19CAR-EGFP$^+$ cells normalized to initial mean percentage of CAR Reporter$^+$ cells. Recombination measured 72h after start of blue light stimulation. Expression = percentage of myc-α-CD38Receptor$^+$ and α-CD19CAR-EGFP$^+$ cells normalized to the initial mean percentage of CAR Reporter$^+$ cells. Plotted mean ± s.d. of n independently tested groups, each with ≥ 10,000 cells analyzed by flow cytometry. P-values: *n.s.* $p > 0.05$, (*) $p \leq 0.05$, (**) $p \leq 0.01$, (***) $p \leq 0.001$ using heteroscedastic two-tailed Student's *t*-Test.

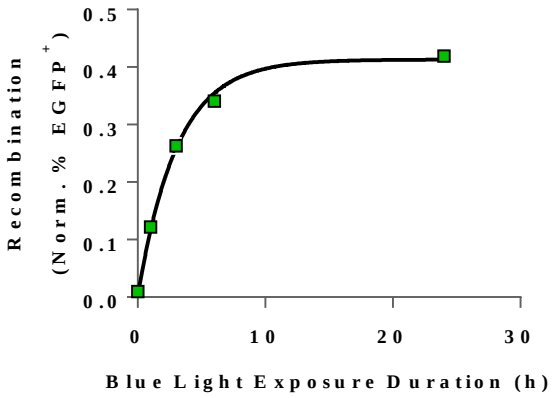

Figure 4.13: Cre-loxP recombination in TamPA-Cre CAR Reporter Jurkat T cells plateaus between 6h and 24h of blue light stimulation. Alternate graphical representation of Figure 4.12D with non-linear fit exponential growth trendline. See Table 4.2 for details.

Table 4.2: Non-linear Fit Trendline Information. Parameters of non-linear fit trendlines in Fig. 4.12E and 4.13 (GraphPad Prism 7.04).

Non-linear Fit for Fig. 4.13	
One phase exponential association	Y=Ymax*(1-exp(-K*X))
Best-fit values	
Ymax	0.413
K	0.3253
HalfLife	2.131
Std. Error	
Ymax	0.005569
K	0.01258
95% CI (profile likelihood)	
Ymax	0.4012 to 0.4251
K	0.2992 to 0.3546
HalfLife	1.955 to 2.317
Goodness of Fit	
Degrees of Freedom	18
R square	0.9942
Absolute Sum of Squares	0.002519
Sy.x	0.01183
Constraints	
K	K > 0
Number of points	
# of X values	20
# Y values analyzed	20
Non-linear Fit for Fig. 4.12E (Receptor Expression)	
One phase exponential decay	Y=Span*exp(-K*X) + Plateau
Best-fit values	
Span	= 1.026
K	0.542
Plateau	0.02641
HalfLife	1.279
Std. Error	
K	0.1417
Plateau	0.07495
95% CI (profile likelihood)	
K	0.3583 to 0.7395
Plateau	-0.1024 to 0.1169
HalfLife	0.9373 to 1.934

Non-linear Fit for Fig. 4E (Receptor Expression) Continued	
Goodness of Fit	
Plateau	-0.1024 to 0.1169
HalfLife	0.9373 to 1.934
Goodness of Fit	
Degrees of Freedom	10
R square	0.9571
Absolute Sum of Squares	0.03617
Sy.x	0.06014
Constraints	
Span	Span = 1.026
K	K > 0
Number of points	
# of X values	12
# Y values analyzed	12
Non-linear Fit for Fig. 4.12E (CAR Expression)	
One phase exponential association	Y=Ymax*(1-exp(-K*X))
Best-fit values	
Ymax	0.4643
K	1.251
HalfLife	0.554
Std. Error	
Ymax	0.008901
K	0.102
95% CI (profile likelihood)	
Ymax	0.4446 to 0.4851
K	1.039 to 1.523
HalfLife	0.455 to 0.6673
Goodness of Fit	
Degrees of Freedom	10
R square	0.8925
Absolute Sum of Squares	0.004884
Sy.x	0.0221
Constraints	
K	K > 0
Number of points	
# of X values	12
# Y values analyzed	12

Figure 4.14: TamPA-Cre drives CAR-mediated T cell activation. (A) Schematic of the tamoxifen- and blue light-induced TamPA-Cre system in CAR Reporter T cells driving recombination and CAR-mediated T cell activation upon binding to TAA^+ Target cells. (B) PA-Cre^+ or (C) TamPA-Cre^+ CAR Reporter Jurkat T cells either were (+ 4-OHT) or were not (- 4-OHT) exposed to tamoxifen, and either were (Light) or were not (Dark) exposed to blue light stimulation following Protocol E (n=4). 48h after the start of blue light stimulation, all samples from (B) and (C) were split into groups that either were (+ Target) or were not (- Target) co-incubated with $CD19^+$ Target cells (1:1) over the next 24h, as reported in (D) and (E) respectively. (n=4). (F) A heat map summary of T cell activation in Reporter, PA-Cre, and TamPA-Cre groups showing the mean of normalized CD69+ cells. Higher activation levels are indicated in red while lower levels are shown in green. Recombination and Activation = percentage of CAR-$EGFP^+$ or $CD69^+$ cells, respectively, normalized to the initial mean percentage of CAR $Reporter^+$ cells, both measured 72h after the start of blue light stimulation. Reporter = CAR Reporter Jurkat cell line. 4-OHT = 500nM. Blue light = 473 ± 29 nm. Plotted mean ± s.d. of n independently tested groups, each with ≥ 10,000 cells analyzed by flow cytometry. P-values: *n.s.* $p > 0.05$, (*) $p \leq 0.05$, (**) $p \leq 0.01$, (***) $p \leq 0.001$ using heteroscedastic two-tailed Student's *t*-Test.

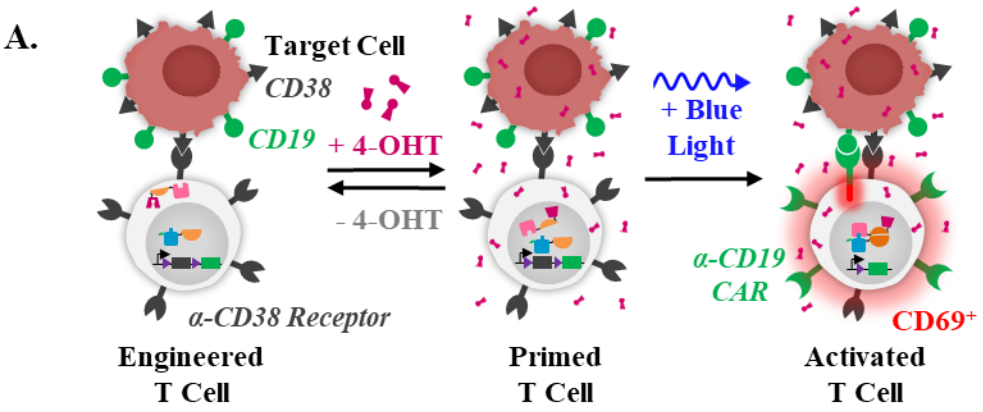

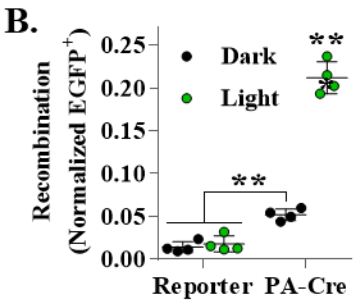

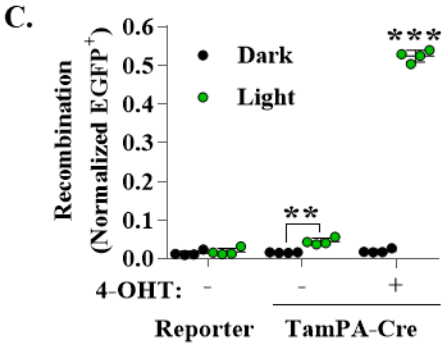

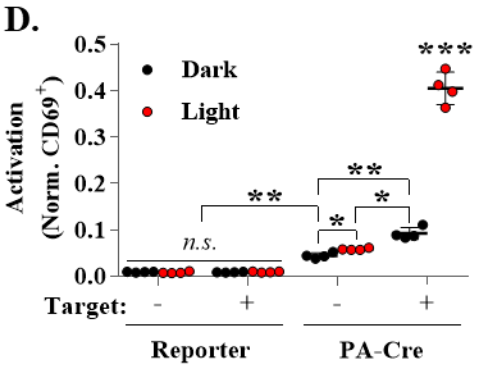

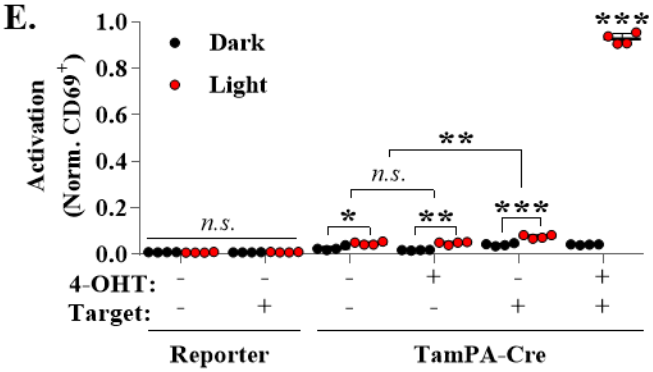

F.

Activation		Reporter	PA-Cre	TamPA-Cre	
		- Tam	- Tam	- Tam	+ Tam
Dark	- Target	0.0088	0.0444	0.0264	0.0179
	+ Target	0.0088	0.0925	0.0418	0.0416
Light	- Target	0.0081	0.0583	0.0472	0.0483
	+ Target	0.0094	0.4055	0.0762	0.9268

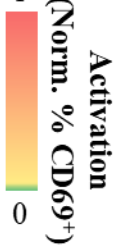

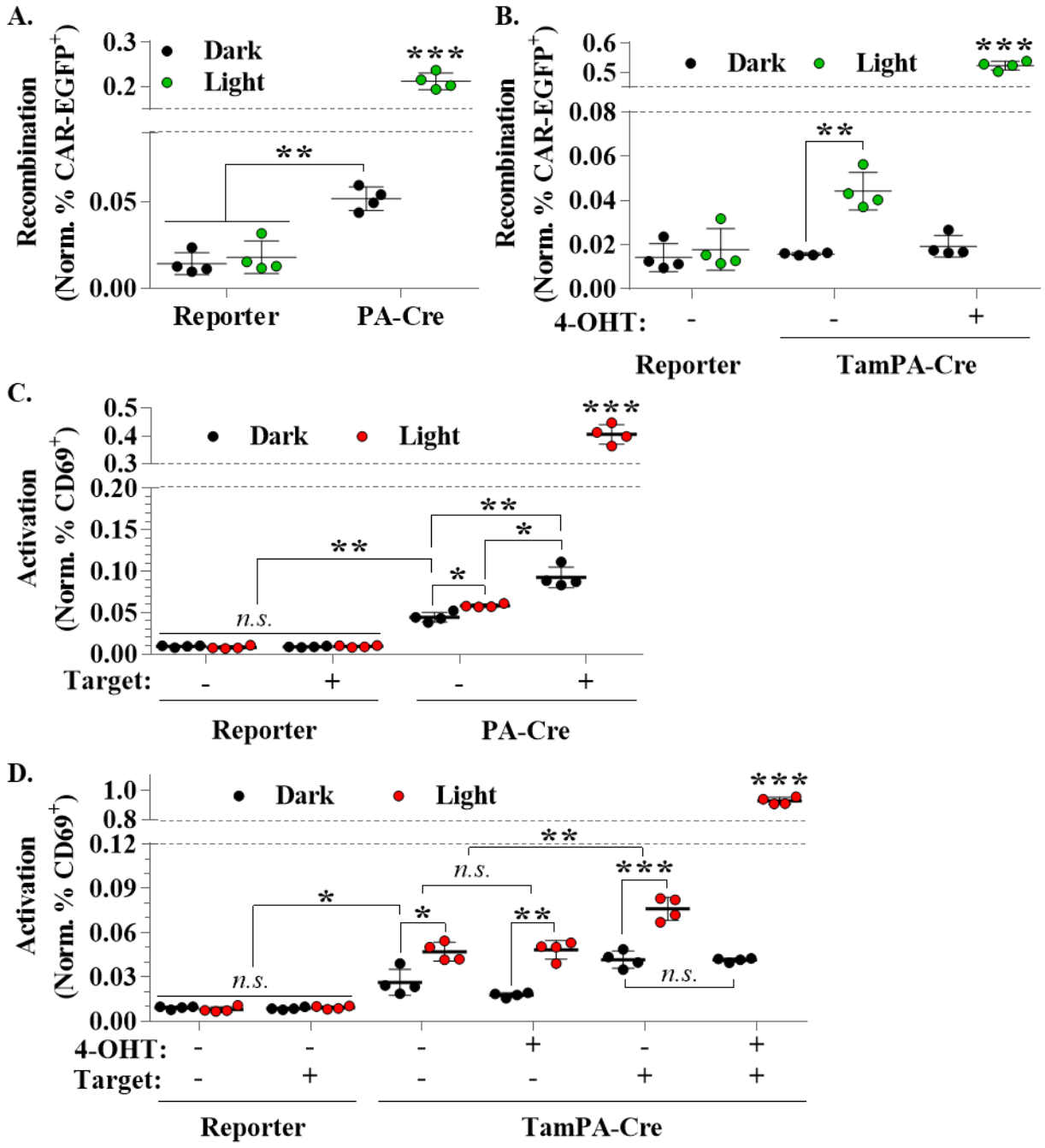

Figure 4.15: Expanded lower range of plots in Fig. 4.14B-E. 4.15A = 4.14B, 4.15B = 4.14C, 4.15C = 4.14D, 4.15D = 4.14E. Plotted mean ± s.d. of n independently tested groups, each with ≥ 10,000 cells analyzed by flow cytometry. P-values: *n.s.* $p > 0.05$, (*) $p \leq 0.05$, (**) $p \leq 0.01$, (***) $p \leq 0.001$ using heteroscedastic two-tailed Student's *t*-Test.

4.5 Acknowledgements

Chapter 4, in part, is currently being prepared for submission for publication of the material as it may appear in ACS Synthetic Biology, 2019, Thangaraj, Jeyan; Kyriakakis, Phillip; Pan, Yijia; Limsakul, Praopim; Wu, Yiqian; Huang, Ziliang; Wang, Yingxiao; Molly Elizabeth Allen was the primary investigator and author of this material.

CHAPTER 5:

Summary and Future Directions

In this dissertation, I documented my efforts to expedite CAR development and improve CAR T cell therapy safety using light to both detect and drive CAR-mediated T cell activation. I investigated the use of genetically encoded biosensors to rapidly detect CAR-mediated T cell activation within seconds or minutes of interacting with TAA^+ target cells. With future improvements to the dynamic fluorescence range of biosensors, data analysis techniques, and primary T cell gene delivery, biosensors may indeed expedite the process of CAR screening and development. I also pioneered the concept of using light stimulation to limit CAR T cell activity to the tumor site, thereby helping to bypass the challenge of on-target off-tumor toxicity in distant healthy tissues. I found that blue light-inducible transcription- and Cre-recombination-based optogenetic systems both drove premature CAR expression prior to light stimulation. In order to solve this problem, I developed a novel optogenetic tamoxifen- and photoactivatable split Cre system called TamPA-Cre that is capable of strictly regulating robust CAR expression in T cells.

Next-step experiments in mouse models will be necessary to validate TamPA-Cre system functionality *in vivo*. After demonstrating that the α-TAA Receptor allows intravenously-injected engineered T cells to bind to both spatially distinct TAA^+ tumor sites within an immunocompromised mouse model, this approach must show that tamoxifen-primed blue light stimulation localized to only one of the TAA^+ tumor sites drives exclusively local CAR expression and T cell effector cytotoxicity against TAA^+ cancer cells. CAR T cell cytotoxicity

can be assessed non-invasively by quantitatively measuring the size and intensity of both luciferase-expressing TAA^+ tumors over time.

In preparation for stimulating tumor sites deep within the body, it would be beneficial to demonstrate that the TamPA-Cre system can drive recombination in response to NIR lanthanide-doped up-conversion nanoparticles (UCNPs). Streptavidin-conjugated UCNPs capable of converting NIR light (980nm) into blue light (470nm) have already been used to successfully activate optogenetic LOV2-based proteins.[45] Therefore, it would stand to reason that using UCNPs targeted to cancerous tissues would allow for NIR-based non-invasive, localized blue light stimulation of locally attached engineered T cells deep within tissues.

However, I do anticipate facing some challenges in future experiments. Although relatively small without fluorescent protein tags (~1-2kb each), the *CAR*, *Receptor*, and both *TamPA-Cre* components must be reliably delivered into primary human T cells at the appropriate protein expression levels. Current standards of virus-based gene delivery systems are inefficient at introducing multiple genetic constructs into primary T cells simultaneously, let alone at precise copy numbers. Viral particles can also be toxic at high concentrations, and viral packaging limits constrain the size of deliverable genetic material. Non-specific genome insertion can also disrupt the expression of critical endogenous genes and potentially activate oncogenes. Despite the recent development of several optimized protocols,[86-87] direct introduction of construct-encoded nucleic acids and/or proteins into primary T cells via electroporation often kills a majority of T cells, and is increasingly toxic to cells when introducing greater amounts of DNA.

Fortunately, recent developments in CRISPR-Cas9 technology may overcome some of these limitations by allowing large genetic constructs to be integrated into the genome at safe,

and even beneficial loci.[73] Despite ongoing improvements, current CRISPR-Cas9 gene delivery technologies also become less efficient with more constructs. Furthermore, a CRISPR-Cas9-delivered single copy of TamPA-Cre genetic constructs will not likely be sufficient to drive the necessary high levels of protein expression. However, the TamPA-Cre-nH1 system (Fig. 4.6E) may prove functional at lower protein expression levels. Likewise, exchanging the TamPA-Cre Magnet domains for more efficiently-heterodimerizing nMagHigh1 and pMagHigh1 domains will likely further improve functionality at even lower protein expression levels. Additionally, this system would require even less frequent blue light stimulation due to the slower nMagHigh1-pMagHigh1 heterodimer decay rates (half-life: 4.7h).[77]

As is true of most synthetic protein constructs, there is a risk that the foreign Cre and Magnet protein fragments may trigger endogenous immunogenicity in humans. While immunosuppressive regimens are typically administered to patients prior to the infusion of engineered CAR T cells, the risk of long-term immunogenicity may impede clinical applications of the TamPA-Cre system in the near future. On the other hand, this issue is already common to many synthetic proteins, including the CRISPR-Cas9 system.[88] Therefore, future strategies to overcome the immunogenicity of other proteins may also be applicable to the TamPA-Cre system.

The TamPA-Cre system is also highly versatile. It can be utilized to lend high-spatiotemporal control to any Cre-loxP recombination system. Additionally, the TamPA-Cre system can easily be integrated with other genetic systems to further improve on-target off-tumor toxicity. For example, replacing the Receptor and/or CAR components with universal SUPRA CARs would allow CAR T cells to rapidly switch between antigen targets *in vivo* to prevent cancer cell escape via antigen loss.[37] Furthermore, the tamoxifen- and light-inducible AND-gate

of the TamPA-Cre system could likewise be adapted to more strictly control, for example, newly developed CRISPR-Cas9-based photoactivatable transcription systems.[81-83] All in all, I have contributed to the esteemed scientific community the first versatile, robust, and highly-controllable optogenetic tool capable of regulating CAR T cell effector functions with high spatiotemporal precision. I hope that the TamPA-Cre system and its future iterations will prove useful in overcoming the problem of on-target off-tumor toxicity that currently limits the CAR T cell therapeutic approach.

REFERENCES

1. Bray, F.; Ferlay, J.; Soerjomataram, I.; Siegel, R. L.; Torre, L. A.; Jemal, A., Global cancer statistics 2018: GLOBOCAN estimates of incidence and mortality worldwide for 36 cancers in 185 countries. *CA Cancer J Clin* **2018,** *68* (6), 394-424.

2. Kalos, M.; Levine, B. L.; Porter, D. L.; Katz, S.; Grupp, S. A.; Bagg, A.; June, C. H., T cells with chimeric antigen receptors have potent antitumor effects and can establish memory in patients with advanced leukemia. *Sci Transl Med* **2011,** *3* (95), 95ra73.

3. Sadelain, M.; Brentjens, R.; Riviere, I., The basic principles of chimeric antigen receptor design. *Cancer Discov* **2013,** *3* (4), 388-98.

4. Porter, D. L.; Levine, B. L.; Kalos, M.; Bagg, A.; June, C. H., Chimeric antigen receptor-modified T cells in chronic lymphoid leukemia. *N Engl J Med* **2011,** *365* (8), 725-33.

5. Grupp, S. A.; Kalos, M.; Barrett, D.; Aplenc, R.; Porter, D. L.; Rheingold, S. R.; Teachey, D. T.; Chew, A.; Hauck, B.; Wright, J. F.; Milone, M. C.; Levine, B. L.; June, C. H., Chimeric antigen receptor-modified T cells for acute lymphoid leukemia. *N Engl J Med* **2013,** *368* (16), 1509-1518.

6. Maude, S. L.; Shpall, E. J.; Grupp, S. A., Chimeric antigen receptor T-cell therapy for ALL. *Hematology Am Soc Hematol Educ Program* **2014,** *2014* (1), 559-64.

7. Maude, S. L.; Teachey, D. T.; Porter, D. L.; Grupp, S. A., CD19-targeted chimeric antigen receptor T-cell therapy for acute lymphoblastic leukemia. *Blood* **2015,** *125* (26), 4017-23.

8. Davila, M. L.; Riviere, I.; Wang, X.; Bartido, S.; Park, J.; Curran, K.; Chung, S. S.; Stefanski, J.; Borquez-Ojeda, O.; Olszewska, M.; Qu, J.; Wasielewska, T.; He, Q.; Fink, M.; Shinglot, H.; Youssif, M.; Satter, M.; Wang, Y.; Hosey, J.; Quintanilla, H.; Halton, E.; Bernal, Y.; Bouhassira, D. C.; Arcila, M. E.; Gonen, M.; Roboz, G. J.; Maslak, P.; Douer, D.; Frattini, M. G.; Giralt, S.; Sadelain, M.; Brentjens, R., Efficacy and toxicity management of 19-28z CAR T cell therapy in B cell acute lymphoblastic leukemia. *Sci Transl Med* **2014,** *6* (224), 224ra25.

9. Alonso-Camino, V.; Harwood, S. L.; Alvarez-Mendez, A.; Alvarez-Vallina, L., Efficacy and toxicity management of CAR-T-cell immunotherapy: a matter of responsiveness control or tumour-specificity? *Biochem Soc Trans* **2016,** *44* (2), 406-11.

10. Frey, N.; Porter, D., Cytokine Release Syndrome with Chimeric Antigen Receptor T Cell Therapy. *Biol Blood Marrow Transplant* **2018**.

11. Teachey, D. T.; Lacey, S. F.; Shaw, P. A.; Melenhorst, J. J.; Maude, S. L.; Frey, N.; Pequignot, E.; Gonzalez, V. E.; Chen, F.; Finklestein, J.; Barrett, D. M.; Weiss, S. L.; Fitzgerald, J. C.; Berg, R. A.; Aplenc, R.; Callahan, C.; Rheingold, S. R.; Zheng, Z.; Rose-John, S.; White, J. C.; Nazimuddin, F.; Wertheim, G.; Levine, B. L.; June, C. H.; Porter, D. L.; Grupp, S. A., Identification of Predictive Biomarkers for Cytokine Release Syndrome after Chimeric Antigen Receptor T-cell Therapy for Acute Lymphoblastic Leukemia. *Cancer Discov* **2016,** *6* (6), 664-79.

12. Morgan, R. A.; Yang, J. C.; Kitano, M.; Dudley, M. E.; Laurencot, C. M.; Rosenberg, S. A., Case Report of a Serious Adverse Event Following the Administration of T Cells Transduced With a Chimeric Antigen Receptor Recognizing ERBB2. *Mol Ther* **2010,** *18* (4), 843-851.

13. Lamers, C., Treatment of metastatic renal cell cancer with autologous T cells genetically retargeted against carbonic anhydrase IX - first clinical experience. *Hum Gene Ther* **2009,** *20* (11), 1544-1545.

14. Thistlethwaite, F. C.; Gilham, D. E.; Guest, R. D.; Rothwell, D. G.; Pillai, M.; Burt, D. J.; Byatte, A. J.; Kirillova, N.; Valle, J. W.; Sharma, S. K.; Chester, K. A.; Westwood, N. B.; Halford, S. E. R.; Nabarro, S.; Wan, S.; Austin, E.; Hawkins, R. E., The clinical efficacy of first-generation carcinoembryonic antigen (CEACAM5)-specific CAR T cells is limited by poor persistence and transient pre-conditioning-dependent respiratory toxicity. *Cancer Immunol Immun* **2017,** *66* (11), 1425-1436.

15. Kloss, C. C.; Condomines, M.; Cartellieri, M.; Bachmann, M.; Sadelain, M., Combinatorial antigen recognition with balanced signaling promotes selective tumor eradication by engineered T cells. *Nat Biotechnol* **2013,** *31* (1), 71-+.

16. Chen, L.; Flies, D. B., Molecular mechanisms of T cell co-stimulation and co-inhibition. *Nat Rev Immunol* **2013,** *13* (4), 227-42.

17. Hebeisen, M.; Allard, M.; Gannon, P. O.; Schmidt, J.; Speiser, D. E.; Rufer, N., Identifying Individual T Cell Receptors of Optimal Avidity for Tumor Antigens. *Front Immunol* **2015,** *6*, 582.

18. Chakravarti, D.; Wong, W. W., Synthetic biology in cell-based cancer immunotherapy. *Trends Biotechnol* **2015,** *33* (8), 449-61.

19. Okazaki, T.; Honjo, T., PD-1 and PD-1 ligands: from discovery to clinical application. *Int Immunol* **2007,** *19* (7), 813-24.

20. Schmidt, A.; Oberle, N.; Krammer, P. H., Molecular mechanisms of treg-mediated T cell suppression. *Front Immunol* **2012,** *3*, 51.

21. Lewis, R. S., Calcium signaling mechanisms in T lymphocytes. *Annu Rev Immunol* **2001,** *19*, 497-521.

22. Fooksman, D. R.; Vardhana, S.; Vasiliver-Shamis, G.; Liese, J.; Blair, D. A.; Waite, J.; Sacristan, C.; Victora, G. D.; Zanin-Zhorov, A.; Dustin, M. L., Functional anatomy of T cell activation and synapse formation. *Annu Rev Immunol* **2010,** *28*, 79-105.

23. James, J. R.; Vale, R. D., Biophysical mechanism of T-cell receptor triggering in a reconstituted system. *Nature* **2012,** *487* (7405), 64-9.

24. Liao, W.; Lin, J. X.; Leonard, W. J., Interleukin-2 at the Crossroads of Effector Responses, Tolerance, and Immunotherapy. *Immunity* **2013,** *38* (1), 13-25.

25. Sample, V.; Mehta, S.; Zhang, J., Genetically encoded molecular probes to visualize and perturb signaling dynamics in living biological systems. *J Cell Sci* **2014,** *127* (Pt 6), 1151-60.

26. Carlson, H. J.; Campbell, R. E., Genetically encoded FRET-based biosensors for multiparameter fluorescence imaging. *Curr Opin Biotechnol* **2009,** *20* (1), 19-27.

27. Zhang, J.; Allen, M. D., FRET-based biosensors for protein kinases: illuminating the kinome. *Mol Biosyst* **2007,** *3* (11), 759-65.

28. Mehta, S.; Zhang, J., Reporting from the field: genetically encoded fluorescent reporters uncover signaling dynamics in living biological systems. *Annu Rev Biochem* **2011,** *80*, 375-401.

29. Komatsu, N.; Aoki, K.; Yamada, M.; Yukinaga, H.; Fujita, Y.; Kamioka, Y.; Matsuda, M., Development of an optimized backbone of FRET biosensors for kinases and GTPases. *Mol Biol Cell* **2011,** *22* (23), 4647-56.

30. Nagai, T.; Yamada, S.; Tominaga, T.; Ichikawa, M.; Miyawaki, A., Expanded dynamic range of fluorescent indicators for Ca(2+) by circularly permuted yellow fluorescent proteins. *Proc Natl Acad Sci U S A* **2004,** *101* (29), 10554-9.

31. Kanchiswamy, C. N.; Malnoy, M.; Occhipinti, A.; Maffei, M. E., Calcium imaging perspectives in plants. *Int J Mol Sci* **2014,** *15* (3), 3842-59.

32. Weinberg, B. H.; Pham, N. T. H.; Caraballo, L. D.; Lozanoski, T.; Engel, A.; Bhatia, S.; Wong, W. W., Large-scale design of robust genetic circuits with multiple inputs and outputs for mammalian cells. *Nat Biotechnol* **2017,** *35* (5), 453-462.

33. Fedorov, V. D.; Themeli, M.; Sadelain, M., PD-1-and CTLA-4-Based Inhibitory Chimeric Antigen Receptors (iCARs) Divert Off-Target Immunotherapy Responses. *Sci Transl Med* **2013,** *5* (215).

34. Di Stasi, A.; Tey, S. K.; Dotti, G.; Fujita, Y.; Kennedy-Nasser, A.; Martinez, C.; Straathof, K.; Liu, E.; Durett, A. G.; Grilley, B.; Liu, H.; Cruz, C. R.; Savoldo, B.; Gee, A. P.; Schindler, J.; Krance, R. A.; Heslop, H. E.; Spencer, D. M.; Rooney, C. M.; Brenner, M. K., Inducible Apoptosis as a Safety Switch for Adoptive Cell Therapy. *New Engl J Med* **2011,** *365* (18), 1673-1683.

35. Wu, C. Y.; Roybal, K. T.; Puchner, E. M.; Onuffer, J.; Lim, W. A., Remote control of therapeutic T cells through a small molecule-gated chimeric receptor. *Science* **2015,** *350* (6258).

36. Roybal, K. T.; Rupp, L. J.; Morsut, L.; Walker, W. J.; McNally, K. A.; Park, J. S.; Lim, W. A., Precision Tumor Recognition by T Cells With Combinatorial Antigen-Sensing Circuits. *Cell* **2016,** *164* (4), 770-779.

37. Cho, J. H.; Collins, J. J.; Wong, W. W., Universal Chimeric Antigen Receptors for Multiplexed and Logical Control of T Cell Responses. *Cell* **2018,** *173* (6), 1426-1438 e11.

38. Xu, Y.; Kim, M.; Hyun, Y., Optogenetic control of chemokine receptor signal and T cell migration. *Mol Biol Cell* **2014,** *25*.

39. Ueda, Y.; Sato, M., Induction of Signal Transduction by Using Non-Channelrhodopsin-Type Optogenetic Tools. *Chembiochem* **2018,** *19* (12), 1217-1231.

40. Tan, P.; He, L.; Han, G.; Zhou, Y., Optogenetic Immunomodulation: Shedding Light on Antitumor Immunity. *Trends Biotechnol* **2017,** *35* (3), 215-226.

41. Huang, X.; Yang, P.; Ouyang, X.; Chen, L.; Deng, X. W., Photoactivated UVR8-COP1 module determines photomorphogenic UV-B signaling output in Arabidopsis. *PLoS Genet* **2014,** *10* (3), e1004218.

42. Sinha, D. K.; Neveu, P.; Gagey, N.; Aujard, I.; Benbrahim-Bouzidi, C.; Le Saux, T.; Rampon, C.; Gauron, C.; Goetz, B.; Dubruille, S.; Baaden, M.; Volovitch, M.; Bensimon, D.; Vriz, S.; Jullien, L.,

Photocontrol of protein activity in cultured cells and zebrafish with one- and two-photon illumination. *Chembiochem* **2010,** *11* (5), 653-63.

43. Il Park, S.; Brenner, D. S.; Shin, G.; Morgan, C. D.; Copits, B. A.; Chung, H. U.; Pullen, M. Y.; Noh, K. N.; Davidson, S.; Oh, S. J.; Yoon, J.; Jang, K. I.; Samineni, V. K.; Norman, M.; Grajales-Reyes, J. G.; Vogt, S. K.; Sundaram, S. S.; Wilson, K. M.; Ha, J. S.; Xu, R. X.; Pan, T. S.; Kim, T. I.; Huang, Y. G.; Montana, M. C.; Golden, J. P.; Bruchas, M. R.; Gereau, R. W.; Rogers, J. A., Soft, stretchable, fully implantable miniaturized optoelectronic systems for wireless optogenetics. *Nat Biotechnol* **2015,** *33* (12), 1280-+.

44. Jeong, J. W.; McCall, J. G.; Shin, G.; Zhang, Y. H.; Al-Hasani, R.; Kim, M.; Li, S.; Sim, J. Y.; Jang, K. I.; Shi, Y.; Hong, D. Y.; Liu, Y. H.; Schmitz, G. P.; Xia, L.; He, Z. B.; Gamble, P.; Ray, W. Z.; Huang, Y. G.; Bruchas, M. R.; Rogers, J. A., Wireless Optofluidic Systems for Programmable In Vivo Pharmacology and Optogenetics. *Cell* **2015,** *162* (3), 662-674.

45. He, L.; Zhang, Y.; Ma, G.; Tan, P.; Li, Z.; Zang, S.; Wu, X.; Jing, J.; Fang, S.; Zhou, L.; Wang, Y.; Huang, Y.; Hogan, P. G.; Han, G.; Zhou, Y., Near-infrared photoactivatable control of Ca(2+) signaling and optogenetic immunomodulation. *Elife* **2015,** *4*.

46. Yu, N.; Huang, L.; Zhou, Y.; Xue, T.; Chen, Z.; Han, G., Near-Infrared-Light Activatable Nanoparticles for Deep-Tissue-Penetrating Wireless Optogenetics. *Adv Healthc Mater* **2019**, e1801132.

47. Nihongaki, Y.; Kawano, F.; Nakajima, T.; Sato, M., Photoactivatable CRISPR-Cas9 for optogenetic genome editing. *Nat Biotechnol* **2015,** *33* (7), 755-60.

48. Kawano, F.; Okazaki, R.; Yazawa, M.; Sato, M., A photoactivatable Cre-loxP recombination system for optogenetic genome engineering. *Nat Chem Biol* **2016,** *12* (12), 1059-+.

49. Taslimi, A.; Zoltowski, B.; Miranda, J. G.; Pathak, G. P.; Hughes, R. M.; Tucker, C. L., Optimized second-generation CRY2-CIB dimerizers and photoactivatable Cre recombinase. *Nat Chem Biol* **2016,** *12* (6), 425-30.

50. Feil, R.; Wagner, J.; Metzger, D.; Chambon, P., Regulation of Cre recombinase activity by mutated estrogen receptor ligand-binding domains. *Biochem Bioph Res Co* **1997,** *237* (3), 752-757.

51. Hirrlinger, J.; Requardt, R. P.; Winkler, U.; Wilhelm, F.; Schulze, C.; Hirrlinger, P. G., Split-CreERT2: Temporal Control of DNA Recombination Mediated by Split-Cre Protein Fragment Complementation. *Plos One* **2009,** *4* (12).

52. Besser, S.; Wilhelm, F.; Winkler, U.; Requardt, R.; Schulze, C.; Hirrlinger, P. G.; Hirrlinger, J., Split-Cre and Split-Creert2: Versatile Genetic Coincidence Detectors for Precise Analysis of Cell Populations in Vivo. *Glia* **2011,** *59*, S100-S100.

53. Paster, W.; Paar, C.; Eckerstorfer, P.; Jakober, A.; Drbal, K.; Schutz, G. J.; Sonnleitner, A.; Stockinger, H., Genetically encoded Forster resonance energy transfer sensors for the conformation of the Src family kinase Lck. *J Immunol* **2009,** *182* (4), 2160-7.

54. Ouyang, M.; Wan, R.; Qin, Q.; Peng, Q.; Wang, P.; Wu, J.; Allen, M.; Shi, Y.; Laub, S.; Deng, L.; Lu, S.; Wang, Y., Sensitive FRET Biosensor Reveals Fyn Kinase Regulation by Submembrane Localization. *ACS Sens* **2019,** *4* (1), 76-86.

55. Randriamampita, C.; Mouchacca, P.; Malissen, B.; Marguet, D.; Trautmann, A.; Lellouch, A. C., A novel ZAP-70 dependent FRET based biosensor reveals kinase activity at both the immunological synapse and the antisynapse. *Plos One* **2008,** *3* (1), e1521.

56. Harvey, C. D.; Ehrhardt, A. G.; Cellurale, C.; Zhong, H.; Yasuda, R.; Davis, R. J.; Svoboda, K., A genetically encoded fluorescent sensor of ERK activity. *Proc Natl Acad Sci U S A* **2008,** *105* (49), 19264-9.

57. Vandame, P.; Spriet, C.; Riquet, F.; Trinel, D.; Cailliau-Maggio, K.; Bodart, J. F., Optimization of ERK activity biosensors for both ratiometric and lifetime FRET measurements. *Sensors (Basel)* **2014,** *14* (1), 1140-54.

58. Fosbrink, M.; Aye-Han, N. N.; Cheong, R.; Levchenko, A.; Zhang, J., Visualization of JNK activity dynamics with a genetically encoded fluorescent biosensor. *Proc Natl Acad Sci U S A* **2010,** *107* (12), 5459-64.

59. Liu, S.; Zhang, J.; Xiang, Y. K., FRET-based direct detection of dynamic protein kinase A activity on the sarcoplasmic reticulum in cardiomyocytes. *Biochem Biophys Res Commun* **2011,** *404* (2), 581-6.

60. Zhao, Y.; Araki, S.; Wu, J.; Teramoto, T.; Chang, Y. F.; Nakano, M.; Abdelfattah, A. S.; Fujiwara, M.; Ishihara, T.; Nagai, T.; Campbell, R. E., An expanded palette of genetically encoded Ca(2)(+) indicators. *Science* **2011,** *333* (6051), 1888-91.

61. Joseph, N.; Reicher, B.; Barda-Saad, M., The calcium feedback loop and T cell activation: how cytoskeleton networks control intracellular calcium flux. *Biochim Biophys Acta* **2014,** *1838* (2), 557-68.

62. Wulfing, C.; Rabinowitz, J. D.; Beeson, C.; Sjaastad, M. D.; McConnell, H. M.; Davis, M. M., Kinetics and extent of T cell activation as measured with the calcium signal. *J Exp Med* **1997,** *185* (10), 1815-25.

63. Salles, A.; Billaudeau, C.; Serge, A.; Bernard, A. M.; Phelipot, M. C.; Bertaux, N.; Fallet, M.; Grenot, P.; Marguet, D.; He, H. T.; Hamon, Y., Barcoding T cell calcium response diversity with methods for automated and accurate analysis of cell signals (MAAACS). *PLoS Comput Biol* **2013,** *9* (9), e1003245.

64. Kochenderfer, J. N.; Rosenberg, S. A., Treating B-cell cancer with T cells expressing anti-CD19 chimeric antigen receptors. *Nat Rev Clin Oncol* **2013,** *10* (5), 267-76.

65. Mihara, K.; Yanagihara, K.; Takigahira, M.; Imai, C.; Kitanaka, A.; Takihara, Y.; Kimura, A., Activated T-cell-mediated Immunotherapy With a Chimeric Receptor Against CD38 in B-cell Non-Hodgkin Lymphoma. *Journal of Immunotherapy* **2009,** *32* (7), 737-743.

66. Abraham, R. T.; Weiss, A., Jurkat T cells and development of the T-cell receptor signalling paradigm. *Nat Rev Immunol* **2004,** *4* (4), 301-8.

67. Paredes, R. M.; Etzler, J. C.; Watts, L. T.; Zheng, W.; Lechleiter, J. D., Chemical calcium indicators. *Methods* **2008,** *46* (3), 143-51.

68. Komatsubara, A. T.; Matsuda, M.; Aoki, K., Quantitative analysis of recombination between YFP and CFP genes of FRET biosensors introduced by lentiviral or retroviral gene transfer. *Sci Rep* **2015,** *5*, 13283.

69. Rydzek, J.; Nerreter, T.; Peng, H.; Jutz, S.; Leitner, J.; Steinberger, P.; Einsele, H.; Rader, C.; Hudecek, M., Chimeric Antigen Receptor Library Screening Using a Novel NF-kappaB/NFAT Reporter Cell Platform. *Mol Ther* **2018**.

70. Konermann, S.; Brigham, M. D.; Trevino, A.; Hsu, P. D.; Heidenreich, M.; Cong, L.; Platt, R. J.; Scott, D. A.; Church, G. M.; Zhang, F., Optical control of mammalian endogenous transcription and epigenetic states. *Nature* **2013,** *500* (7463), 472-476.

71. Niopek, D.; Benzinger, D.; Roensch, J.; Draebing, T.; Wehler, P.; Eils, R.; Di Ventura, B., Engineering light-inducible nuclear localization signals for precise spatiotemporal control of protein dynamics in living cells. *Nature Communications* **2014,** *5*.

72. Niopek, D.; Benzinger, D.; Roensch, J.; Draebing, T.; Wehler, P.; Eils, R.; Di Ventura, B., Engineering light-inducible nuclear localization signals for precise spatiotemporal control of protein dynamics in living cells. *Nat Commun* **2014,** *5*, 4404.

73. Eyquem, J.; Mansilla-Soto, J.; Giavridis, T.; van der Stegen, S. J.; Hamieh, M.; Cunanan, K. M.; Odak, A.; Gonen, M.; Sadelain, M., Targeting a CAR to the TRAC locus with CRISPR/Cas9 enhances tumour rejection. *Nature* **2017,** *543* (7643), 113-117.

74. Shaner, N. C.; Lambert, G. G.; Chammas, A.; Ni, Y.; Cranfill, P. J.; Baird, M. A.; Sell, B. R.; Allen, J. R.; Day, R. N.; Israelsson, M.; Davidson, M. W.; Wang, J., A bright monomeric green fluorescent protein derived from Branchiostoma lanceolatum. *Nat Methods* **2013,** *10* (5), 407-9.

75. Feil, S.; Valtcheva, N.; Feil, R., Inducible Cre mice. *Methods Mol Biol* **2009,** *530*, 343-63.

76. Casanova, E.; Fehsenfeld, S.; Lemberger, T.; Shimshek, D. R.; Sprengel, R.; Mantamadiotis, T., ER-based double iCre fusion protein allows partial recombination in forebrain. *Genesis* **2002,** *34* (3), 208-14.

77. Kawano, F.; Suzuki, H.; Furuya, A.; Sato, M., Engineered pairs of distinct photoswitches for optogenetic control of cellular proteins. *Nat Commun* **2015,** *6*, 6256.

78. Drent, E.; Groen, R. W.; Noort, W. A.; Themeli, M.; Lammerts van Bueren, J. J.; Parren, P. W.; Kuball, J.; Sebestyen, Z.; Yuan, H.; de Bruijn, J.; van de Donk, N. W.; Martens, A. C.; Lokhorst, H. M.; Mutis, T., Pre-clinical evaluation of CD38 chimeric antigen receptor engineered T cells for the treatment of multiple myeloma. *Haematologica* **2016,** *101* (5), 616-25.

79. Roybal, K. T.; Rupp, L. J.; Morsut, L.; Walker, W. J.; McNally, K. A.; Park, J. S.; Lim, W. A., Precision Tumor Recognition by T Cells With Combinatorial Antigen-Sensing Circuits. *Cell* **2016,** *164* (4), 770-9.

80. Cho, J. H.; Collins, J. J.; Wong, W. W., Universal Chimeric Antigen Receptors for Multiplexed and Logical Control of T Cell Responses. *Cell* **2018**.

81. Nihongaki, Y.; Yamamoto, S.; Kawano, F.; Suzuki, H.; Sato, M., CRISPR-Cas9-based Photoactivatable Transcription System. *Chemistry & Biology* **2015,** *22* (2), 169-174.

82. Nihongaki, Y.; Furuhata, Y.; Otabe, T.; Hasegawa, S.; Yoshimoto, K.; Sato, M., CRISPR-Cas9-based photoactivatable transcription systems to induce neuronal differentiation. *Nature Methods* **2017,** *14* (10), 963-+.

83. Zhou, X. X.; Zou, X.; Chung, H. K.; Gao, Y.; Liu, Y.; Qi, L. S.; Lin, M. Z., A Single-Chain Photoswitchable CRISPR-Cas9 Architecture for Light-Inducible Gene Editing and Transcription. *ACS Chem Biol* **2018,** *13* (2), 443-448.

84. Gargett, T.; Brown, M. P., The inducible caspase-9 suicide gene system as a "safety switch" to limit on-target, off-tumor toxicities of chimeric antigen receptor T cells. *Front Pharmacol* **2014,** *5*, 235.

85. Kristianto, J.; Johnson, M. G.; Zastrow, R. K.; Radcliff, A. B.; Blank, R. D., Spontaneous recombinase activity of Cre-ERT2 in vivo. *Transgenic Res* **2017,** *26* (3), 411-417.

86. Roth, T. L.; Puig-Saus, C.; Yu, R.; Shifrut, E.; Carnevale, J.; Li, P. J.; Hiatt, J.; Saco, J.; Krystofinski, P.; Li, H.; Tobin, V.; Nguyen, D. N.; Lee, M. R.; Putnam, A. L.; Ferris, A. L.; Chen, J. W.; Schickel, J. N.; Pellerin, L.; Carmody, D.; Alkorta-Aranburu, G.; Del Gaudio, D.; Matsumoto, H.; Morell, M.; Mao, Y.; Cho, M.; Quadros, R. M.; Gurumurthy, C. B.; Smith, B.; Haugwitz, M.; Hughes, S. H.; Weissman, J. S.; Schumann, K.; Esensten, J. H.; May, A. P.; Ashworth, A.; Kupfer, G. M.; Greeley, S. A. W.; Bacchetta, R.; Meffre, E.; Roncarolo, M. G.; Romberg, N.; Herold, K. C.; Ribas, A.; Leonetti, M. D.; Marson, A., Reprogramming human T cell function and specificity with non-viral genome targeting. *Nature* **2018,** *559* (7714), 405-409.

87. Zhao, Y.; Zheng, Z.; Cohen, C. J.; Gattinoni, L.; Palmer, D. C.; Restifo, N. P.; Rosenberg, S. A.; Morgan, R. A., High-efficiency transfection of primary human and mouse T lymphocytes using RNA electroporation. *Mol Ther* **2006,** *13* (1), 151-9.

88. Crudele, J. M.; Chamberlain, J. S., Cas9 immunity creates challenges for CRISPR gene editing therapies. *Nat Commun* **2018,** *9* (1), 3497.